

โครงสร้างทางเรขาคณิตและสมบัติเชิงอิเล็กทรอนิกส์ของสารยับยั้ง
เอช ไอ วี-1 โปรตีนเอส: อนุพันธ์ C₆₀



นางสาวศิริพร พรหมศรี

สถาบันวิทยบริการ
จุฬาลงกรณ์มหาวิทยาลัย

วิทยานิพนธ์นี้เป็นส่วนหนึ่งของการศึกษาตามหลักสูตรปริญญาวิทยาศาสตรมหาบัณฑิต

สาขาวิชาเคมี ภาควิชาเคมี

คณะวิทยาศาสตร์ จุฬาลงกรณ์มหาวิทยาลัย

ปีการศึกษา 2545

ISBN 974-17-3131-7

ลิขสิทธิ์ของจุฬาลงกรณ์มหาวิทยาลัย

GEOMETRIC STRUCTURES AND ELECTRONIC PROPERTIES OF HIV-1
PROTEINASE INHIBITOR: C₆₀ DERIVATIVES



MISS SIRIPORN PROMSRI

สถาบันวิทยบริการ

จุฬาลงกรณ์มหาวิทยาลัย
A Thesis Submitted in Partial Fulfillment of the Requirements
for the Degree of Master of Science in Chemistry

Department of Chemistry

Faculty of Science

Chulalongkorn University

Academic year 2002

ISBN 974-17-3131-7

Thesis Title Geometric Structures and Electronic Properties of HIV-1
Proteinase Inhibitor: C₆₀ Derivatives
By Miss Siriporn Promsri
Field of Study Chemistry
Thesis Advisor Associate Professor Supot Hannongbua, Ph. D.
Thesis Co-advisor Associate Professor Vudhichai Parasuk, Ph. D.

Accepted by the Faculty of Science, Chulalongkorn University in Partial
Fulfillment of the Requirements for the Master's Degree

..... Dean of Faculty of Science
(Associate Professor Wanchai Phothiphichitr, Ph. D.)

THESIS COMMITTEE

..... Chairman
(Associate Professor Sirirat Kokpol, Ph. D.)

..... Thesis Advisor
(Associate Professor Supot Hannongbua, Ph. D.)

..... Thesis Co-advisor
(Associate Professor Vudhichai Parasuk, Ph. D.)

..... Member
(Assistant Professor Surapong Pinitglang, Ph. D.)

..... Member
(Vannajan Sanghiran Lee, Ph. D.)

ศิริพร พรหมศรี: โครงสร้างทางเรขาคณิตและสมบัติเชิงอิเล็กทรอนิกส์ของสารยับยั้ง เอช ไอ
 วี-1 โปรตีนเอส: อนุพันธ์ C_{60} (GEOMETRIC STRUCTURES AND
 ELECTRONIC PROPERTIES OF HIV-1 PROTEINASE INHIBITOR: C_{60}
 DERIVATIVES) อาจารย์ที่ปรึกษา: รศ. ดร. สุพจน์ หารหนองบัว, อาจารย์ที่ปรึกษาร่วม:
 รศ. ดร. วุฒิชัย พาราสุข, 136 หน้า. ISBN 974-17-3131-7

ศึกษาโครงสร้างและสมบัติเชิงอิเล็กทรอนิกส์ของอนุกรมอนุพันธ์ C_{60} ด้วยวิธีทางเคมีควอนตัมโดยใช้วิธีอเนียม (ONIOM) เพื่อหาโครงสร้างที่เสถียรที่สุดของสารและใช้วิธีเดนซิติฟังก์ชันแนลในการคำนวณเพื่อหาสมบัติเชิงโมเลกุลและสมบัติเชิงอิเล็กทรอนิกส์ที่ระดับเบซิทเซททชยชชนิด 6-31G (d) ซึ่งพบว่าผลกระทบที่เกิดกับประจุสุทธิอันเกิดจากหมู่ฟังก์ชันนั้นมีผลมากที่สุดต่ออะตอมในตำแหน่งที่เชื่อมต่อระหว่างโมเลกุล C_{60} กับหมู่ฟังก์ชัน โดยทำให้เกิดการเปลี่ยนแปลงประจุสุทธิในระยะกว่า 5 อังสตรอมจากพันธะ คาร์บอน-- คาร์บอน ที่เชื่อมต่อระหว่างหมู่ฟังก์ชันกับ C_{60} นอกจากนี้ยังพบบริเวณที่มีศักย์ไฟฟ้าสถิตที่มีค่าสูงอยู่ 2 บริเวณด้วยกัน คือ บริเวณอะตอมออกซิเจนของหมู่ไฮดรอกซิลและอะตอมไฮโดรเจนของหมู่ไฮดรอกซิล โดยที่อะตอมไฮโดรเจนของหมู่ไฮดรอกซิลเป็นบริเวณที่มีค่าศักย์ไฟฟ้าสถิตเป็นค่าบวกมากที่สุด ซึ่งลักษณะทางไฟฟ้าสถิตแสดงความเป็นไฮโดรโฟบิก หรือ ไฮโปฟิลิกของสารซึ่งบ่งชี้ว่าสารเหล่านี้เกิดอันตรกิริยากับเอนไซม์อย่างไร

สถาบันวิทยบริการ
 จุฬาลงกรณ์มหาวิทยาลัย

ภาควิชา.....เคมี.....ลายมือชื่อนิสิต.....
 สาขาวิชา.....เคมี.....ลายมือชื่ออาจารย์ที่ปรึกษา.....
 ปีการศึกษา.....2545.....ลายมือชื่ออาจารย์ที่ปรึกษาร่วม.....

4372427623: MAJOR CHEMISTRY

SIRIPORN PROMSRI: GEOMETRIC STRUCTURES AND ELECTRONIC PROPERTIES OF HIV-1 PROTEINASE INHIBITOR: C₆₀ DERIVATIVES. THESIS ADVISOR: ASSOC. PROF. DR. SUPOT HANNONGBUA, THESIS CO-ADVISOR: ASSOC. PROF. DR. VUDHICHAIR PARASUK, 136 pp. ISBN 974-17-3131-7.

Quantum chemical methods were performed to study structure and electronic properties of a series of C₆₀ derivatives. The integrated, ONIOM molecular orbital method was applied to optimize the structure of all compounds while the DFT/B3LYP (6-31G (d)) calculations were performed to examine molecular and electronic properties. It was found that strongest effect of functional group on the net charges takes place on the linked atoms between C₆₀ and its side chain. The functional group leads to the changes of atomic net charges on the C₆₀ surface up to 5 Å far from C—C bond where the functional group binds to the surface. Two localized electrostatic potential regions are observed, for the selected compounds, near the hydroxyl oxygen and the hydroxyl hydrogen. The hydroxyl hydrogen atom is the center for most positive potential. These electrostatic features are likely to be the modulator of hydrophobicity or lipophilicity of the compounds and, hence, indicate how they interact with the receptor.

สถาบันวิทยบริการ
จุฬาลงกรณ์มหาวิทยาลัย

Department Chemistry Student's signature

Field of study Chemistry Advisor's signature

Academic year 2002 Co-advisor's signature

ACKNOWLEDGEMENTS

I would like to express my sincere gratitude to Associate Professor Dr. Supot Hannongbua, my advisor, for his understanding, useful guidance, and kind suggestion and encouragement throughout this study. Gratefully thanks to Associate Professor Dr. Vudhichai Parasuk, my co-advisor, for all the help and good advise. Special thanks to Associate Professor Dr. Sirirat Kokpol, Assistant Professor Dr. Surapong Pinitglang and Dr. Vannajan Sanghiran Lee who act as the thesis committee.

I also would like to acknowledge the computational chemistry unit cell (CCUC) for computer resources and other facilities. Also gratefully acknowledge the National Center for Genetic Engineering and Biotechnology (BIOTEC) for financial support during the study.

I also would like to thank Professor Dr. Keiji Morokuma for valuable suggestions and discussions in ONIOM method.

Finally, I would like to give all gratitude affectionately to my beloved parents for all their love, support and encouragement during the whole period of my study and for always letting me that choose my own path. Thanks my sister for all joys and fights we have shared and for being such wonderful sister.

สถาบันวิทยบริการ
จุฬาลงกรณ์มหาวิทยาลัย

CONTENTS

	Pages
ABSTRACT IN THAI	iv
ABSTRACT IN ENGLISH	v
ACKNOWLEDGEMENT	vi
CONTENTS	vii
LIST OF FIGURES	x
LIST OF TABLES	xiii
CHAPTER 1 INTRODUCTION	1
1.1. Acquired Immune Deficiency Syndrome (AIDS).....	1
1.2. Human Immunodeficiency Virus (HIV).....	2
1.3. Replication of HIV.....	3
1.4. HIV-1 Proteinase (HIV-1 PR).....	5
1.5. HIV-1 Proteinase Inhibitors.....	9
1.6. Fullerene (C ₆₀) Derivatives.....	10
1.6.1. Introduction.....	10
1.6.2. Enzymatic Inhibition and Anti-HIV Activity.....	11
1.7. Objectives of the Present Study.....	13
CHAPTER 2 THEORY	14
2.1. Quantum Mechanics.....	14
2.1.1. Introduction.....	14
2.1.2. <i>Ab initio</i> Methods.....	17
2.1.2.1. Hartree-Fock Theory.....	17
2.1.2.2. Basis Sets.....	21
2.1.3. Semi-empirical Methods.....	24
2.1.4. Density Functional Theory.....	26
2.1.4.1. Basic Theory.....	26
2.1.4.2. Local density Methods.....	28

CONTENTS (cont.)

	Pages
2.1.4.3.Gradient Corrected Methods.....	29
2.1.4.4.Hybrid Methods.....	32
2.2. The ONIOM (our Own N-layered Integrated molecular Orbital and molecular Mechanics) Method.....	33
2.3. Electrostatics.....	36
2.3.1. Basic Theorems in Electrostatics.....	36
2.3.2. Molecular Electrostatic Potential (MESP): Theoretical Computation and Graphics Visualization.....	40
2.3.2.1.MESP from Density Functional Theory.....	41
2.3.2.2.MESP Visualization.....	42
2.3.3. Applications of Molecular Electrostatic Potential.....	43
2.3.3.1.Introduction.....	43
2.3.3.2.Biological and Medicinal Chemistry.....	44
CHAPTER 3 DETAILS OF THE CALCULATIONS	45
3.1. Geometry Optimization of C ₆₀ Derivatives.....	45
3.1.1. Structure of C ₆₀ Derivatives.....	45
3.1.2. Optimization Algorithm.....	47
3.2. Electronic Features of the C ₆₀ Derivatives.....	48
CHAPTER 4 RESULTS AND DISCUSSIONS	49
4.1. Optimized Geometry of the C ₆₀ Derivatives.....	49
4.2. Electronic and Molecular Properties.....	51
4.2.1. Effect of Functional Groups on Molecular Orbital Properties...	51
4.2.2. Effect of Functional Groups on Atomic Net Charge.....	52
4.2.3. Effect of Functional Groups on the Molecular Geometry.....	56
4.2.4. Electrostatic Potential (ESP).....	59

CONTENTS (cont.)

	Pages
CHAPTER 5 CONCLUSIONS	65
FURTHER WORKS.....	67
REFERENCES.....	68
APPENDICES.....	78
APPENDIX A PARAMETERS OF C ₆₀ DERIVETIVES.....	79
APPENDIX B MOLECULAR ELECTROSTATIC POTENTIAL VISUALIZATION.....	108
APPENDIX C MANUSCRIPT.....	120
VITAE.....	136

สถาบันวิทยบริการ
จุฬาลงกรณ์มหาวิทยาลัย

LIST OF FIGURES

		Pages
Figure 1.1	A Schematic drawing of the mature HIV-virion.....	3
Figure 1.2	A schematic representation of the replication cycle of HIV.....	4
Figure 1.3	Ribbon drawing of (a) apo- and (b) inhibited HIV proteinase showing the relatively open and closed position of the flaps (top of images).....	5
Figure 1.4	Cleavage site of HIV pretease in the Gag and Pol polyproteins...	6
Figure 1.5	Schematic representation of the catalytic mechanism of aspartic acid proteinase.....	7
Figure 1.6	General scheme of active site interaction in HIV PR with a putative substrate or peptide-based inhibitor.....	8
Figure 1.7	Six clinically FDA approved proteinase inhibitors (FDA stands for Food and Drug Administration).....	9
Figure 2.1	(a) Comparison of exponential and Gaussian functions. (b) Comparison of the same exponential function and a sum of three Gaussians.....	20
Figure 2.2	Basis set improvements.....	23
Figure 2.3	Schematic representation of two-layered ONIOM extrapolation scheme.....	34
Figure 2.4	Illustration of Gauss' law for a charge enclosed in a closed surface S	37
Figure 2.5	Electric field in the neighborhood of a point P , position of a stable equilibrium for a positive charge.....	40
Figure 3.1	Fullerene (C_{60}) derivatives used in this study.....	46
Figure 3.2	Optimized structure of C_{60} derivatives using ONIOM method (a) low level region and (b) high level region (ball and stick).....	47
Figure 4.1	Definition of structural parameters of C_{60} derivative compounds I – IV with atomic numbering.....	49

LIST OF FIGURES (cont.)

		Pages
Figure 4.2	Definition of structural parameters of C ₆₀ derivative compounds VII-X with atomic numbering.....	50
Figure 4.3	The selected carbon atoms with labeling for atomic net charges determination of (a) compounds I-VI and (b) compounds VII-X.....	53
Figure 4.4	The plots of atomic net charges of all 10 C ₆₀ derivatives; (a) compounds I-VI and (b) compounds VII-X.....	55
Figure 4.5	The six selected bond lengths on the C ₆₀ surface which are in the region 5 Å from the bridged atoms.....	56
Figure 4.6	The plots of selected bond-length of all compounds; (a) compounds I-VI and (b) compounds VII-X.....	58
Figure 4.7	Molecular electrostatic potential energy isosurfaces of the selected compounds superimposed onto total electron density (0.004 e/au ³) of compounds (solid view).....	62
Figure 4.8	Molecular electrostatic potential energy isosurfaces of the selected compounds superimposed onto total electron density (0.004 e/au ³) of compounds (mesh view).....	63
Figure 4.9	(a) Stereoview and (b) electrostatic potential contours plot of the compound III comparison between the optional structures obtained from quantum chemical calculation (blue) and molecular dynamics simulations (black).....	64
Figure B.1	Schematic representation of methodology details and calculations of molecular electrostatic maps.....	109
Figure B.2	Dialog boxes of drawing tools and conformational search in HyperChem package.....	110
Figure B.3	ONIOM layer assignment illustration in <i>Gaussview</i> program.....	111
Figure B.4	Dialog box of <i>Gaussian</i> calculation setup in <i>Gaussview</i> program.....	112

LIST OF FIGURES (cont.)

	Pages
Figure B.5 Show the section in the Cubes and Surfaces dialog box.....	118
Figure B.6 Show the section of map values from a 2 nd function in the Cubes and Surfaces dialog box.....	118
Figure B.7 Three-dimensional plot showing MESP isosurface.....	119



สถาบันวิทยบริการ
จุฬาลงกรณ์มหาวิทยาลัย

LIST OF TABLES

		Pages
Table 3.1	K_i and EC_{50} of the 10 investigated compounds as shown in Figure 3.1.....	45
Table 3.2	ONIOM model structures employed 2-layer calculation for optimization (ONIOM2).....	48
Table 4.1	The HOMO-LUMO energy gaps of all 10 C_{60} derivatives and of C_{60}	51
Table 4.2	The minimum of electrostatic potential of all 10 C_{60} derivatives..	61
Table 4.3	The maximum of electrostatic potential of all 10 C_{60} derivatives..	61
Table A.1	Structural parameters of compounds I-VI obtained from ONIOM calculations.....	80
Table A.2	Structural parameters of compounds VII-X obtained from ONIOM calculations.....	91
Table A.3	The net charges (in a.u.) of atoms of C_{60} derivatives in group 1 obtained using B3LYP/6-31G (d).....	102
Table A.4	The net charges (in a.u.) of atoms of C_{60} derivatives in group 2 obtained using B3LYP/6-31G (d).....	105

CHAPTER 1

INTRODUCTION

1.1. Acquired Immune Deficiency Syndrome (AIDS)

In mid-1981, five cases of a rare of pneumonia (*Pneumocystis carinii*) and severe viral infections in previously healthy young adults were rather quietly reported in Los Angeles.¹ Soon, an increased occurrence of unusual cases of pneumonia and Kaposi's cancer together with other opportunistic infections, was observed among previously healthy homosexual men and intravenous drug abusers in the USA.^{2, 3} The disease was accompanied by a depressed immune system and a susceptibility to opportunistic infections. This syndrome became known as Acquired Immune Deficiency Syndrome (AIDS).⁴

In 1983 the causative agent of AIDS was identified as a human retrovirus, first isolated in France from a patient with multiple lymphadenopathies⁵, a condition linked to AIDS, and subsequently in 1984, from AIDS patient.^{6,7} Initially, three different names were given to the virus isolated from AIDS patients; human T lymphotropic virus III (HTLV-III)⁶, lymphadenopathy-associated virus (LAV)⁸, and AIDS-associated retrovirus (ARV). Eventually the AIDS-causing virus was in 1986 given an alternative name, human immunodeficiency virus (HIV).⁹

By the end of 2001, approximately 42 million people were living with human immunodeficiency virus (HIV)¹⁰, and more than 20 million people worldwide had lost their lives to AIDS.¹¹ As the number of people infected with HIV continues to mount, efforts to provide care for those affected are just as critical as strategies for prevention, and have become an integral part of the response to control the HIV/AIDS pandemic.

1.2. Human Immunodeficiency Virus (HIV)

HIV-1 and HIV-2 are RNA viruses and belong to the family of retroviruses, *Retroviridae* (*retro*, backwards). The genome of retroviruses consists of duplicate copies of positive single-stranded RNA. Once a cell has become infected with a retrovirus the viral genetic information will be transformed from RNA to DNA, catalyzed by viral enzyme reverse transcriptase. The name retrovirus is derived from this unique event, which is completely opposite to the normal process where RNA is transcribed from DNA. Retroviruses are divided into seven genera, where the genus *Lentivirus* (*lenti*, slow), is characterized by the slow development of disease after infection. HIV is a typical lentivirus, since it usually has a disease latency of several years.¹²

A schematic drawing of the mature HIV virion is shown in Figure 1.1. The virion is almost spherical and is about one ten-thousandth of a millimeter across (ca. 100 nm).¹³ The virus is surrounded by a lipid bilayer derived from the host cell and contains several cellular membrane proteins.¹⁴ The outer portion of this envelope is spotted with surface glycoprotein gp120 (named for its approximate molecular weight) adhered to transmembrane protein gp41 (see Figure 1.1). These surface proteins play a crucial role when HIV binds to and enters the host cells. A shell of the matrix protein (p17) in Figure 1.1 lines the inner surface of the viral membrane, and a conical capsid core particle constructed out of the capsid protein (p24) is located in the center of the virus. The capsid particle encapsulates two copies of the viral genome, stabilized by the nucleocapsid protein (p7), and also contains three essential virally encoded enzymes: protease (PR), reverse transcriptase (RT), and integrase (IN).¹⁵

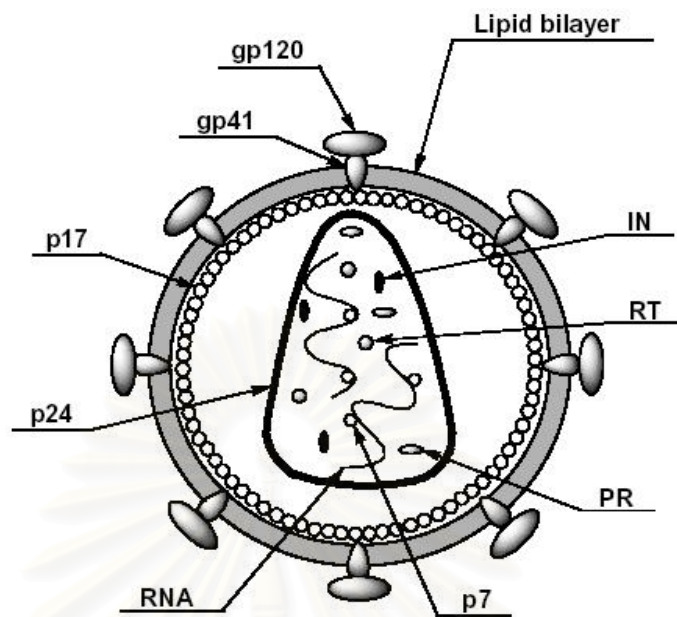


Figure 1.1 A Schematic drawing of the mature HIV-virion.¹³

1.3. Replication of HIV

A schematic representation of the replication cycle of HIV appears in Figure 1.2. The attachment of the viral surface protein (gp120) to the CD4-receptor, located on various cells within the immune system, initiates the replicative cycle of HIV.¹⁶ Attached virions utilize several additional cell-surface proteins to promote the fusion of the viral and host cellular membranes.^{17,18} Membrane fusion is followed by a poorly understood uncoating event of the capsid that allows the release of the viral content into the host-cell cytosol. The single-stranded viral RNA complexes with reverse transcriptase, which catalyses the reverse transcription to yield a double-stranded DNA molecule.¹⁹⁻²¹ The double-stranded viral DNA is then transported into the cell nucleus and is permanently integrated into the host genome by the catalytic activity of the viral integrase. The integrated viral DNA is designated *provirus*.²²

By an unknown activation process the cell initiates the transcription of the proviral DNA by the host cellular RNA polymerase II. Initially, short spliced RNA species that encode the regulatory proteins Tat, Rev, and Nef are synthesized. Tat acts as a stimulator of the transcription of the proviral DNA to enhance the production of

viral RNA.²³⁻²⁵ Full-length and singly spliced RNA is needed in the cytoplasm for the synthesis of Gag and Gag-Pol polyproteins, and for packing into new virions. Rev binds to the full length and singly spliced RNA in the nucleus and protects it from further splicing and actively transports it to the cytosol. In this manner, Rev acts as a switch between the early synthesis of highly spliced RNAs and the later synthesis of unspliced and singly spliced RNAs. Nef acts as a down-regulator of the number of CD4 receptors on the surface of the infected cell.²⁶

Translations of the unspliced RNA by the ribosomes produce the polyproteins Gag and Gag-Pol. These polyproteins are transported to the plasma membrane with two molecules of viral RNA. They assemble together with the envelope protein to form an immature virus particle that is released from the cell by budding from the cell surface. To become infectious, the virion has to pass through a maturation process where the enzyme HIV protease cleaves the polyproteins into functional enzymes and structural proteins. The mature HIV virion is now ready to infect a new cell and start a new replication cycle.^{15,22}

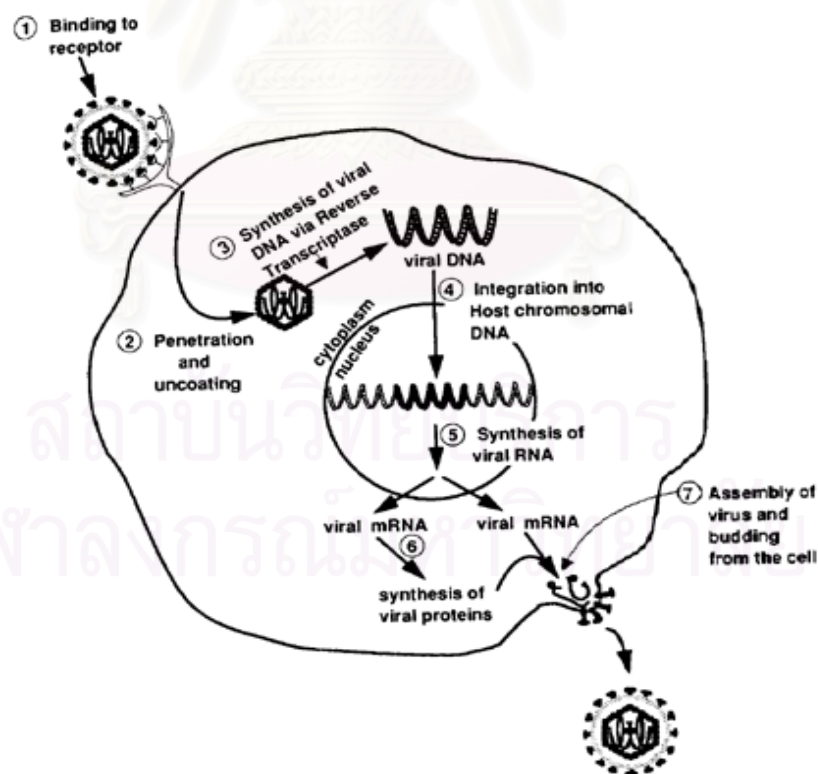


Figure 1.2 A schematic representation of the replication cycle of HIV.²⁷

1.4.HIV-1 Protease (HIV-1 PR)

The HIV-1 protease (HIV-1 PR) was postulated to belong to the family of aspartic acid protease based on the identification of the Asp-Thr-Gly catalytic triad.²⁸ Other members of this family, including the endogenous enzyme Pepsin, Cathepsin D and Renin, are single chain proteins of over 300 residues folded into two domains; each of which supplies a catalytic triad Asp-(Ser/Thr)-Gly. HIV-1 PR is much smaller at only 99 residues in length and possesses only a single Asp-Thr-Gly triad so a homodimeric structure was proposed.²⁹ Both of these conjectures were later confirmed by X-ray crystallographic analysis of the apoenzyme^{30,31} and of a HIV-1 PR-inhibitor complex.^{32,33}

Some general features of the HIV-1 protease structure can be described (Figure 1.3); (i) the two monomers are identical and form a C_2 -symmetric elliptical-shaped enzyme. (ii) The N- and C- terminal of each monomer are juxtaposed in a four-stranded β -sheet that serves to hold the dimer together (the dimer interface). (iii) Each monomer has a hydrophobic core consisting of two loops, one of which includes the active site aspartic acid. (iv) The dimers come together to create an extended substrate-binding cleft capable of interacting with a minimum of seven consecutive amino acids in the substrate. (v) Each monomer contributes a flexible flap that folds down to make important contacts with the bound substrate.³⁴

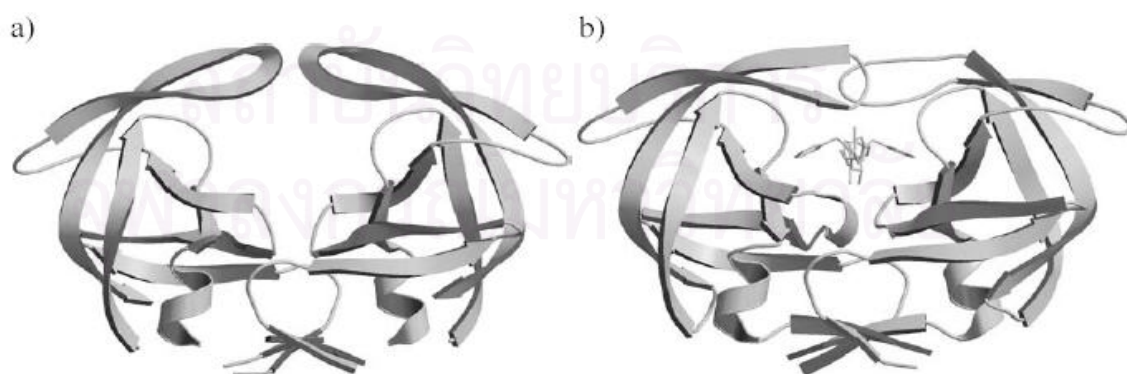


Figure 1.3 Ribbon drawing of (a) apo- and (b) inhibited HIV protease showing the relatively open and closed position of the flaps (top of images).^{29,32}

The HIV-1 PR processes the Gag and Gag-Pol polyproteins proteolytically at specific cleavage sites as shown in Figure 1.4.^{35,36} The HIV-1 PR is specific for cleavage of these sites *in vivo*, although the general sequence homologies among these are small.

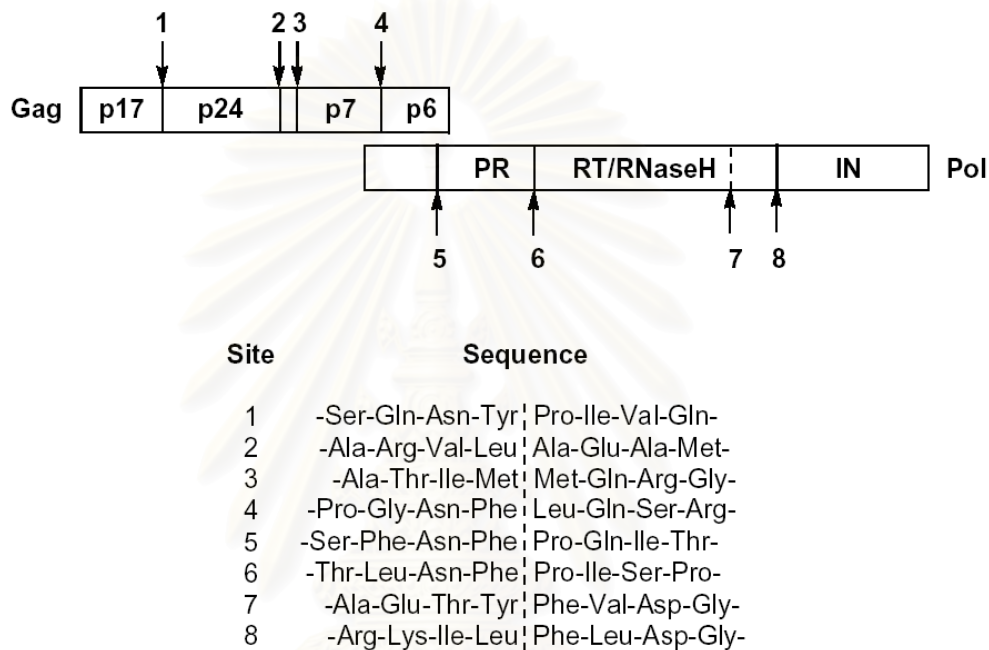


Figure 1.4 Cleavage site of HIV pretease in the Gag and Pol polyproteins.^{35,36}

The HIV-1 PR cleaves a variety of peptide bonds in the viral polyproteins during the course of its action to produce the individual proteins of the mature virus. The active site constellation of two proximal carboxyl group from the Asp25/Asp25' residues (one from each monomer). Several studies, experimental and *ab initio* calculations, of the protein cleavage mechanism have been performed. A schematic representation of the mechanism is outlined in Figure 1.5.³⁷⁻⁴¹ Hydration of the amide carbonyl group, with a water molecule accommodated between the two side-chains of the aspartic acid residues 25/25', give a putative tetrahedral intermediate that is suggested to be an approximate representation of the transition state of the proteolytic reaction.

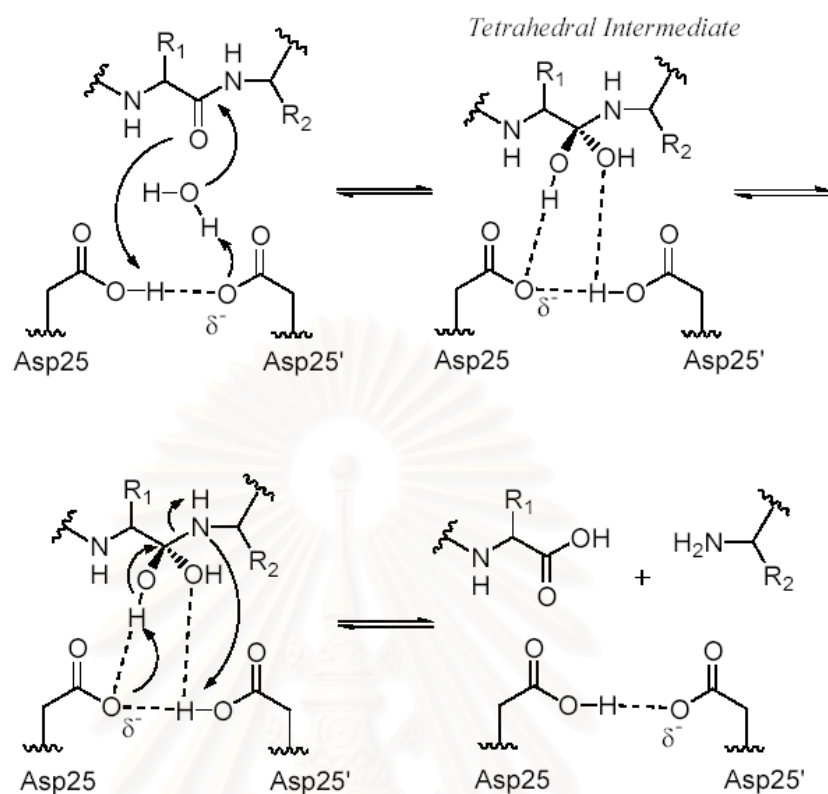


Figure 1.5 Schematic representation of the catalytic mechanism of aspartic acid protease.³⁸

To date, several hundred crystal structures have been solved for various HIV protease/inhibitor complexes – a testimony to the importance placed on structural information in the process of inhibitor design. Structural comparison of the inhibitor complexes reveals certain common features (Figure 1.6).^{31,36,42-47} The inhibitor and enzyme make a pattern of complementary hydrogen bonds between their backbone atoms. The enzyme also contains a number of well-defined pockets, or subsites, in its active site region into which inhibitor side-chains protrude, resulting in tight binding interaction between enzyme and inhibitor. Since a similar pattern of hydrogen bonds is believed to reside in the pattern of largely nonpolar subsite interactions between inhibitor and enzyme side-chain atoms. Overall, knowledge of the structure and function of HIV-1PR and its relationship to other aspartic proteinases has led to the successful development of a wide variety of potent and chemically diverse inhibitors.

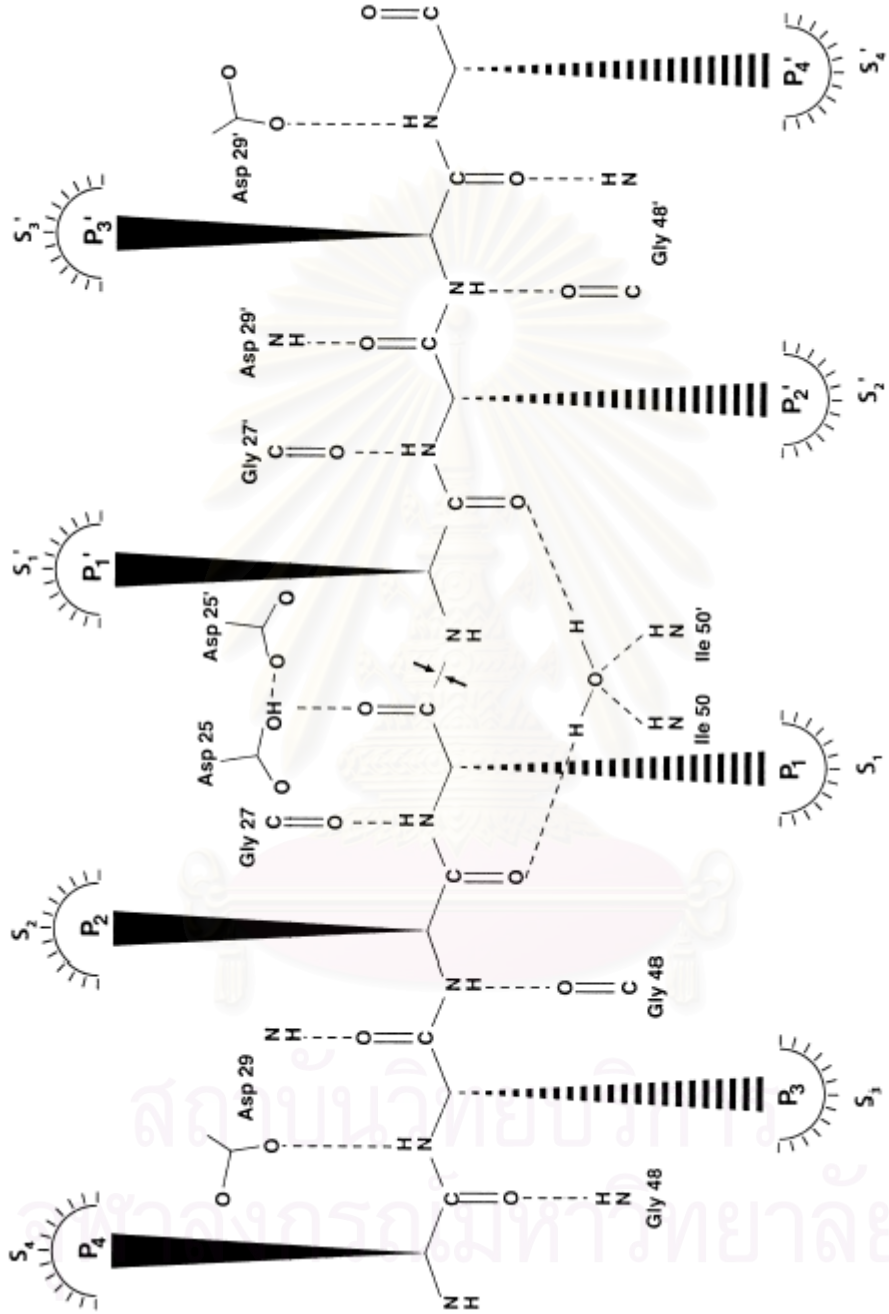


Figure 1.6 General scheme of active site interaction in HIV PR with a putative substrate or peptide-based inhibitor.⁴⁷

1.5. HIV-1 Protease Inhibitors

HIV protease was first suggested as a potential target for AIDS therapy by Kramer et al. after it was shown that a frameshift mutation in the protease region of the pol-gene prevented cleavage of the Gag polyprotein precursor, which is essential for the maturation of the HIV particles.⁴⁸ Blockage of HIV protease leads to the formation of immature non-infectious virions.⁴⁹ Compounds, having the ability to inhibit this protease have been studied intensively during the last decade and numerous reports of potent HIV-1 protease inhibitors have been published.^{35,47,50-53}

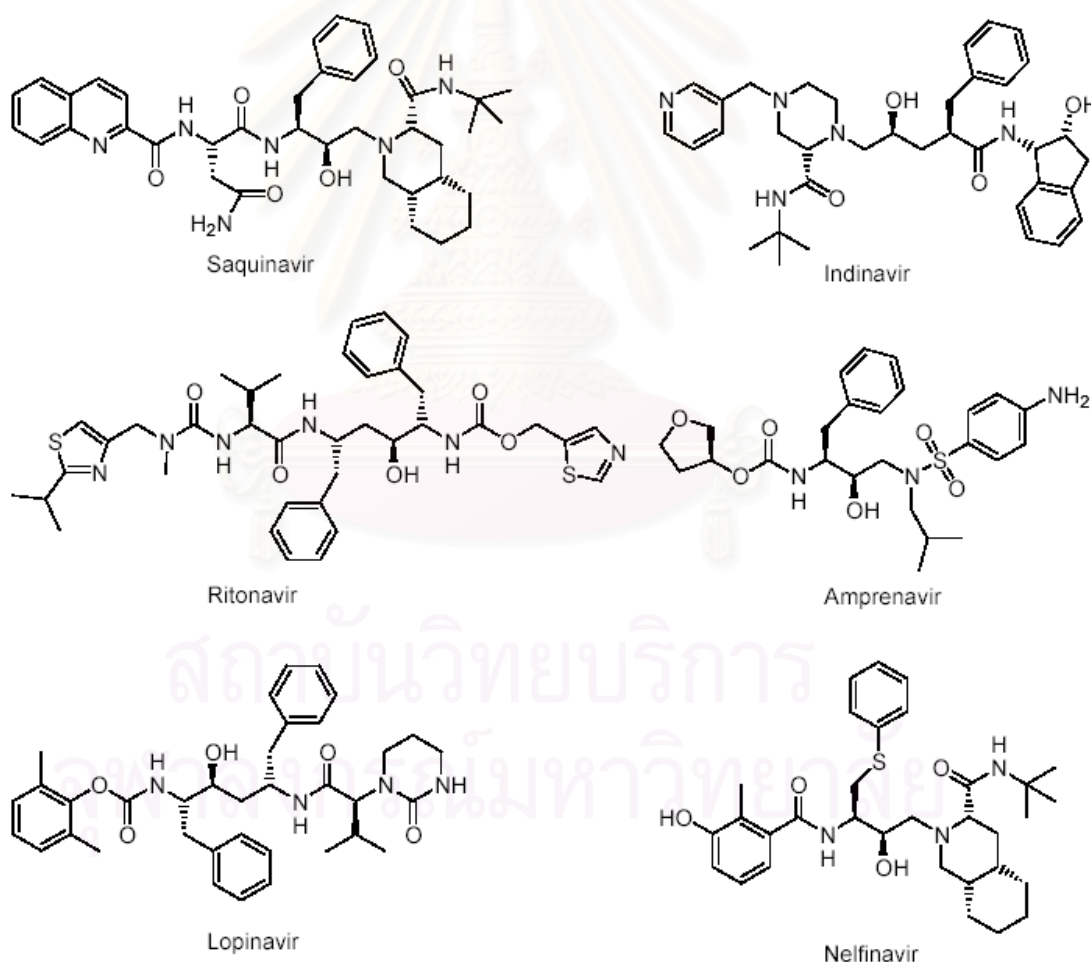


Figure 1.7 Six clinically FDA approved protease inhibitors (FDA stands for Food and Drug Administration).

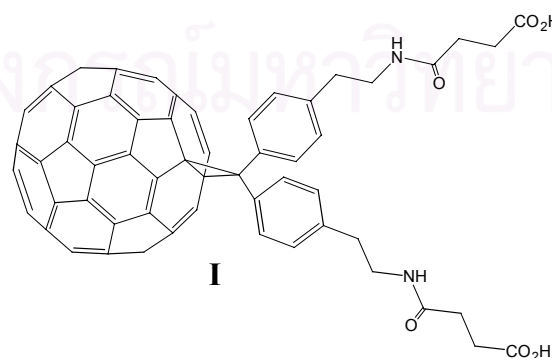
Saquinavir was the first approved protease inhibitor and has been in clinical use since 1995.⁵⁴ Presently, there are six clinically approved protease inhibitors which are peptide-analogue inhibitors and have excellent oral bioavailability (Figure 1.7). Although the inhibitors on the market are highly selective, however, they induce side effects such as lipodystrophy, hyperlipidaemia, insulin resistance, and emergence of resistant mutants upon prolonged use.⁵⁵⁻⁵⁸ Therefore there will probably be a constant demand for new HIV protease inhibitors.

Many groups have been pursuing a different nonpeptide template for the development of HIV protease inhibitors.⁵⁹ Friedman et al. discovered that water-soluble methanofullerene derivative was a competitive inhibitor of HIV-1 protease by theoretical approach.⁶⁰ Then they identified fullerene (C₆₀) derivatives with K_i value, the binding constant of the inhibitor to the enzyme, in the micromolar to nanomolar range.⁶¹

1.6. Fullerene (C₆₀) Derivatives

1.6.1 Introduction

Interesting biological properties of fullerenes derivatives have been demonstrated in the last few years. Specific biological applications of fullerenes are discovered in the following order: enzymatic inhibition and anti-HIV activity, DNA cleavage and photodynamic therapy, neuroprotective properties, antiapoptotic activity, antibacterial activity and miscellaneous uses.⁶² Of particular relevance to the present work was the discovery by Friedman et al. [60] that a water-soluble methanofullerene derivative **I** was a competitive inhibitor of HIV-1 protease with a K_i of 5.3 μM .



1.6.2. Enzymatic inhibition and anti-HIV activity

Based on molecular modeling, Friedman et al. anticipated that a C₆₀ molecule fit nicely into the hydrophobic cavity of the HIV-1 protease. Using the program DOCK3 and MINDOCK they were able to fit a minimized structure of C₆₀ into the enzyme active site.⁶¹ Good Van der Waals interactions with the hydrophobic surface resulted when the C₆₀ was squarely in the center of the cavity. The complexes generated via computer models suggest that the virucidal activity of C₆₀ derivatives results from a snug fit of the fullerene into the active site of the HIV-1 protease, thereby removing at least 298 Å² of primarily nonpolar surface from solvent exposure and driving ligand/protein association. The free energy of binding was estimated to be 8-12 kcal/mol, corresponding to a dissociation constant K_d of 10⁻⁶-10⁻⁹ M. In this model, interaction of the catalytic aspartate residues of the enzyme with the fullerene was not specifically taken into account. A computer-minimized inclusion complex of the water-soluble C₆₀ derivative **I**, prepared in three steps from C₆₀ by Sijbesma et al.⁶³, again positions the fullerene in the center of the hydrophobic cavity at the enzyme active site. Experimentally, fullerene **I** was found to be a competitive inhibitor of recombinant affinity-purified HIV-1 protease, with a K_i value of 5.3 μM. For comparison, the best peptide-based protease inhibitors are effective in the subnanomolar range, while nonpeptide inhibitors are effective in the high nanomolar range.

Fullerene derivative **I** was tested by Schinazi et al.⁶⁴ for antiviral activity in cells acutely and chronically infected with HIV-1 and in cell-free systems. In human peripheral blood mononuclear cells (PBMC) infected with HIV type ILA-I, the antiviral activity (EC₅₀: effective concentration causing a 50% response, the lower the value the greater the toxicity) of **I** was also active against chronically infected H9 cells and human PBMC acutely infected with HIV-2_{ROD}. While the anti-AIDS drug 3'-azido-3'-deoxythymidine (AZT) has significantly greater activity against acutely infected cell, it is not active in chronically infected H9 cells. When cell-free HIV-1 was incubated with **I** at concentrations of 5-25 μM, virus infectivity was reduced by more than 95% relative to controls, demonstrating that **I** interacts directly with the virus. Since agents used to treat viruses frequently lead to the development of drug

resistant viral strains, fullerene **I** was tested against AZT in acutely infected primary human lymphocytes. The activity of **I** was the same in both cases, indicating no cross-resistance between **I** and AZT. This suggests that combination therapy using water-soluble fullerene derivatives and AZT might be fruitful.

Eleven additional C_{60} derivatives synthesized at New York University by Wilson, Schuster, and co-workers were tested as DMSO/water emulsions against human PBMC infected with HIV-1.⁶⁵ All but one of these showed antiviral activity (EC_{50}) in the low micromolar range. Although the mechanism of anti-HIV activity of these compounds has not been established using cell-free assays, it appears that anti-HIV activity and low toxicity seem to be general properties of many types of C_{60} derivatives, although the pattern of activity may vary from compound to compound. It will also be interesting to see if these fullerenes have activity against other viruses.

The advantages of C_{60} derivatives for blocking the active site of HIV-1 protease over those known in the art are twofold. First of all, the C_{60} derivatives represent nonpeptide-based compounds that, through careful modeling, result in effective, tightly binding HIV-1 protease inhibitors. Second, the buckminsterfullerenes present a rigid, conformationally restricted scaffold upon which to mount nonpolar chemical moieties for establishing a hydrophobic interaction between the nonpolar active site surface of HIV-1 protease and the C_{60} surface. Because of the steric bulk of C_{60} and its complementarity to the active site surface, there are severe limitations to the orientations it can adopt within the active site. Essentially, the principal degree of freedom of a C_{60} derivative within the active site is rotation around the central axis of symmetry. All of these attributes simplify the problem of predicting the binding modes of various derivatives.

1.7. Objectives of the Present Study

This work is part of the structure based drug design research project aimed at the discovery of novel and selective HIV-1 protease inhibitors, with the study of physical properties of compounds. The specific objectives of this study are:

- (i) To study the structure and orientation of the functional groups of C_{60} derivatives.
- (ii) To study effects of the functional groups on the changes of molecular geometries and distribution of electron on the surface of C_{60} .



สถาบันวิทยบริการ
จุฬาลงกรณ์มหาวิทยาลัย

CHAPTER 2

THEORY

2.1. Quantum Mechanics

2.1.1. Introduction

Quantum mechanics (QM) is the correct mathematical description of the behavior of electrons and thus of chemistry. In theory, QM can predict any property of an individual atom or molecule exactly. In practice, the QM equations have only been solved exactly for one electron systems. A myriad collection of methods has been developed for approximating the solution for multiple electron systems. These approximations can be very useful, but this requires an amount of sophistication on the part of the researcher to know when each approximation is valid and how accurate the results are likely to be.

Two equivalent formulations of QM were devised by Schrödinger and Heisenberg. However, the uncertainty principle of Heisenberg, which is authentically the limitation of the obtained microscopic information of a system, seems to be essential as the consequences of the wave-particle duality. Here, only the Schrödinger form, since it is the basis for nearly all computational chemistry methods, has been briefly reviewed.

The Schrödinger equation is

$$\hat{H}\Psi = E\Psi \quad (2.1)$$

where \hat{H} is the Hamiltonian operator, Ψ the wave function, and E the energy. In the language of mathematics, an equation of this form is called an eigen equation. Ψ is

then called the eigenfunction and E an eigenvalue. The operator and eigenfunction can be a matrix and vector, respectively, but this is not always the case.

The wave function Ψ is a function of the electron and nuclear positions. As the name implies, this is the description of an electron as a wave. This is a probabilistic description of electron behavior. As such, it can describe the probability of electrons being in certain locations, but it cannot predict exactly where electrons are located. The wave function is also called a probability amplitude because it is the square of the wave function that yields probabilities. This is the only rigorously correct meaning of a wave function. In order to obtain a physically relevant solution of the Schrödinger equation, the wave function must be continuous, single-valued, normalizable, and antisymmetric with respect to the interchange of electrons.

For molecule, the Hamiltonian operator \hat{H} is, in general,

$$\begin{aligned}\hat{H} &= -\sum_i \frac{\hbar^2}{2m_e} \nabla_i^2 + \sum_k \frac{\hbar^2}{2m_k} \nabla_k^2 - \sum_i \sum_k \frac{e^2 Z_k}{r_{ik}} + \sum_{i < j} \frac{e^2}{r_{ij}} + \sum_{k < l} \frac{e^2 Z_k Z_l}{r_{kl}} \\ &= T_N + T_e + V_{ne} + V_{ee} + V_{NN}\end{aligned}\quad (2.2)$$

where i and j run over electrons, k and l run over nuclei, \hbar is Planck's constant divided by 2π , m_e is the mass of the electron, m_k is the mass of nucleus K , ∇^2 is the Laplacian operator, e is the charge on the electron, Z is an atomic number, and r_{ab} is the distance between particles a and b . T_N denotes nuclear kinetic, T_e electron kinetic, V_{ne} nuclear-electron attraction, V_{ee} electron-electron repulsion and V_{NN} nuclear-nuclear repulsion. Note that Ψ is thus a function of $3n$ coordinates where n is the total number of particles (nuclei and electrons), e.g., the x , y , and z Cartesian coordinates specific to each particle.

In currently available software, the Hamiltonian above is nearly never used. The problem can be simplified by separating the nuclear and electron motions. This is

called the Born-Oppenheimer approximation. It is convenient to decouple these two motions, and compute electronic energies for fixed nuclear positions. That is, the nuclear kinetic energy term is taken to be independent of the electrons, correlation in the attractive electron–nuclear potential energy term is eliminated, and the repulsive nuclear–nuclear potential energy term becomes a simply evaluated constant for a given geometry. Thus, the electronic Schrödinger equation is taken to be

$$(T_e + V_{ne} + V_{ee}) \Psi_{\text{el}}(\mathbf{q}_i; \mathbf{q}_k) = E_{\text{el}} \Psi_{\text{el}}(\mathbf{q}_i; \mathbf{q}_k) \quad (2.3)$$

where the subscript ‘el’ emphasizes the invocation of the Born–Openheimer approximation and the electronic coordinates \mathbf{q}_i are independent variables but the nuclear coordinate \mathbf{q}_k are parameters. The eigenvalue of the electronic Schrödinger equation is called the ‘electronic energy’.

Once a wave function has been determined, any property of the individual molecule can be determined. This is done by taking the expectation value of the operator for that property, denoted with angled brackets $\langle \rangle$. For example, the energy is the expectation value of the Hamiltonian operator given by

$$\langle E \rangle = \int \Psi^* \hat{H} \Psi \quad (2.4)$$

For an exact solution, this is the same as the energy predicted by the Schrödinger equation. For an approximate wave function, this gives an approximation of the energy. This is called variational energy because it is always greater than or equal to the exact energy. By substituting different operators, it is possible to obtain different observable properties, such as the dipole moment or electron density. Properties other than the energy are not variational, because only Hamiltonian is used to obtain the wave function in the widely used computational chemistry methods.

Another way of obtaining molecular properties is to use the Hellmann-Feynman theorem. This theorem states that the derivative of energy with respect to some property P is given by

$$\frac{dE}{dP} = \left\langle \frac{\partial \hat{H}}{\partial P} \right\rangle \quad (2.5)$$

This relationship is often used for computing electrostatic properties. Not all, but variation methods approximation methods obey the Hellmann-Feynman theorem. Some of the variational methods were also discussed in this chapter.

2.1.2. *Ab initio* Methods

The term *ab initio* is Latin for “from the beginning”. This name is given to computations that are derived directly from theoretical principles with no inclusion of experimental data. This is an approximate quantum mechanical calculation. The approximations made are usually mathematical approximations, such as using a simpler functional form for a function or finding an approximate solution to a differential equation.

All molecular wave functions are approximate; some are just more approximate than others. We can solve the Schrödinger equation exactly for the hydrogen atom but not even, despite what many textbooks say, for the hydrogen molecule ion, H_2^+ .

2.1.2.1. Hartree-Fock Theory

The orbital model is a very attractive one, and it can obviously be used to successfully model atoms, molecules and the solid state because it is now part of the language of elementary descriptive chemistry. The essence of this Hartree-Fock (HF) model is to solve the electronic Schrödinger equation for a single electron moving in a potential that averages out the effects of the nuclei and the remaining

electrons. Electron repulsion is certainly not taken to be zero, but the HF model cannot treat the finer details of electronic structure theory that are caused by the instantaneous repulsion between electrons. So, dispersion forces cannot be treated at the HF level of theory.

The basic physical idea of HF theory is a simple one and can be tied in very nicely with the electron density. The physical significance of the density function $\rho_i(\mathbf{r}, s)$; $\rho_i(\mathbf{r}, s) d\tau ds$ gives the chance of finding any electron simultaneously in the spin-space volume elements $d\tau$ and ds , with the other electrons anywhere in space and with either spin. $P(\mathbf{r}) d\tau$ gives the corresponding chance of finding any electron with either spin in the spatial volume element $d\tau$.

The vast majority of known molecules are organic, totally lacking in symmetry and having singlet electronic ground states which can be written in the language of elementary descriptive chemistry as configurations $\psi_A^2 \psi_B^2 \dots \psi_M^2$.

If there are m doubly occupied molecular orbitals, and the number of electrons is $2m$. In the original Hartree model, the many-electron wave function was written as a straightforward product of one-electron orbital ψ_A , ψ_B and so on

$$\psi_e(\mathbf{r}_1, s_1, \mathbf{r}_2, s_2, \dots, \mathbf{r}_{2m}, s_{2m}) = \psi_A(\mathbf{r}_1)\alpha(s_1)\psi_A(\mathbf{r}_2)\beta(s_2) \dots \psi_M(\mathbf{r}_{2m})\beta(s_{2m}) \quad (2.6)$$

The simplest antisymmetric combination of molecular orbitals (MOs) is a matrix determinant. A HF wave function is constructed by assigning electrons to molecular orbitals in pairs of opposite spin, and then forming a determinant using two spin functions α and β . For molecule containing $2m$ electrons, the wave function is referred to as a 'Slater determinant', and takes the form:

$$\psi_e(\mathbf{r}_1, s_1, \mathbf{r}_2, s_2, \dots, \mathbf{r}_{2m}, s_{2m}) = \begin{vmatrix} \psi_A(\mathbf{r}_1)\alpha(s_1) & \psi_A(\mathbf{r}_1)\beta(s_1) & \dots & \psi_M(\mathbf{r}_1)\beta(s_1) \\ \psi_A(\mathbf{r}_2)\alpha(s_2) & \psi_A(\mathbf{r}_2)\beta(s_2) & \dots & \psi_M(\mathbf{r}_2)\beta(s_2) \\ \dots & \dots & \dots & \dots \\ \psi_A(\mathbf{r}_{2m})\alpha(s_{2m}) & \psi_A(\mathbf{r}_{2m})\beta(s_{2m}) & \dots & \psi_M(\mathbf{r}_{2m})\beta(s_{2m}) \end{vmatrix} \quad (2.7)$$

At the minimum, each electron moves in an average field due to the other electrons and the nuclei. Small variations in the form of the orbitals at this point do not change the energy or the electric field.

Linear combinations of atomic orbitals (LCAO)

Although there is no exact analytical solution to the time-independent molecular Schrödinger equation for systems containing more than one electron, approximate solutions can be obtained using standard numerical techniques. The approach of all *ab initio* techniques is to build the total wave function from a ‘basis’ set of mathematical functions capable of reproducing critical properties of the system. An individual molecular orbital may then be expressed as

$$\phi_i(\mathbf{r}) = \sum_{\mu=1}^N c_{\mu i} \chi_{\mu}(\mathbf{r}), \quad (2.8)$$

where $\chi_{\mu}(\mathbf{r})$ are the basis functions, and the coefficients $c_{\mu i}$ are adjustable parameters. For a molecular wavefunction, the electronic orbitals of the constituent atoms form a natural set of basis functions. These atomic orbitals can in turn be represented by different types of mathematical functions. A highly accurate set of atomic orbitals (Slater-type orbitals or STOs) are based on hydrogenic wavefunctions having the form

$$\chi_{STO}(\mathbf{r}) \approx C e^{-a r}. \quad (2.9)$$

Exponential functions are not well suited to numerical manipulation, so most electronic structure calculations approximate STOs with a linear combination of Gaussian-type functions,

$$\chi_{STO-NG}(\mathbf{r}) \approx \chi_{\mu} = \sum_{\nu} d_{\mu\nu} e^{-\alpha_{\nu} r^2}, \quad (2.10)$$

where $d_{\mu\nu}$ and α_ν are adjustable parameters. As can be seen from Fig. 2.1, Gaussian-type functions provide reasonable approximations of STOs, except at very small or very large electron-nucleus separations.

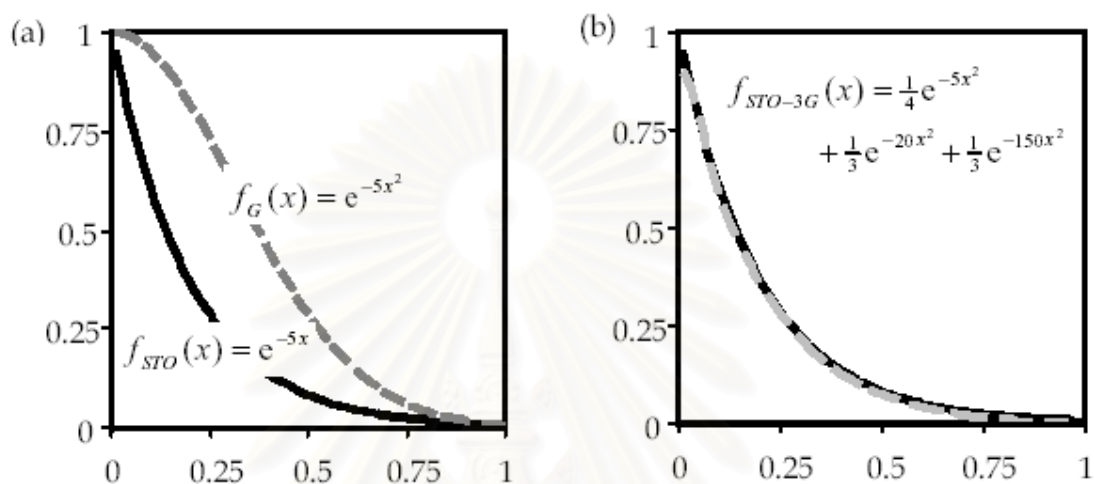


Figure 2.1 (a) Comparison of exponential and Gaussian functions. (b) Comparison of the same exponential function and a sum of three Gaussians.

Linear combinations of ‘primitive’ Gaussian functions are referred to as ‘contracted’ Gaussians. Standard *ab initio* software packages offer a choice of basis sets containing contracted Gaussians optimized to reproduce the chemistry of a large range of molecular systems.

The Roothan–Hall equation

From a method for constructing a determinantal wave function from a set of LCAO-MOs. It remains now to define a method to determine the MO expansion coefficients $c_{\mu i}$ (Eq. 2.8) which optimize the molecular wave function for a particular system. The variational nature of the model guarantees that the energy eigenvalue solution for any approximate wave function is always greater than the energy obtained using the exact wave function. It follows that the set of coefficients that minimize the

energy of the resultant wavefunction will give the best approximation to the exact wave function from a chosen basis set.

The variational constraint leads to a set of algebraic equations (Roothan-Hall) for $c_{\mu i}$, expressed in matrix form as

$$\mathbf{FC} = \mathbf{SC}\boldsymbol{\varepsilon} \quad (2.11)$$

where

- \mathbf{C} is the matrix of MO expansion coefficient;
- \mathbf{F} is the Fock matrix, which is the sum of a term representing the energy of a single electron in the field of the bare atomic nuclei and a term describing electron–electron repulsion within an averaged field of electron density;
- \mathbf{S} is a matrix describing the overlap of molecular orbitals; and
- $\boldsymbol{\varepsilon}$ is a diagonal matrix containing the one-electron energies of each molecular orbital χ_{μ} .

Since the terms within the Fock matrix \mathbf{F} depend upon the electron density, which in turn, depends upon molecular wave function defined by the matrix of MO expansion coefficients \mathbf{C} , the Roothan-Hall equations are nonlinear, and must be solved by an iterative procedure termed the ‘self-consistent field’ (SCF) method. Upon convergence of the SCF method, the minimum-energy MOs produce the electric field which generate the same orbitals (hence, the self-consistency).

2.1.2.2. Basis Sets

In general, a basis set is an assortment of mathematical functions used to solve a differential equation. In quantum chemical calculations, the term ‘basis set’ is applied to a collection of contracted Gaussians representing atomic orbitals, which are optimized to reproduce the desired chemical properties of a system.

Standard *ab initio* software packages generally provide a choice of basis sets that vary both in size and in their description of the electrons in different

atomic orbitals. Larger basis sets include more and a greater range of basis functions. Therefore, larger basis sets can better refine the approximation to the ‘true’ molecular wave function, but require correspondingly more computer resources. Alternatively, accurate wave functions may be obtained from different treatments of electrons in atoms. For instance, molecules containing large atoms ($Z > 30$) are often modeled using basis sets incorporating approximate treatments of inner-shell electrons which account for relativistic phenomena.

‘Minimal’ basis sets contain the minimum number of AO basis functions needed to describe each atom (*e.g.*, 1s for H and He; 1s, 2s, 2px, 2py, 2pz for Li to Ne). An example of a minimal basis set is STO-3G, which uses three Gaussian-type functions (3G) per basis function to approximate the atomic Slater-type orbitals (*see* Fig. 2.1b). Although minimal basis sets are not recommended for consistent and accurate predictions of molecular energies, their simple structure provides a good tool for visualizing qualitative aspects of chemical bonding. Improvements on minimal basis sets are described below and illustrated in Fig. 2.2.

Split valence basis sets

In split valence basis sets, additional basis functions (one contracted Gaussian plus some primitive Gaussians) are allocated to each valence atomic orbital. The resultant linear combination allows the atomic orbitals to adjust independently for a given molecular environment. Split valence basis sets are characterised by the number of functions assigned to valence orbitals. ‘Double zeta’ basis sets use two basis functions to describe valence electrons, ‘triple zeta’ use three functions, and so forth. Basis sets developed by Pople and coworkers⁶⁶ are denoted by the number of Gaussian functions used to describe inner and outer shell electrons. Thus ‘6-31G’ describes an inner shell atomic orbital with a contracted Gaussian composed of six primitive Gaussians, an inner valence shell with a contracted Gaussian composed of three primitives, and an outer valence shell with one primitive. Other split-valence sets include 3-21G, 4-31G, and 6-311G.

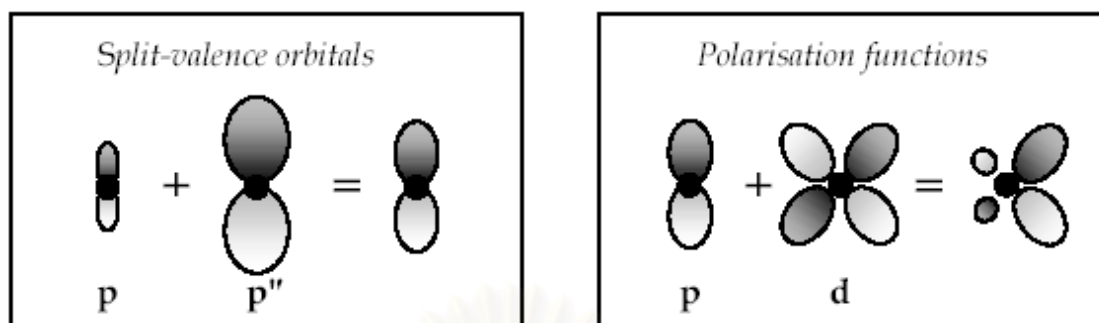


Figure 2.2 Basis set improvements.

Polarized basis sets

Polarization functions can be added to basis sets to allow for non-uniform displacement of charge away from atomic nuclei, thereby improving descriptions of chemical bonding. Polarisation functions describe orbitals of higher angular momentum quantum number than those required for the isolated atom (*e.g.*, *p*-type functions for H and He, and *d*-type functions for atoms with $Z > 2$), and are added to the valence electron shells. For example, the 6-31G(d) basis set is constructed by adding six *d*-type Gaussian primitives to the 6-31G description of each non-hydrogen atom. The 6-31G(d,p) is identical to 6-31G(d) for heavy atoms, but adds a set of Gaussian *p*-type functions to hydrogen and helium atoms. The addition of *p*-orbitals to hydrogen is particularly important in systems where hydrogen is a bridging atom.

Diffuse basis sets

Species with significant electron density far removed from the nuclear centers (*e.g.*, anions, lone pairs and excited states) require diffuse functions to account for the outermost weakly bound electrons. Diffuse basis sets are recommended for calculations of electron affinities, proton affinities, inversion barriers and bond angles in anions. The addition of diffuse *s*- and *p*-type Gaussian functions to non-hydrogen atoms is denoted by a plus sign—as in ‘3-21+G’. Further addition of diffuse functions to both hydrogen and larger atoms is indicated by a double plus.

2.1.3. Semi-empirical Methods

Semi-empirical methods increase the speed of computation by using approximations of *ab initio* techniques (*e.g.*, by limiting choices of molecular orbitals or considering only valence electrons) which have been fitted to experimental data (for instance, structures and formation energies of organic molecules). Until recently, the size of many energetic molecules placed them beyond the scope of *ab initio* calculations. However, semi-empirical methods have been calibrated to typical organic or biological systems and tend to be inaccurate for problems involving hydrogen-bonding, chemical transitions or nitrated compounds.^{67, 68}

Several semi-empirical methods are available and appear in commercially available computational chemistry software packages such as HyperChem⁶⁹ and Chem3D⁷⁰. Some of the more common semi-empirical methods can be grouped according to their treatment of electron-electron interactions.⁶⁹

The extended Hückel method

Extended Hückel calculations neglect all electron-electron interactions, making them computationally fast but not very accurate. The model provides a qualitative estimate of the shapes and relative energies of molecular orbitals, and approximates the spatial distribution of electron density. Extended Hückel models are good for chemical visualisation and can be applied to ‘frontier orbital’ treatments of chemical reactivity.

Neglect of differential overlap (NDO)

NDO models neglect some but not all of the electron-electron interactions. The Hartree-Fock Self-Consistent Field (HF-SCF) method is used to solve the Schrödinger equation with various approximations:

- *Complete NDO (CNDO)* - the product of two atomic orbitals on different atoms is set equal to zero everywhere.

- *Intermediate NDO (INDO)* - differential overlap between orbitals on the same atom are taken into account in the description of electron-electron repulsion, but differential overlap between orbitals on different atoms is neglected.
- *Modified INDO, version 3 (MINDO/3)* - reparameterized version of INDO optimized to predict good enthalpies of formation and reasonable molecular geometries for a range of chemical systems, in particular, sulphur-containing compounds, carbocations, and polynitro organic compounds.⁷¹
- *Zerner's INDO methods (ZINDO/1 and ZINDO/S)* - Michael Zerner.s (University of Florida) versions of INDO developed for use with molecular systems containing transition metals.

Neglect of diatomic differential overlap (NDDO)

NDDO methods build upon the INDO model by including the overlap density between two orbitals on one atom interacting with the overlap density between two orbitals on the same or another atom.

- *Modified NDO (MNDO)* - a method introduced to correct some of the problems associated with MINDO/3. In general, MNDO overestimates activation barriers to chemical reactions.
- *Austin Method, version 1 (AM1)* - a reparameterised version of MNDO which includes changes in nuclear repulsion terms.⁷²
- *Parameterisation Model, version 3 (PM3)* - a second reparameterisation of MNDO, functionally similar to AM1, but with some significant improvements. The PM3 Hamiltonian contains essentially the same elements as that for AM1, but the parameters for the PM3 model were derived using an automated parameterization procedure.⁷³ By contrast, many of the parameters in AM1 were obtained by applying chemical knowledge and 'intuition'. As a consequence, some of the parameters have significantly different values in AM1 and PM3, even though both methods use the same functional form and they both predict various thermodynamic and structural properties to approximately the same level of accuracy. Some problems do remain with PM3. One of the most important of these is the rotational barrier of the amide bond, which is much too low and in some cases almost non-existent. This problem can

be corrected through the use of an empirical torsional potential. There has been considerable debate over the relative merits of the AM1 and PM3 approaches to parametrization.

2.1.4. Density Functional Theory

Density functional theory (DFT) has become very popular in recent years. This is justified based on the pragmatic observation that it is less computationally intensive than other methods with similar accuracy. This theory has been developed more recently than other *ab initio* methods. Because of this, there are classes of problems which are not yet explored with this theory, making it all the more crucial to test the accuracy of the method before applying it to unknown systems.

2.1.4.1. Basic Theory

The premise behind DFT is that the energy of a molecule can be determined from the electron density instead of a wave function. This theory originated with a theorem by Hohenberg and Kohn⁷⁴ that stated this was possible. The original theorem applied only to finding the ground-state electronic energy of a molecule. A practical application of this theory was developed by Kohn and Sham who formulated a method similar in structure to the Hartree-Fock method.

In this formulation, the electron density is expressed as a linear combination of basis functions similar in mathematical form to HF orbitals. A determinant is then formed from these functions, called Kohn-Sham orbitals. It is the electron density from this determinant of orbitals that is used to compute the energy. This procedure is necessary because Fermion systems can only have electron densities that arise from an antisymmetric wave function. There has been some debate over the interpretation of Kohn-Sham orbitals. It is certain that they are not mathematically equivalent to either HF orbitals or natural orbitals from correlated calculations. However, Kohn-Sham orbitals do describe the behavior of electrons in a molecule, just as the other orbitals mentioned do. DFT orbital eigenvalues do not match the energies obtained from photoelectron spectroscopy experiments as well as HF orbital energies

do. The questions still being debated are how to assign similarities and how to physically interpret the differences.

A density functional is used to obtain the energy for the electron density. A functional is a function of a function, in this case, the electron density. The exact density functional is not known. Therefore, there is a whole list of different functionals that may have advantages or disadvantages. Some of these functionals were developed from fundamental quantum mechanics and some were developed by parameterizing functions to best reproduce experimental results. Thus, there are in essence *ab initio* and semiempirical versions of DFT. DFT tends to be classified either as an *ab initio* method or in a class by itself.

The advantage of using electron density is that the integrals for Coulomb repulsion need be done only over the electron density, which is a three-dimensional function, thus scaling as N^3 . Furthermore, at least some electron correlation can be included in the calculation. These results in faster calculations than HF calculations (which scale as N^4) and computations those are a bit more accurate as well. The better DFT functionals give results with an accuracy similar to that of and MP2 calculation.

Density functionals can be broken down into several classes. The simplest is called the $X\alpha$ method. This type of calculation includes electron exchange but not correlation. It was introduced by J. C. Slater, who in attempting to make an approximation to Hartree-Fock unwittingly discovered the simplest form of DFT. The $X\alpha$ method is similar in accuracy to HF and sometimes better.

The simplest approximation to the complete problem is one based only on the electron density, called a local density approximation (LDA). For high-spin systems, this is called the local spin density approximation (LSDA). LDA calculations have been widely used for band structure calculations. Their performance is less impressive for molecular calculations, where both qualitative and quantitative errors are encountered. For example, bonds tend to be too short and too strong. In recent years, LDA, LSDA, and VWN (the Vosko, Wilks, and Nusair functional) have become synonymous in the literature.

A more complex set of functionals utilizes the electron density and its gradient. These are called gradient-corrected methods. There are also hybrid

methods that combine functionals from other methods with pieces of a Hartree-Fock calculation, usually the exchange integrals.

In general, gradient-corrected or hybrid calculations give the most accurate results. However, there are a few cases where $X\alpha$ and LDA do quite well. LDA is known to give less accurate geometries and predicts binding energies significantly too large. The current generations of hybrid functionals are a bit more accurate than the present gradient-corrected techniques.

2.1.4.2. Local density Methods

In the *Local Density Approximation* (LDA) it is assumed that the density locally can be treated as a uniform electron gas, or equivalently that the density is slowly varying function. The exchange energy for a uniform electron gas is given by the Dirac formula.

$$E_x^{\text{LDA}}[\rho] = -C_x \int \rho^{4/3}(\mathbf{r}) d\mathbf{r} \quad (2.12)$$

$$\varepsilon_x^{\text{LDA}}[\rho] = -C_x \rho^{1/3} \quad (2.13)$$

In the more general case, where the α and β densities are not equal, LDA (where the sum of the α and β densities is raised to the 4/3 power) has been virtually abandoned and replaced by the *Local Spin Density Approximation* (LSDA) (which is given as the sum of the individual densities raised to the 4/3 power), eq. (2.14)

$$E_x^{\text{LSDA}}[\rho] = -2^{1/3} C_x \int [\rho_\alpha^{4/3} + \rho_\beta^{4/3}] d\mathbf{r} \quad (2.14)$$

$$\varepsilon_x^{\text{LSDA}}[\rho] = -C_x \rho [\rho_\alpha^{1/3} + \rho_\beta^{1/3}] \quad (2.15)$$

LSDA may also be written in terms of the total density and the spin polarization.

$$\varepsilon_x^{\text{LSDA}}[\rho] = -\frac{1}{2} C_x \rho^{1/3} [(1 + \zeta)^{4/3} + (1 - \zeta)^{4/3}] \quad (2.16)$$

The correlation energy of a uniform electron gas has been determined by Monte Carlo methods for a number of different densities. In order to use these results in DFT calculations, it is desirable to have a suitable analytic interpolation formula. This has been constructed by Vosko, Wilk and Nusair (VWN)⁷⁵ and is in general considered to be a very accurate fit. It interpolates between the unpolarized ($\zeta = 0$) and spin polarized ($\zeta = 1$) limits by the following functional.

$$\varepsilon_c^{\text{VWN}}(r_s, \zeta) = \varepsilon_c(r_s, 0) + \varepsilon_a(r_s) \left[\frac{f(\zeta)}{f'(0)} \right] [1 - \zeta^4] + [\varepsilon_c(r_s, 1) - \varepsilon_c(r_s, 0)] f(\zeta) \zeta^4$$

$$f(\zeta) = \frac{(1 + \zeta)^{4/3} + (1 - \zeta)^{4/3} - 2}{2(2^{1/3} - 1)} \quad (2.17)$$

The LSDA approximation in general underestimates the exchange energy by $\sim 10\%$, thereby creating errors which are larger than the whole correlation energy. Electron correlation is furthermore overestimated, often by a factor close to 2, and bond strengths are as a consequent overestimated. Despite the simplicity of the fundamental assumptions, LSDA methods are often found to provide results with accuracy similar to that obtained by wave mechanics HF methods.

2.1.4.3. Gradient Corrected Methods

Improvements over the LSDA approach have to consider a non-uniform electron gas. A step in this direction is to make the exchange and correlation energies dependent not only the electron density, but also on derivatives of the density. Such methods are known as *Gradient Corrected or Generalized Gradient Approximation* (GGA) methods (a straightforward Taylor expansion does not lead to as improvement over LSDA, it actually makes things worse, thus the name generalized gradient approximation). GGA methods are also sometimes referred to as *non-local* methods, although this is somewhat misleading since the functionals depend only on the density (and derivatives) at a given point, not on a space volume as for example the Hartree-Fock exchange energy.

Perdew and Wang (PW86)⁷⁶ proposed modifying the LSDA exchange expression to that shown in eq. 2.18, where x is a dimensionless gradient variable, and a , b and c being suitable constants (summation over equivalent expressions for the α and β densities is implicitly assumed).

$$\begin{aligned}\varepsilon_x^{\text{PW86}} &= \varepsilon_x^{\text{LDA}} \left(1 + a x^2 + b x^4 + c x^6\right)^{1/15} \\ x &= \frac{|\nabla\rho|}{\rho^{4/3}}\end{aligned}\quad (2.18)$$

Becke proposed a widely used correction to the LSDA exchange energy, which has the correct $-r^{-1}$ asymptotic behavior for the energy density (but not for the exchange potential).

$$\begin{aligned}\varepsilon_x^{\text{B88}} &= \varepsilon_x^{\text{LDA}} + \Delta\varepsilon_x^{\text{B88}} \\ \Delta\varepsilon_x^{\text{B88}} &= -\beta\rho^{1/3} \frac{x^2}{1 + 6\beta x \sinh^{-1} x}\end{aligned}\quad (2.19)$$

The β parameter is determined by fitting to known atomic data and x is defined in eq. 2.18.

Perdew and Wang have proposed an exchange functional similar to B88 to be used in connection with the PW91 correlation functional given below.

$$\varepsilon_x^{\text{PW91}} = \varepsilon_x^{\text{LDA}} \left(\frac{1 + x a_1 \sinh^{-1}(x a_2) + \left(a_3 + a_4 e^{-b x^2}\right) x^2}{1 + x a_1 \sinh^{-1}(x a_2) + a_5 x^2} \right) \quad (2.20)$$

There have been various gradient corrected functional forms proposed for the correlation energy. One popular functional (not a correction) is due to Lee, Yang and Parr (LYP)⁷⁷ and has the form

$$\begin{aligned}
\varepsilon_c^{\text{LYP}} &= -a \frac{\gamma}{(1+d\rho^{-1/3})} - ab \frac{\gamma e^{-c\rho^{-1/3}}}{9(1+d\rho^{1/3})\rho^{8/3}} \\
&\quad \times \left[18(2^{2/3})C_F(\rho_\alpha^{8/3} + \rho_\beta^{8/3}) - 18\rho t_W \right. \\
&\quad \left. + \rho_\alpha(2t_W^\alpha + \nabla^2\rho_\alpha) + \rho_\beta(2t_W^\beta + \nabla^2\rho_\beta) \right] \\
\gamma &= 2 \left[1 - \frac{\rho_\alpha^2 + \rho_\beta^2}{\rho^2} \right] \\
t_W^\sigma &= \frac{1}{8} \left(\frac{|\nabla\rho_\sigma|^2}{\rho_\sigma} - \nabla^2\rho_\sigma \right)
\end{aligned} \tag{2.21}$$

where the a , b , c and d parameters are determined by fitting to data for the helium atom. The t_W functional is known as the local Weizsacker kinetic energy density. Note that the γ -factor becomes zero when all the spins are aligned ($\rho = \rho_\alpha$, $\rho_\beta = 0$), i.e. the LYP functional does not predict any parallel spin correlation in such a case (e.g. The LYP correlation energy in triplet He is Zero). The appearance of the second derivative of the density can be removed by partial integration to give eq. (2.22).

$$\begin{aligned}
\varepsilon_c^{\text{LYP}} &= -4\alpha \frac{\rho_\alpha\rho_\beta}{\rho^2(1+d\rho^{-1/3})} \\
&\quad - ab\omega \left\{ \frac{\rho_\alpha\rho_\beta}{18} \left[144(2^{2/3})C_F(\rho_\alpha^{8/3} + \rho_\beta^{8/3}) + (47-7\delta)|\nabla\rho|^2 \right. \right. \\
&\quad \left. \left. - (45-\delta)(|\nabla\rho_\alpha|^2 + |\nabla\rho_\beta|^2) + 2\rho^{-1}(11-\delta)(\rho_\alpha|\nabla\rho_\alpha|^2 + \rho_\beta|\nabla\rho_\beta|^2) \right] \right. \\
&\quad \left. + \frac{2}{3}\rho^2(|\nabla\rho_\alpha|^2 + |\nabla\rho_\beta|^2 - |\nabla\rho|^2) - (\rho_\alpha^2|\nabla\rho_\beta|^2 + \rho_\beta^2|\nabla\rho_\alpha|^2) \right\} \\
\omega &= \frac{e^{-c\rho^{-1/3}}}{(1+d\rho^{-1/3})\rho^{14/3}} \\
\delta &= c\rho^{1/3} + \frac{d\rho^{-1/3}}{(1+d\rho^{-1/3})}
\end{aligned} \tag{2.22}$$

2.1.4.4. Hybrid Methods

From the Hamiltonian and the definition of the exchange-correlation energy and exact connection can be made between the exchange-correlation energy and the corresponding potential connecting the non-interacting reference and the actual system. The resulting equation is called the *Adiabatic Connection Formula* (ACF) and involves an integration over the parameter λ which “turns on” the electron-electron interaction.

$$E_{xc} = \int_0^1 \langle \Psi_\lambda | \mathbf{V}_{xc}(\lambda) | \Psi_\lambda \rangle d\lambda \quad (2.23)$$

In the crudest approximation (taking \mathbf{V}_{xc} to be linear in λ) the integral is given as the average of the values at the two end-points.

$$E_{xc} \approx \frac{1}{2} \langle \Psi_0 | \mathbf{V}_{xc}(0) | \Psi_0 \rangle + \frac{1}{2} \langle \Psi_1 | \mathbf{V}_{xc}(1) | \Psi_1 \rangle \quad (2.24)$$

In the $\lambda = 0$ limit, the electrons are non-interacting and there is consequently no correlation energy, only exchange energy. Furthermore, since the exact wave function in this case is a single Slater determinant composed of KS orbitals, the exchange energy is exactly that given by Hartree-Fock theory. If the KS orbitals are identical to the HF orbitals, the “exact” exchange is precisely the exchange energy calculated by HF wave mechanics methods.

$$E_{xc}^{B3} = (1 - a)E_x^{LSDA} + aE_x^{exact} + b\Delta E_x^{BSS} + E_c^{LSDA} + c\Delta E_c^{GGA} \quad (2.25)$$

Models which include exact exchange are often called *hybrid* methods, the names *Adiabatic Connection Model* (ACM) and *Becke 3 parameter functional* (B3) are examples of such hybrid models defined by eq. (2.25). The a , b and c parameters are determined by fitting to experimental data and depend on the form chosen for E_c^{GGA} , typical values are $a \sim 0.2$, $b \sim 0.7$ and $c \sim 0.8$. Owing to the substantially better

performance of such parameterized functionals the Half-and-Half model is rarely used anymore. The B3 procedure has been generalized to include more fitting parameters, however, the improvement is rather small.

2.2. The ONIOM (our Own N-layered Integrated molecular Orbital and molecular Mechanics) Method⁷⁸

Although the density functional theory obtained from the combination with coulomb and exchange integrals has led to theoretical methods which scaled almost linearly with the size of the system, the accurate *ab initio* modeling of chemical systems containing a large number of atoms is still a challenging task. Morokuma et al.⁷⁹ proposed the Integrated Molecular Orbital and Molecular Mechanics (IMOMM) method which partitioned the system into 2 parts where different levels of theory are treated. Soon afterward, it was realized that the extrapolation scheme in IMOMM could be generalized to combine two MO methods as well. This resulted in a combined MO + MO method, which was referred to as the Integrated Molecular Orbital and Molecular Orbital method (IMOMO).⁸⁰ Later, the integration of more than two methods was accomplished, and the entire suite of integrated methods was named the ONIOM method. Thus, IMOMO encompasses both two-layered ONIOM2 (MO:MO) and three-layered ONIOM3 (MO:MO:MO), and IMOMM is in principle equivalent to ONIOM2 (MO:MM) and ONIOM3 (MO:MO:MM). Thus, interesting or difficult part of the system is treated with more accurate method while the rest of the system is treated with the less accurate method. By this approach, a lot of computation time can be saved and “real” instead of “model” system can be studied. The crucial aspect in this and other hybrid schemes is the interaction between the inner and the outer part (higher level of theory)/(lower level of theory) of the system.

Hybrid Calculations with ONIOM

In the two-layered ONIOM method, the total energy of the system is obtained from three independent calculations:

$$E^{\text{ONIOM2}} = E_{\text{model}}^{\text{high}} + E_{\text{real}}^{\text{low}} - E_{\text{model}}^{\text{low}}, \quad (2.26)$$

where *real* denotes the full system, which is treated at the *low* level, while *model* denotes the part of the system for which the energy is calculated at both *high* and *low* levels. The concept of the ONIOM method is represented schematically in Figure 2.3. One can see that the method can be regarded as an extrapolation scheme. Beginning at $E_{\text{model}}^{\text{low}}$, the extrapolation to the high-level calculation ($E_{\text{model}}^{\text{high}} - E_{\text{model}}^{\text{low}}$) and the extrapolation to the real system ($E_{\text{real}}^{\text{low}} - E_{\text{model}}^{\text{low}}$) are assumed to produce an estimate for $E_{\text{real}}^{\text{high}}$.

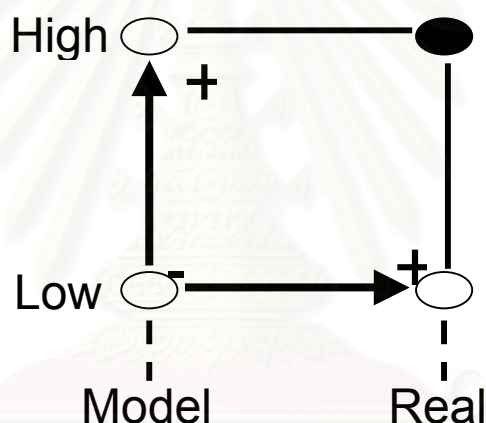


Figure 2.3 Schematic representation of two-layered ONIOM extrapolation scheme.

As can be seen, there is no restriction on the methods used at various levels (high, medium, low), and various MO and MM combinations discussed above can be derived. Combining different levels of MO methods is a unique feature of the ONIOM method. It turns out that MO:MO integration is rather straightforward, and virtually no special attention is required. On the other hand, the integration in ONIOM of MO and MM methods, combining two methods with very different philosophies, leads to many serious problems, as with all of the QM/MM methods. The integration of two MO levels with one MM level, ONIOM3 (MO:MO:MM), is unique, a feature absent from other QM/MM methods. In MO–MM combinations, the interaction between the MO

and MM regions can be treated at the MM level, i.e., with so-called mechanical embedding, or, alternatively, in the QM Hamiltonian, with so-called electronic embedding.

In the construction of the ONIOM model system, atoms that belong to the high-level layer have the same coordinates as the corresponding atoms in the real system. Even during geometry optimizations, these coordinates remain identical to one another. When no bond exists between the two layers, the first derivative of the energy with respect to the geometry is easy to obtain:

$$\frac{\partial E^{\text{ONIOM}}}{\partial q} = \frac{\partial E_{\text{mod el}}^{\text{high}}}{\partial q} + \frac{\partial E_{\text{real}}^{\text{low}}}{\partial q} - \frac{\partial E_{\text{mod el}}^{\text{low}}}{\partial q} \quad (2.27)$$

However, the link atoms used in the model system do not exist in the real system, and one of the main issues in this type of hybrid method is their geometrical placement, or how the geometry of the model system is related to that of the real system. The link atoms are connected to the high-level layer with the same angular and dihedral values as the link atom hosts (LAHs, the atoms replaced by the link atoms in the model system) in the real system. Now steric effects of the substituents are also taken into account in the two model system calculations. In earlier implementation in the IMOMM method, used fixed (standard) bond lengths between the link atoms and the high-level layer, as well as fixed bond lengths between the LAH atoms and the high-level layer. Although this scheme works well for geometry optimization, one degree of freedom is lost for each link between the high- and low-level layers, which causes problems, for example, with dynamics or frequency calculations.

In the later implementation, the angles and dihedrals are treated in the same manner as in the IMOMM scheme, while the bond distances between the high-level layer and the link atoms are obtained by scaling the corresponding distances between the high-level layer and the LAH atoms:

$$\mathbf{R}_{\text{link}} = \mathbf{R}_{\text{high-level atom}} + g(\mathbf{R}_{\text{LAH}} - \mathbf{R}_{\text{high-level atom}}), \quad (2.28)$$

where $\mathbf{R}_{\text{high-level atom}}$ denotes the atom in the high-level layer to which the link atom is connected. The scaling factor g is chosen so that reasonable bond lengths between the

LAH atoms and high-level-layer atoms also yield reasonable bond lengths between the link atoms and high-level-layer atoms. In this case, one must use the Jacobian J to convert the coordinate system for the model system to the coordinate system for the real system:

$$\frac{\partial E^{\text{ONIOM}}}{\partial q} = \frac{\partial E_{\text{model}}^{\text{high}}}{\partial q} \cdot J + \frac{\partial E_{\text{real}}^{\text{low}}}{\partial q} - \frac{\partial E_{\text{model}}^{\text{low}}}{\partial q} \cdot J, \quad (2.29)$$

The Hessian or higher-order derivatives can be uniquely defined in a similar fashion. Any method for the investigation of potential energy surfaces based on conventional techniques can now be used with the ONIOM method.

2.2. Electrostatics

2.3.1. Basic Theorems in Electrostatics

The electrostatic potential for a combination of discrete charges $\{q_\alpha\}$ placed at $\{r_\alpha\}$ and a smeared distribution $\rho(r)$ can be written by employing the superposition principle, as

$$V(\mathbf{r}) = \frac{1}{4\pi\epsilon_0} \left\{ \sum_{\alpha} \frac{q_{\alpha}}{|\mathbf{r} - \mathbf{r}_{\alpha}|} + \int \frac{\rho(\mathbf{r}')}{|\mathbf{r} - \mathbf{r}'|} d^3r' \right\} \quad (2.30)$$

The electric field $\mathbf{E}(\mathbf{r})$ due to this combination of charges is obtained by taking the gradient of $V(\mathbf{r})$ in Eq.2.30 and employing $\mathbf{E}(\mathbf{r}) = -\nabla V(\mathbf{r})$. This yield

$$\mathbf{E}(\mathbf{r}) = \frac{-1}{4\pi\epsilon_0} \left\{ \sum_{\alpha} \frac{q_{\alpha}(\mathbf{r} - \mathbf{r}_{\alpha})}{|\mathbf{r} - \mathbf{r}_{\alpha}|^3} + \int \frac{\rho(\mathbf{r}')(\mathbf{r} - \mathbf{r}')}{|\mathbf{r} - \mathbf{r}'|^3} d^3r' \right\} \quad (2.31)$$

There exists yet another relation in integral form, viz. Gauss' law, for this purpose. This is expressed as

$$\oint \mathbf{E} \cdot d\mathbf{S} = \frac{1}{\epsilon_0} \sum_i q_i \quad (2.32)$$

where q_i 's are the charges enclosed *inside* the surface S , and \mathbf{E} denotes the corresponding electric field. The surface integral on the l.h.s. equals $\oint \mathbf{n} \cdot d\mathbf{S}$ where \mathbf{n} is the out ward normal, and ds is an infinitesimal area as shown in Fig. 2.4. As a special case, it is clear that $\oint \mathbf{n} \cdot d\mathbf{S} = 0$ if the surface encloses no net charge. Gauss' law as expressed by Eq.2.32 is also called the fundamental theorem of electrostatics. Its integral form for a continuous charge density distribution is given by

$$\oint_s \mathbf{E} \cdot d\mathbf{S} = \frac{1}{\epsilon_0} \int \rho(r) d^3r \quad (2.33)$$

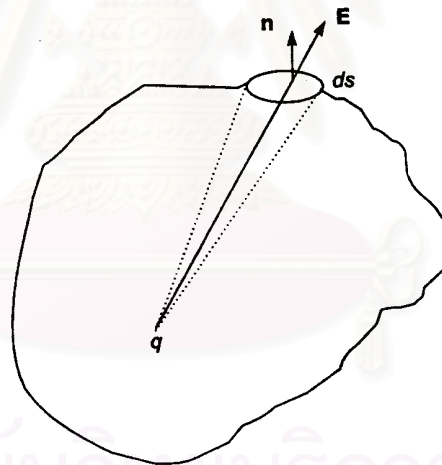


Figure 2.4 Illustration of Gauss' law for a charge enclosed in a closed surface S . Here, ds is a small surface element and \mathbf{n} is a unit outward normal to the surface element ds .

Note that Eqs.2.32 and 2.33 are based on the inverse square law⁸¹ (which implicitly the central nature of the force) and the principle of superposition. Since all these conditions hold good for the gravitational field as well, a relation similar to Eq.2.33 is valid for the gravitational case also, if $\rho(r)$ is treated as matter density.

It is possible to reduce Gauss' law to its differential form by employing the so called divergence theorem

$$\oint \mathbf{A} \cdot d\mathbf{S} = \oint \mathbf{A} \cdot \mathbf{n} ds = \int_{\Omega} \nabla \cdot \mathbf{A} d\tau \quad (2.34)$$

for a closed surface \mathbf{S} which encloses a volume Ω . In order to obtain a "local" version of Gauss' law, consider an infinitesimally small cube. The flux out of such a cube is given by $\nabla \cdot \mathbf{E} d\tau$ where $d\tau$ is the volume of the cube. The charge inside the tiny volume $d\tau$ is $\rho d\tau$. Equating these, one obtains the differential form of Gauss' law, viz.

$$\nabla \cdot \mathbf{E} = \rho / \epsilon_0 \quad (2.35)$$

Equation 2.36 is very useful for solving problems in electrostatics.⁸¹ A related form, called the Poisson equation, is obtained substituting $\mathbf{E} = -\nabla V$ in Eq.2.36:

$$\nabla^2 V(r) = -\rho(r) / \epsilon_0 \quad (2.36)$$

What is the energy associated with an electric field? Consider, for simplicity, a set of point charges $\{q_\alpha\}$ placed at $\{r_\alpha\}$. The Energy associated with this assembly of charges is given by

$$U = \frac{1}{2} \sum_{i \neq j} \frac{q_i q_j}{4\pi\epsilon_0 r_{ij}} \quad (2.37)$$

This may be alternatively written as

$$U = \frac{1}{2} \sum_j q_j \sum_{i \neq j} \left\{ \frac{q_i}{4\pi\epsilon_0 r_{ij}} \right\} \quad (2.38)$$

Note that inclusion of the factor $\frac{1}{2}$ is necessary in Eqs.2.38 and 2.39 in order to avoid double counting of the electrostatic interactions. Further, the term in curly brackets in Eq.2.39 is just the electrostatic potential V_j at r_j generated by point charges $\{q_i\}$ located at sites $\{r_i\}$. Hence,

$$U = \frac{1}{2} \sum_j q_j V_j \quad (2.39)$$

For the continuous case wherein the charge distribution is described by a function $\rho(r)$, the summation in the energy expression 2.40 is replaced by a suitable integration

$$U = \frac{1}{2} \int \rho(r) V(r) d^3r \quad (2.40)$$

This may be written in yet another form, by employing the Poisson equation and vector integral theorems, as

$$U = \frac{1}{2\epsilon_0} \int |\nabla V|^2 d^3r \quad (2.41)$$

If the charge density at a point r is zero, Eq.2.36 reduces to Laplace's equation, viz.

$$\nabla^2 V(r) = 0 \quad (2.42)$$

Thus, for a system containing only point charges, $\nabla^2 V(r) = 0$ at all points, except at the charge sites. This shows that for such a system of charges, the electric potential cannot show a maximum or minimum except at those points where the charges are located. For a (nondegenerate) maximum (minimum) in $V(r)$ to occur at a point, a necessary condition is that $\nabla^2 V(r) < 0$ (> 0) which is in violation of Eq.2.42 above. Using this property, it can be shown that no charges can be in *stable*

equilibrium in an electric field produced by a collection of charges. This result is known as Earnshaw's theorem. For a test positive charge q to be in equilibrium at a point, the field there must be zero, and moving the away from P in any direction should lead to a restoring force opposing the displacement.⁸² This situation is depicted schematically in Figure 2.5.

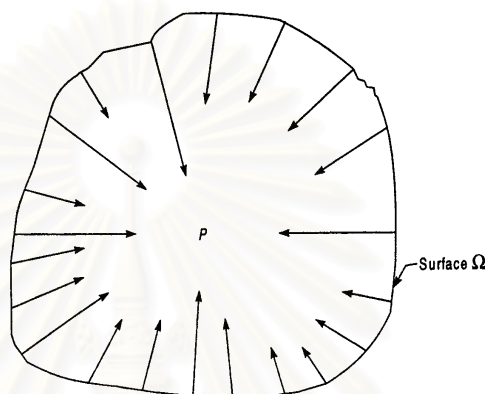


Figure 2.5 Electric field in the neighborhood of a point P , position of a stable equilibrium for a positive charge

It may be seen from this figure that $\mathbf{E} = -\nabla V$ must point inwards to the point P . Thus, $\int_{\Omega} \nabla V \cdot d\mathbf{S}$ must be negative, which contradicts Gauss' theorem since there is no negative charge in this infinitesimally small region. Note that test charge is not to be counted explicitly. Furthermore, it is positive rather than negative, as implied by Gauss's theorem. One may have a charged particle in equilibrium in an electrical field: for example, at those points P where $\mathbf{E} = 0$ in Figure 2.5. However, such an equilibrium is *not* a stable one.

2.3.2. Molecular Electrostatic Potential (MESP): Theoretical Computation and Graphics Visualization

Equation 2.31 is applicable to a molecular charge distribution which is essentially a collection of (static) positive discrete nuclear charges $\{Z_{\alpha}\}$ and a continuous negative electron density distribution described by $\rho(r)$. The MESP thus generated is given in atomic units as

$$V(r) = \sum_{\alpha} \frac{Z_{\alpha}}{|r-r_{\alpha}|} - \int \frac{\rho(r')}{|r-r'|} d^3r' \quad (2.43)$$

The MESP defined by Eq.2.43 bears some interesting characteristics. The first term therein is the bare-nuclear potential, V_{bn} , which is always non-negative. V_{bn} is incapable of exhibiting (non-nuclear) maxima, as well as minima. At the (point) nuclei, V_{bn} tends to assume infinite value, which could be treated as a pseudo maximum. The second term in Eq.2.43 is the negative potential engendered by the continuous electron charge density. The resultant total MESP thus generated can attain positive as well as negative values through zero, a feature which is rather unique and not exhibited individually by the electronic or the bare-nuclear contributions to the total potential.

Yet another salient feature of MESP brought out by Eq.2.43 is the amplification of the second term in the vicinity of an electron-rich region. This amplification effect may be attributed to the $1/|r-r'|$ weight attached within the electronic term of that equation. Thus, attainment of negative MESP values in a region of space is an indicator of electron localization therein. These characteristics make the MESP a very attractive tool for studying the molecular reactive. Many other applications of MESP are also summarized.

2.3.2.1. MESP from Density Functional Theory

The MESP obtained within the framework of the density functional theory (DFT) is also generally found to be in good qualitative agreement with the corresponding HF-SCF one. DFT-based MESP^{83,84} has been recently employed for the determination of covalent radii. The suitability of the DFT method towards the calculation of electrostatic properties of molecules has recently been assessed.^{85,86} The ESP and related properties of molecules containing phosphorus, sulfur and chlorine atoms (which are more difficult to represent than those involving only first row atoms) are found to be remarkably improved on including two sets of d orbitals on these atoms and p orbitals on the hydrogen atom.⁸⁵ Further, the calculations at the MP2 level have been found to be quite adequate for capturing most of the electron correlation

effects.⁸⁷ It was later observed that DFT methods do not noticeably improve the MESP representation at the Hartree-Fock level. However, a more remarkable improvement was seen on employing hybrid non-local functionals. Since DFT is a computationally economical method, it can be gainfully employed for examining molecular electrostatics of larger systems. It is noteworthy that since 1990, the DFT based methods have gained popularity for tackling large molecular systems.

2.3.2.2. MESP Visualization

It may be noted that the MESP is a three – dimensional quantity, unlike the molecular wave function, which is multi-dimensional in nature. This three-dimensional function can be visualized with the help of a computer wherein various colours can be assigned for representing the value of MESP. Since the MESP can assume both positive and negative values through zero, unlike $\rho(r)$ which attains only non-negative values, one expects that three-dimensional visualization of MESP will yield more detailed information than that furnished by $\rho(r)$ in the study of molecular recognition. With the advent of computer graphics techniques, the three-dimensional visualization of data has become an attractive tool in computational chemistry for interpreting the results obtained in the form of numbers. However, the visualization of $V(r)$ over a dauntingly large numbers of points covering the region of molecular framework needs a sophisticated approach.

Two – dimensional visualization

The MESP can be visualized on various planes with the help of contour lines or pixel plots. In a contour plots, different linestyles or colours may be used for a gradation of $V(r)$ values. In pixel plots, the points are given a colour code according to the MESP values on the grid, and intermediate points are assigned interpolated colours. One plane may be chosen at a time or various planes can be simultaneously displayed in conjunction, so as to get a glimpse of its three-dimensional structure. These planes can be plotted along with a ball-and-stick molecular model for getting a better ‘feel’ of the scalar field.

Three-dimensional visualization

Three-dimensional (3D) views of MESP may be obtained using isovalued surfaces differing in colour and transparency. This can also be achieved with the help of 3D or stacked contours. The contours in parallel planes are plotted simultaneously so as to generate a 3D feel. Another way in which a 3D MESP structure can be studied is to plot the MESP on some predefined surface (e.g. a surface on which $\rho(r)$ is constant, van der Waals surface, minimal surface, covalence surface⁸⁴, etc.) of molecules using suitably chosen colour codes. Various facilities of computer graphics such as rotation, scaling, shifting, etc. may be employed for obtaining a better understanding of the picture. The MESP can also be visualized on a black-and white monitor in the grey scale i.e., by using different densities of black-and-white pixels for the MESP values. It is always useful to visualize the molecule under consideration by a ball-and stick representation along with $V(r)$ for reference. Several computer programs are available which are helpful in the computation of molecular properties and/or graphics visualization of scalar/ vector fields (in particular, that of MESP).⁸⁷ These programs include SPARTAN, Hyperchem, PCModel, Molecular Editor, UNIVIS, POPROT, AVS etc., which run on various machines.

2.3.3. Applications of Molecular Electrostatic Potential

2.3.3.1. Introduction

This monograph has introduced the MESP as an important tool for the investigation of molecular structure and reactivity. Earlier⁸⁸ pioneering applications have focused on locating the sites of electrophilic attack, viz. the negative-valued regions or minima that appear in the MESP maps. A variety of applications are found in organic chemistry, pharmacology, biology, chemistry of explosives, drug designing, etc. wherein MESP has been used as parameter to study the structure-activity relationship (SAR). This Chapter presents applications of MESP involving these aspects

2.3.3.2. Biological and Medicinal Chemistry

We have seen that the MESP and allied entities have been widely employed in the study of the quantitative structure-activity relationship (QSAR) of biomolecules and drugs in medicinal chemistry. Electrostatics of molecules provides a highly informative means of characterizing the essential electronic features of drugs and their stereoelectronic complementarity with the receptor site. Since the receptor recognizes the stereoelectronic effects and not the atoms, studies of two- and three-dimensional MESP and its gradient plot have become a popular tool for characterizing pharmacologically active molecules from an electronic point of view. Graphical representations of this property of biologically active molecules are widely available. The dynamic effects are neglected in the rigid body approximation and the association between host (lock) and guest (key) is considered as the fitting of a key into its lock. Among the steric, hydrophobic and electrostatic interactions which are to be considered in such a molecular 'fit', the electrostatic effects predominate wherever the ionic and polar interactions between the host and the guest molecules are dominant. The MESP features of several drug molecules vis-à-vis the complementarity features with the respective receptor sites have been probed in recent years. It can be seen from various studies on drug activity, that a major role is played by an aromatic ring usually present in the structure. The negative-valued MESP region on the aromatic ring generally accounts for the reactivity towards electrophilic reagents. The aromatic moiety of the drug might be involved in a stacking type of interaction with another aromatic ring located at the receptor site. In the stacking complexes of the nucleic acid bases, for example, the electrostatic component is not necessarily a dominant term of the interaction energy, yet it has a decisive effect on the mutual orientation of the aromatic rings.

In summary, the applications of MESP are found in physics, chemistry, biology, as well as their interfaces. Many of these applications stem from the lock-and-key analogy formulated. The MESP distribution along with its topographical features seems to offer the mechanism for investigating these complementarity features.

CHAPTER 3

DETAILS OF THE CALCULATIONS

3.1. Geometry Optimization of C₆₀ Derivatives

3.1.1. Structure of C₆₀ derivatives

Fullerene (C₆₀) derivatives were selected as targets for this study. Starting geometrical parameters for C₆₀ where C-C = 1.448 Å and C=C = 1.375 Å have been taken from literature.⁸⁹ Then, the functional groups were built and added by HyperChem package. Schematic representations of these compounds, **I-X**, are shown in Figure 3.1. Their antiviral activities as measured by K_i and EC₅₀ values are also given in Table 3.1. These compounds are classified into two groups by the linkage between C₆₀ and its derivatives. The connections are via 3-membered and 6-membered rings for compounds **I-VI** and **VII-X**, respectively.

Table 3.1 K_i and EC₅₀ of the 10 investigated compounds as shown in Figure 3.1.

Compounds	Antiviral Activity	
	EC ₅₀ (μM)	K_i (μM)
I	7.3	5.0
II	2.5	-
III	-	0.103
IV	-	0.32
V	-	2.0
VI	2.7	-
VII	0.88	-
VIII	-	0.15
IX	2.2	-
X	6.3	-

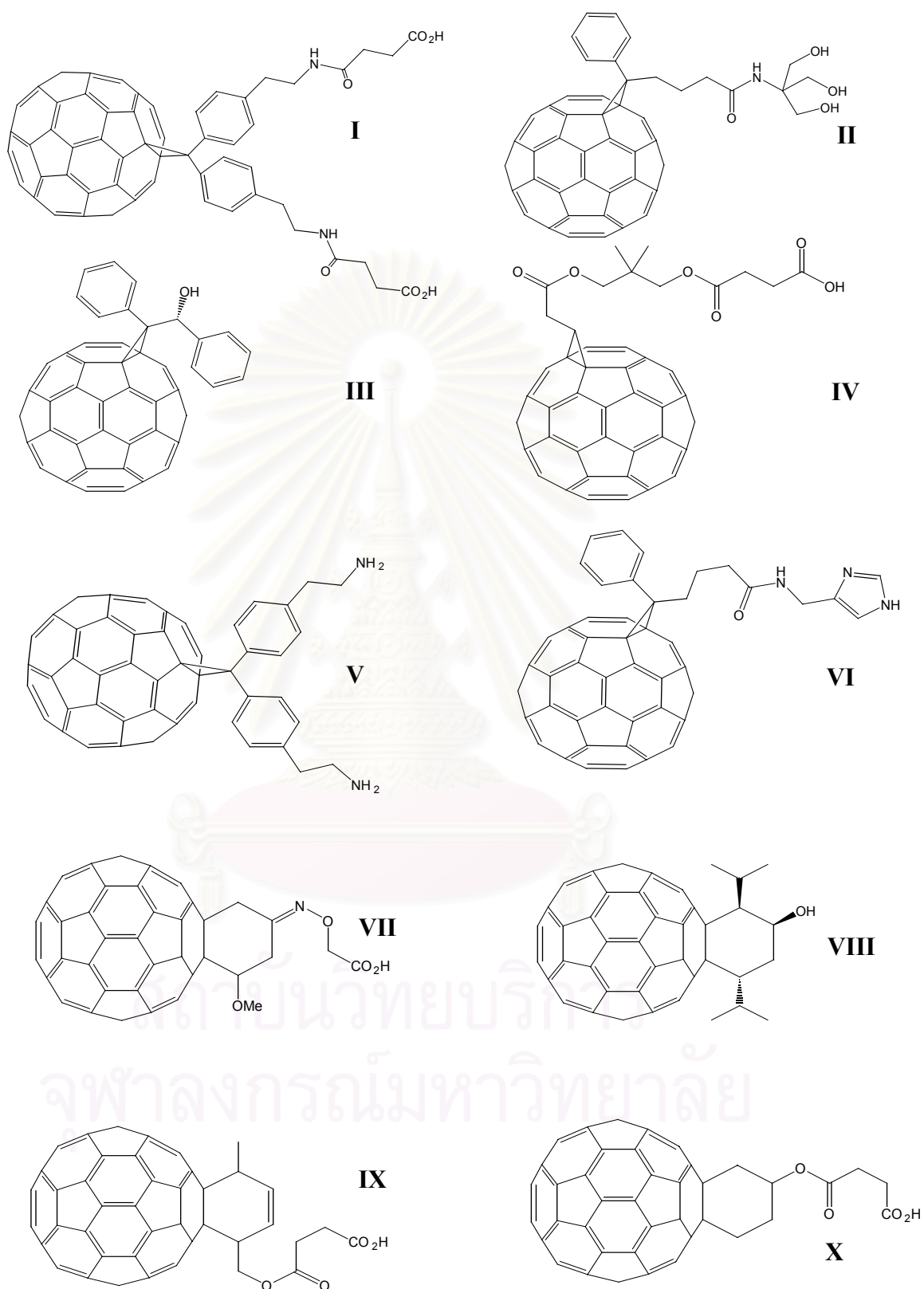


Figure 3.1 Fullerene (C₆₀) derivatives used in this study.

3.1.2. Optimization algorithm

All compounds were pre-optimized at the MM+ using conformational search in HyperChem package. These systems were then partitioned into two ONIOM layers, as shown in Figure 3.2 and Table 3.2. The symbol R denotes the real system consisting of all atoms. The symbol M stands for the small model system, which consisting of its functional group plus the next neighbor rings. A two-layer ONIOM, ONIOM2 (B3LYP/6-31G(d): PM3), was employed for geometry optimizations, using B3LYP/6-31G(d) for the system M (high level) and PM3 for the R system (low level). All computational calculations were performed using the Gaussian98 program.⁹⁰

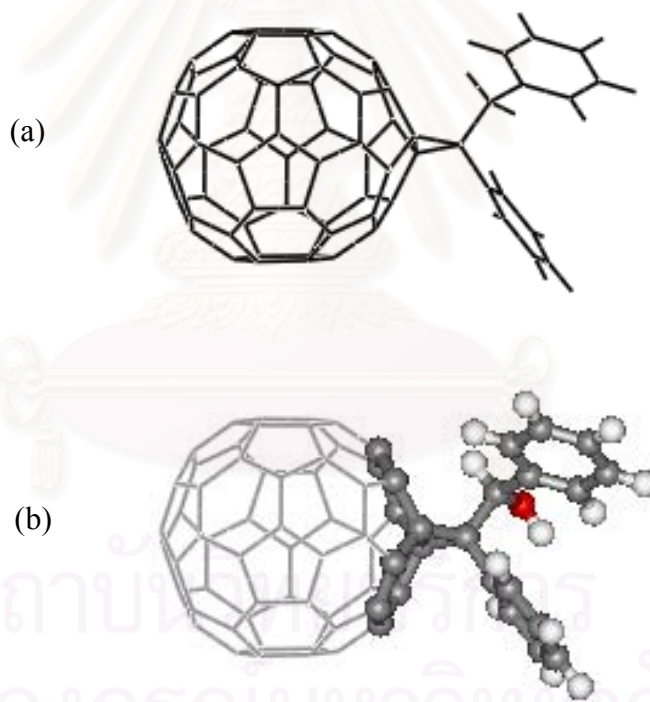


Figure 3.2 Optimized structure of C_{60} derivatives using ONIOM method (a) low level region and (b) high level region (ball and stick).

Table 3.2 ONIOM model structures Employed 2-layer calculation for optimization (ONIOM2).

systems	region	ONIOM2
small model: M	C ₁₀ and side chains	B3LYP/6-31G (d), PM3
real: R	whole molecule	PM3

3.2. Electronic Features of the C₆₀ Derivatives

With the optimal geometry, the B3LYP calculations have been applied to evaluate electronic properties of the compounds. The standard 6-31G(d) basis set was used to determine stabilization energy, HOMO-LUMO energies and electronic properties such as charge distribution on the solubilizing group and electrostatic potential of C₆₀ derivatives. Atomic net charge can be taken from the Mulliken population analysis. Distribution of the charges for all selected-carbon atoms of C₆₀ derivatives has been plotted. Electrostatic potential were calculated using CUBEGEN routine that is utility in Gaussian 98 program.

Molecular electrostatic potential maps for all 10 C₆₀ derivatives were visualized with the aid of the Gaussview program (see appendix B). The electrostatic potentials were sampled over the entire accessible surface of a molecule. The regions of positive electrostatic potential indicate excess positive charge, while regions of negative potential devotes areas of negative charge. Three dimensional isosurfaces of the molecular electrostatic potentials represent electrostatic potentials superimposed onto a surface of electron density. These color-coded isosurface values provide an indication of overall molecular size and of location of negative or positive electrostatic potentials. The most negative electrostatic potential is red, and the most positive electrostatic potential is blue.

CHAPTER 4

RESULTS AND DISCUSSIONS

4.1. Optimized Geometry of the C₆₀ Derivatives

Structural parameters such as bond distance, bond angle and torsion angle of all compounds obtained from ONIOM calculations were presented in an appendix A, Tables A.1 – A.2.

Structural parameter investigation, the structures of compounds **I-VI** and **VII-X** were defined with atomic numbering in Figures 4.1 and 4.2, respectively.

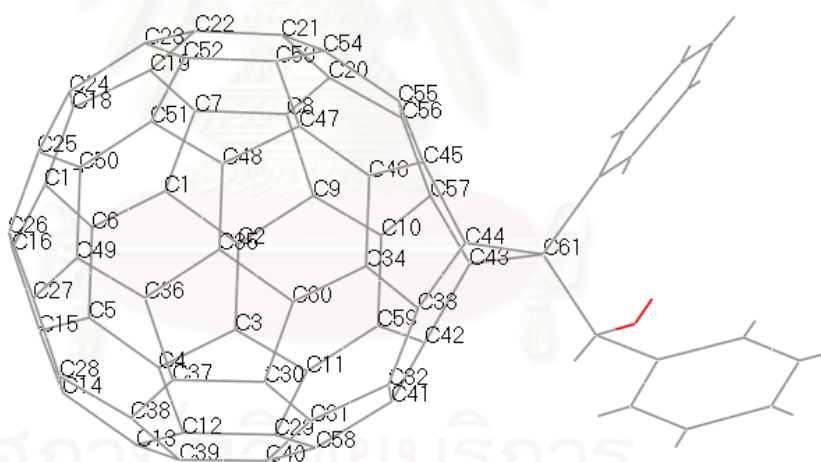


Figure 4.1 Definition of structural parameters of C₆₀ derivative compounds **I – VI** with atomic numbering.

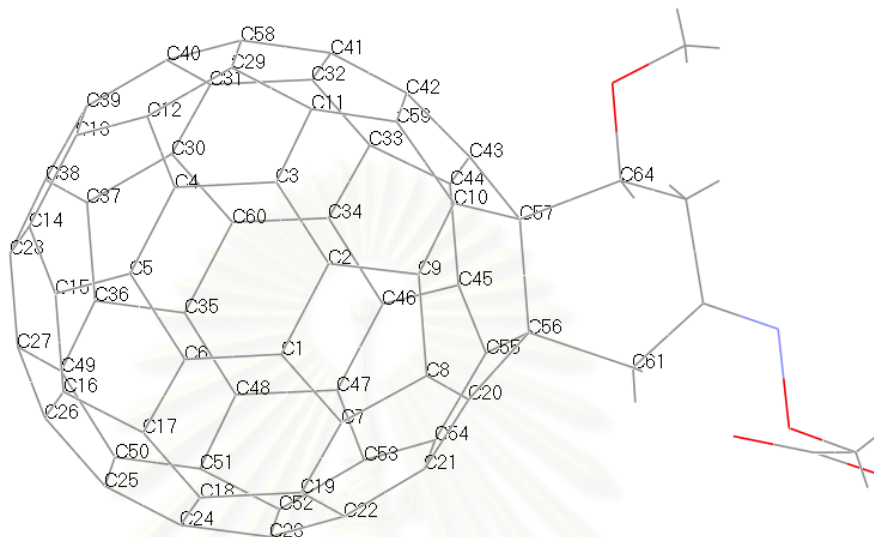


Figure 4.2 Definition of structural parameters of C₆₀ derivative compounds VII-X with atomic numbering.

สถาบันวิทยบริการ
จุฬาลงกรณ์มหาวิทยาลัย

4.2. Electronic and Molecular Properties

One major advantage of quantum chemical calculations over an experimental approach is that they allow the electronic structure to be computed. Therefore, it can obtain electronic properties which are the key to many physical and chemical properties. Some properties can be computed directly from the molecular geometry. Many descriptors for quantitative structure activity can be computed from the geometry only.

4.2.1. Effect of functional groups on Molecular Orbital Properties

The HOMO-LUMO energy gaps of all compounds were shown in Table 4.1. The results show that the energy gaps of C₆₀ derivatives in group 1 (compounds **I-VI**) are almost the same as that of C₆₀ and those of compounds in group 2 (compounds **VII-X**) are slightly narrower than that of C₆₀. However, no significant difference in the HOMO-LUMO energy gap is found among the derivatives in the same group.

Table 4.1 The HOMO-LUMO energy gaps of all 10 C₆₀ derivatives and of C₆₀.

Compound.	HOMO-LUMO energy gap(ev)
I	2.73
II	2.74
III	2.74
IV	2.79
V	2.73
VI	2.73
VII	2.65
VIII	2.63
IX	2.63
X	2.64
C ₆₀	2.73

4.2.2. Effect of functional groups on atomic net charge

Atomic charges cannot be observed experimentally because they do not correspond to any unique physical property. However, quantum chemical calculation can compute electronic structure, especially the charge distribution in molecular systems. It is very effective for some aspects of molecular interaction. Atomic net charges of compounds are taken from Mulliken Population Analysis in quantum chemical calculations. Mulliken analysis can assign an electron population to an orbital that is negative or more than two electrons.

The Mulliken's charges of atoms of C_{60} derivatives both group 1 and group 2 compounds were given in an Appendix A, Tables A.3 and A.4, respectively.

To visualize effect of functional groups on the atomic net charges of the C_{60} derivatives, their structures were fully optimized based on ONIOM (B3LYP/6-31G (d): PM3) calculations. Atomic net charges on carbon atoms around C—C bond which links between C_{60} and its side chain have been analyzed and plotted separately for the two groups of compounds, compounds **I-VI** (group 1) and **VII-X** (group 2), in Figures 4.4a and 4.4b. The selected atoms were labeled and given in Figure 4.3, in which atom numbers C_1 - C_{14} and C_{15} - C_{16} are those of C_{60} surface and its side chain, respectively. It is interesting to note here, therefore, that effect of functional group on the atomic net charges on the C_{60} surface can be observed up to 5 Å far from bridged carbon atoms (C_1 - C_2).

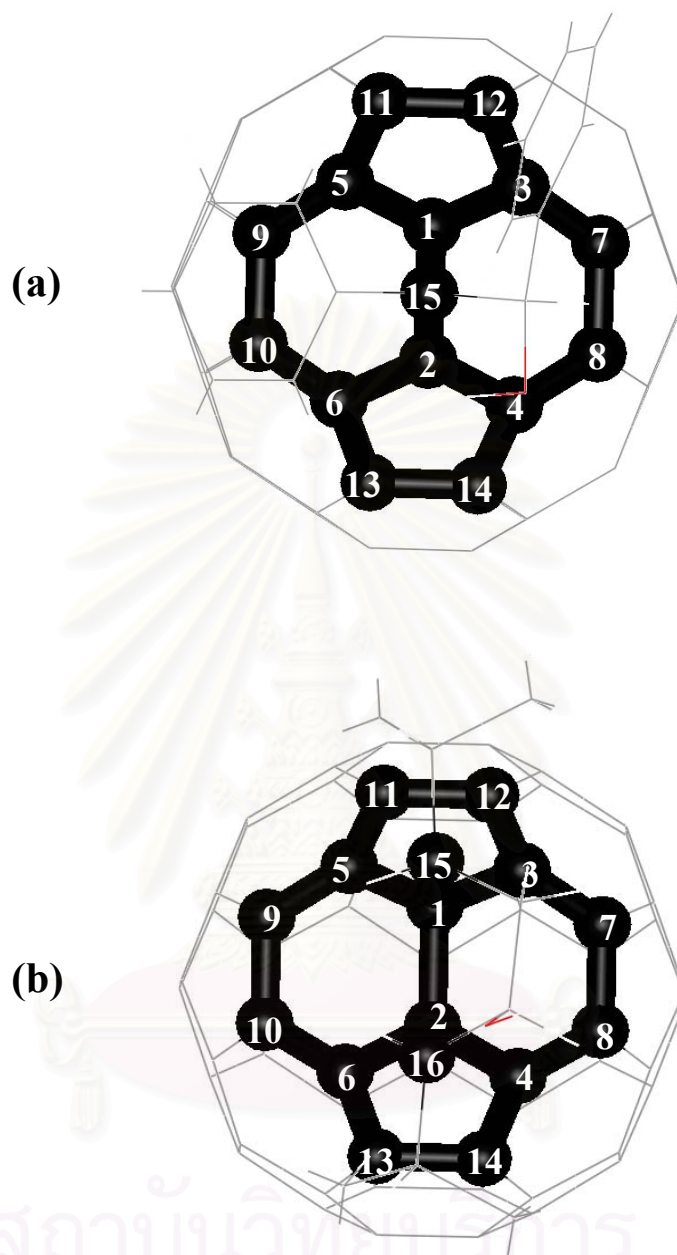


Figure 4.3 The selected carbon atoms with labeling for atomic net charges determination of (a) compounds **I-VI** and (b) compounds **VII-X**.

Atomic net charge on the C₆₀ surface

As expected, strongest effect of functional group on the net charges takes place on the linked atoms, C₁ and C₂. The calculated values are between -0.10 and -0.09 for both groups of derivatives in which the side chains are linked to the C₆₀ surface by the three- and six-membered rings, respectively. Second set of atoms where the net charge of 0.02 – 0.05 is independent of linking type, are C₃-C₆. Effect of linkage has been significantly observed for C₁₁-C₁₄ where the six-membered linkage leads to less negative atomic charges than those of the three-membered ring.

Atomic net charge on the side chain

Effect of side chains and of linkage types is displayed also in Figure 4.4 in terms of atomic net charges of C₁₅ and C₁₅-C₁₆ for compounds group 1 and group 2, respectively. Interest is centered on C₁₅ of the three-membered ring linkage, compound **I-VI**, in which its net charge can be classified into 3 levels. The compounds that their side chains consist of two symmetric benzene rings, compounds **I** and **V**, lead the electron density of about -0.07. This value is significantly lower than that between 0.01 and 0.02 obtained from the other set of compounds that their side chains consist of the single benzene ring, compounds **II**, **III** and **VI**. In addition to the above 2 sets of compounds, the lowest negative charge takes place when the benzene rings are replaced by the open chain, compound **IV**. The calculated value of -0.18 is much lower than those of the other compounds in group 1.

For the second group of compounds, **VII-X**, carbon atoms of the linked six-membered ring, C₁ and C₂, are almost less negative than those of the three-membered rings, compound **I-VI**. The =NO and -OMe functional groups on the six-membered ring of compound **VII** and the -O group of compound **X** donate more electrons into the rings, in comparison to those of compounds **VIII** and **IX**. An unsymmetric distribution taken place for compound **VII**, charge of C₁₅ of about 0.5 atomic unit is much lower than that of C₁₆, is clearly due to the presence of the electron donor -OMe group on C₁₅ (see Figure 1).

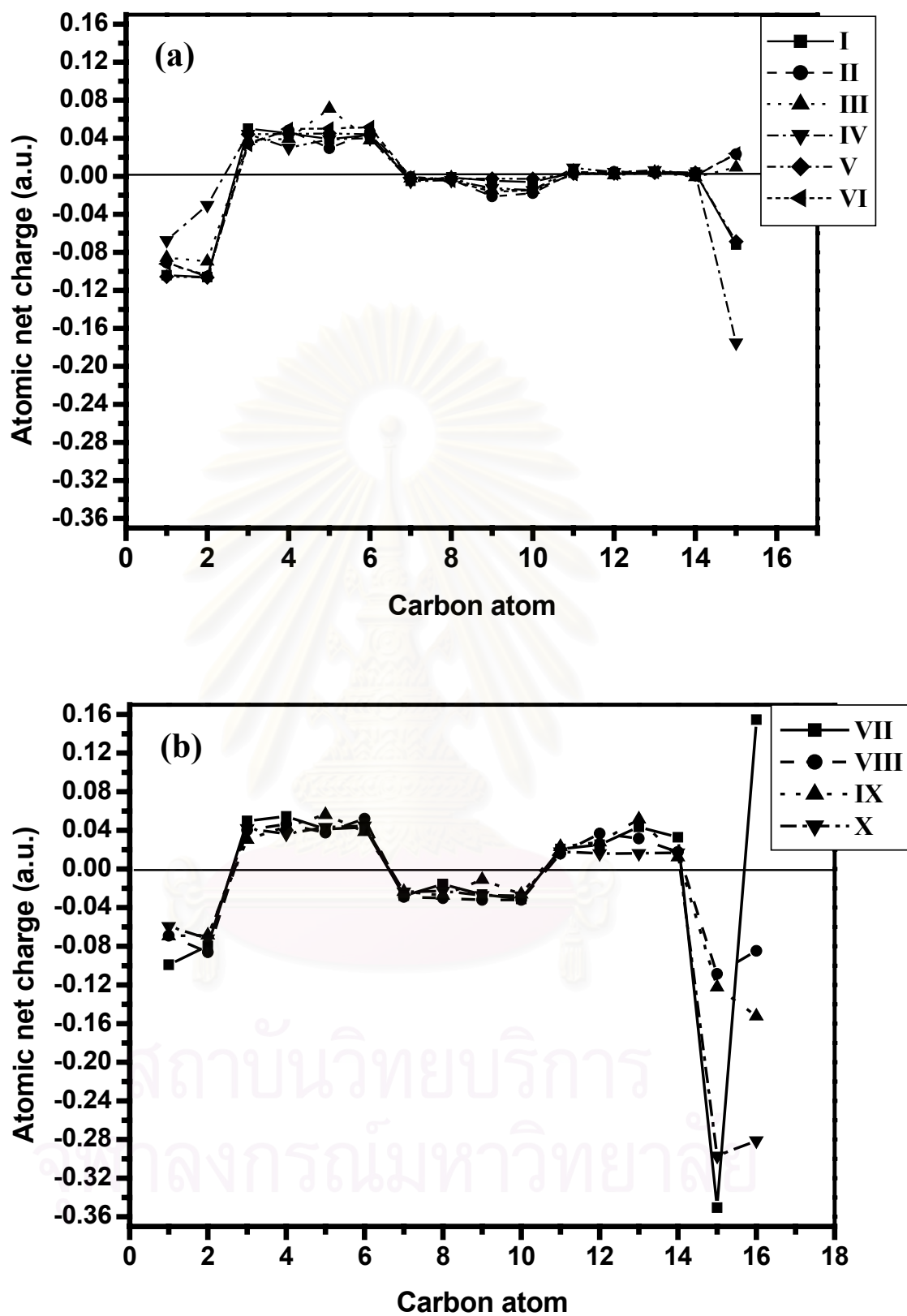


Figure 4.4 The plots of atomic net charges of all 10 C₆₀ derivatives; (a) compounds I-VI and (b) compounds VII-X.

4.2.3. Effect of functional groups on the molecular geometry

With the geometry obtained from the ONIOM (B3LYP/6-31G (d): PM3) optimization, changes of the selected bond lengths of all compounds relative to those of Buckminsterfullerene (C_{60}) were plotted in Figures 4.6a and 4.6b. Six types of C—C bonds on the C_{60} surface which are in the region 5 Å from the bridged atoms were labeled by B1-B6 in Figure 4.5. B3 is only double bond of all investigated ones. B5 and B6 obtained from PM3 only. The average C-C bond lengths of the Buckminsterfullerene which share by the 2 six-membered rings of 1.44 Å (double bond) and by five- and six-membered ring of 1.37 Å (single bond) yielded from our previous work⁸⁸ have been used for comparison.



Figure 4.5 The six selected bond lengths on the C_{60} surface which are in the region 5 Å from the bridged atoms.

It was found in Figure 4.6 that B1 for all compounds which links between C_{60} and its side chain are more than 0.37 Å for compounds **I-VI** (Figure 4.6a) and 0.22 Å for compound **VII-X** (Figure 4.6b) longer than those of Buckminsterfullerene. The corresponding C—C distances of the two groups of derivatives, which longer than 1.81 Å and 1.67 Å for compounds in group 1 and group 2, respectively, indicate that B1 bond for all compounds are totally broken. It is found

that the three-membered linkage effect B1 distance more than the six-membered one. For compound **IV**, dramatic increase of B1 by 0.5 Å relates directly to an increase of electron density on C₁₁, and hence of the three-membered ring connected to C₆₀ surface.

Excluding compound **IV**, the interest is centered on B2. Increases of this C—C bond of group 2 compounds (0.11 Å) are significantly longer than those of group 1 (0.03 Å – 0.05 Å). This fact can be described by a constrain due to an increase of B1, i.e., B2 of compounds in group 1 is higher constrained due to a much higher increase of B2 bond of this group of compounds than that of group 2. Therefore, the trends in increasing B1 and B2 are opposite; the longer B1 bonds with the shorter B2 bonds. As a consequence of increasing B1, B4 bonds for group 1 compounds are slightly longer than those of group 2. In addition, increases of B3 and B5 bonds for compounds in group 1 are larger, in comparison to those of group 2.

Another clear conclusion which can be made from Figure 4.6 is that side chain effects play stronger role on the bond lengths of the six- than those of the five-membered ring of the C₆₀ surface. Changes of the C—C bonds are observed in the following orders: B1 >> B2 ~ B4 > B3 > B6 > B5 for compounds **I-VI** (excluded compound **IV**) and B1 >> B2 > B4 > B3 ~ B6 > B5 for compounds **VII-X**.

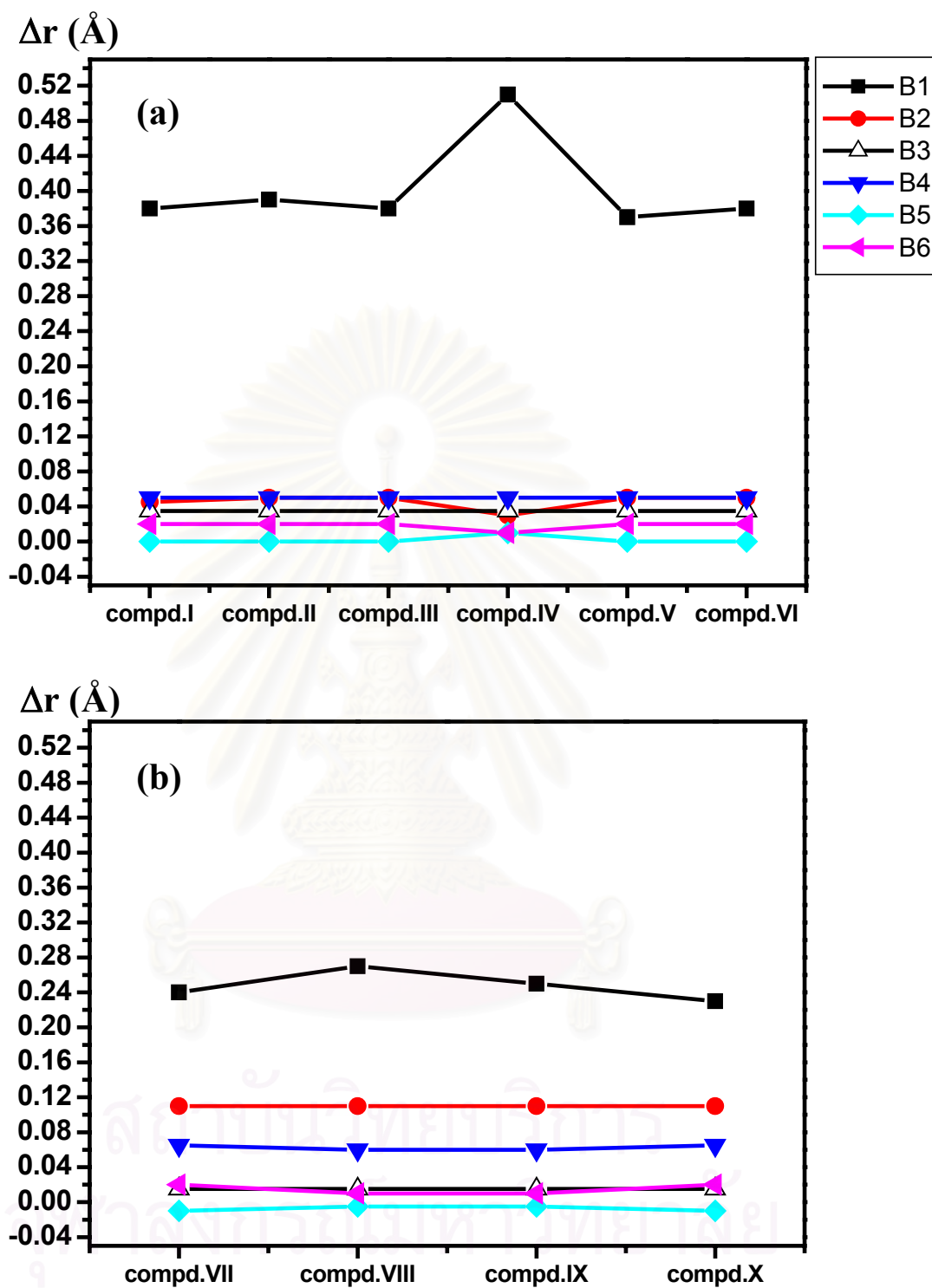


Figure 4.6 The plots of selected bond-length of all compounds; (a) compounds I-VI and (b) compounds VII-X.

4.2.4. Electrostatic Potential (ESP)

The molecular electrostatic potential (MESP) and allied entities have been widely employed in the study of structure-activity relationship of biomolecule and drug design medicinal chemistry. Electrostatics of molecules provides a highly informative means of characterizing the essential electronic features of drugs and their stereoelectronic complementarity with the receptor site. In this study, the three-dimensional MESP plots are employed to investigate the interpretative abilities of some MESP-related with antiviral activity.

The minimum and maximum electrostatic potentials were shown in Tables 4.2 and 4.3, respectively.

Three-dimensional isosurfaces of ESP superimposed onto total electron density and electrostatic potential map of compounds **III**, **VIII**, **IX** and **X** are presented in Figures 4.7 and 4.8. The plots for all compounds show two localized ESP regions. The lowest electrostatic potential (red region) is in the proximity of the lone pair of the hydroxyl oxygen atom, whereas the center for most positive potential (most blue region) lies near the hydroxyl hydrogen atom. These long-range electrostatic features indicate the potential for the inhibitor to participate in intermolecular formation of hydrogen bond with the receptor. The large lateral negative potential in front of the hydroxyl oxygen can be regarded as a nucleophilic region which acts as a magnet toward the electrophilic part of the receptor. This would generate driving force to facilitate the formation of inhibitor-enzyme complex. This fact is known to relate directly to their antiviral activity.

To visualize reliability of the gas phase properties yielded from quantum chemical calculations as described before, the results were compared to those obtained from molecular dynamics (MD) simulations.⁸⁹ Compound **III**, which is the most active compound ($K_i = 150$ nM) among the investigated compounds, was selected. Their structures obtained from the DFT calculations and from MD simulation were compared in Figure 4.9a. The ESP potential for the MD structure was shown in Figure 4.9b.

The plot shows that the two structures are almost identical with the root mean square displacement (RMSD) of 1.02 Å. As a consequence, no difference was found in terms of positive and negative regions of the electrostatic potential obtained from the quantum calculations (compound **III** in Figures 4.7 and 4.8) and MD (Figure 4.9b) geometries. However, it was found that the lowest negative ESP from the quantum calculations structure is slightly higher than that of the MD one.



สถาบันวิทยบริการ
จุฬาลงกรณ์มหาวิทยาลัย

Table 4.2 The minimum of electrostatic potential of all 10 C₆₀ derivatives.

Compound.	Minimum of ESP (a.u.)	Index
I	-79.2010	(128×111×80)
II	-75.1668	(113×101×80)
III	-72.3058	(112×80×79)
VI	-72.5863	(117×82×79)
V	-71.8304	(120×93×80)
VI	-71.9183	(128×91×79)
VII	-70.0541	(111×90×79)
VIII	-69.3719	(99×82×80)
IX	-70.7959	(109×84×79)
X	-68.2570	(107×69×69)

Table 4.3 The maximum of electrostatic potential of all 10 C₆₀ derivatives.

Compound.	Maximum of ESP (a.u.)	Index
I	-19.0430	(128×111×80)
II	-16.3773	(113×101×80)
III	-16.7183	(112×80×79)
VI	-17.8401	(117×82×79)
V	-16.5860	(120×93×80)
VI	-15.2671	(128×91×79)
VII	-15.4935	(111×90×79)
VIII	-17.4475	(99×82×80)
IX	-16.7185	(109×84×79)
X	-14.8683	(107×69×69)

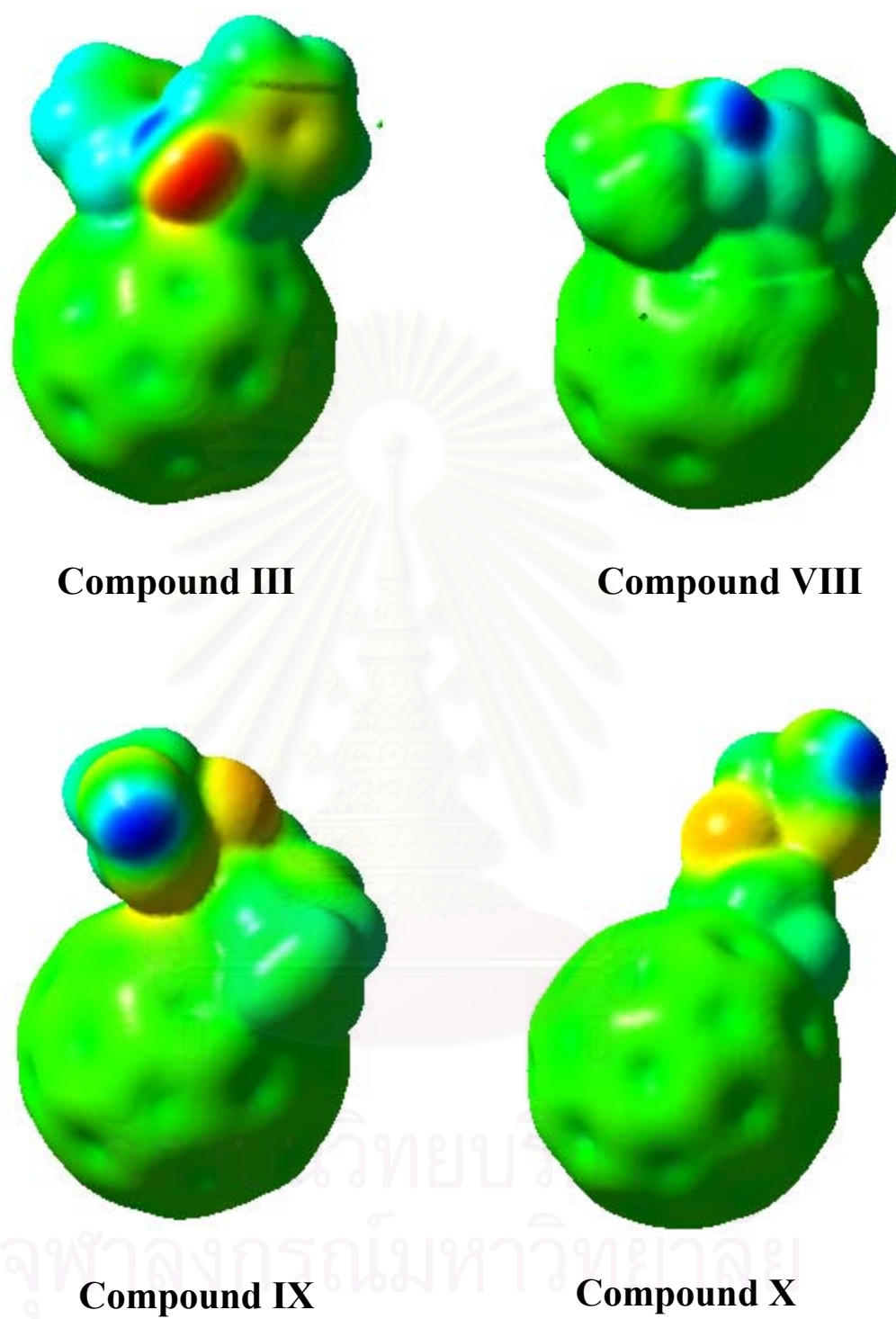


Figure 4.7 Molecular electrostatic potential energy isosurfaces of the selected compounds superimposed onto their total electron density (0.004 e/au^3) (solid view).

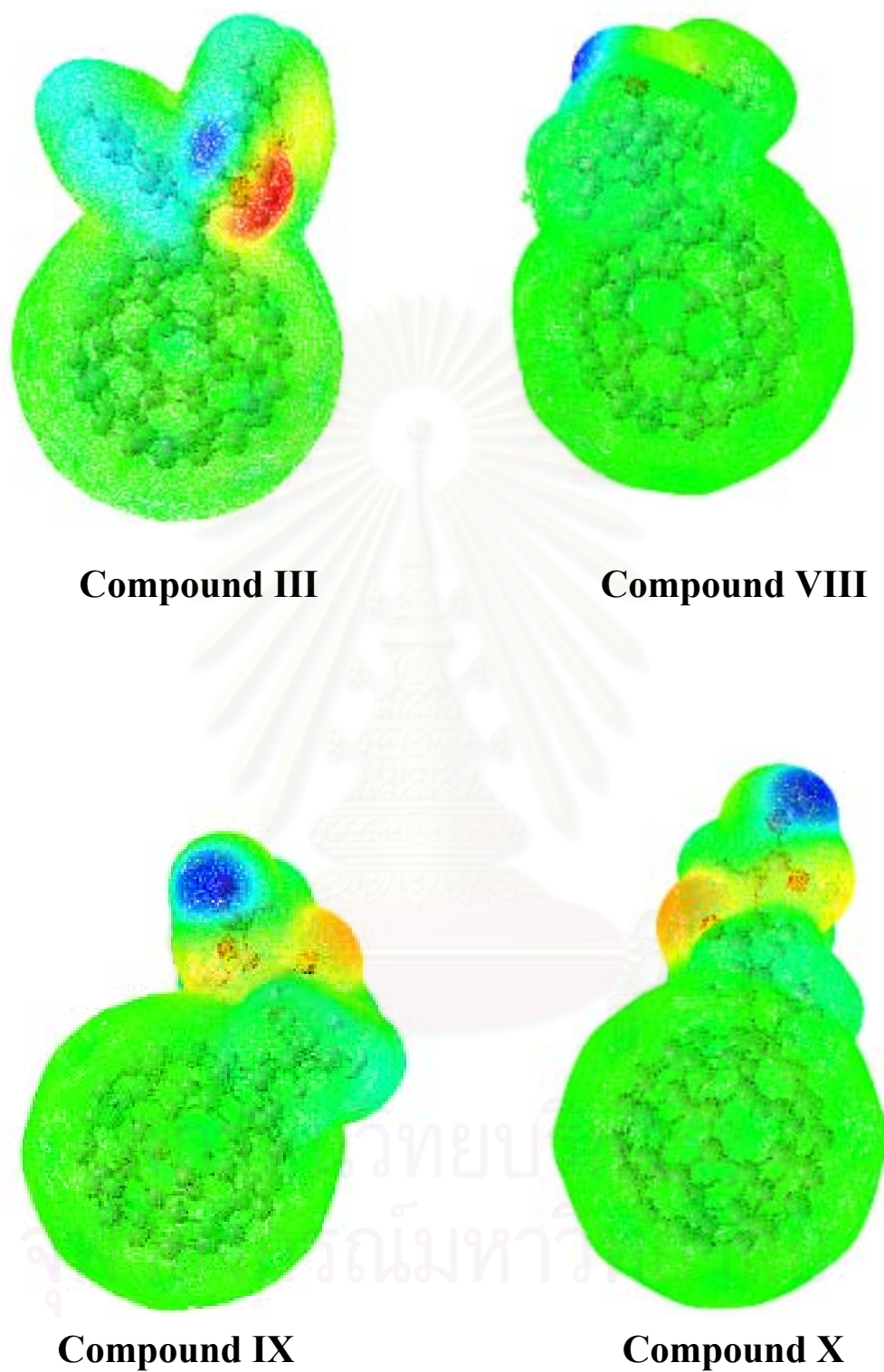


Figure 4.8 Molecular electrostatic potential energy isosurfaces of the selected compounds superimposed onto their total electron density (0.004 e/au³) (mesh view).

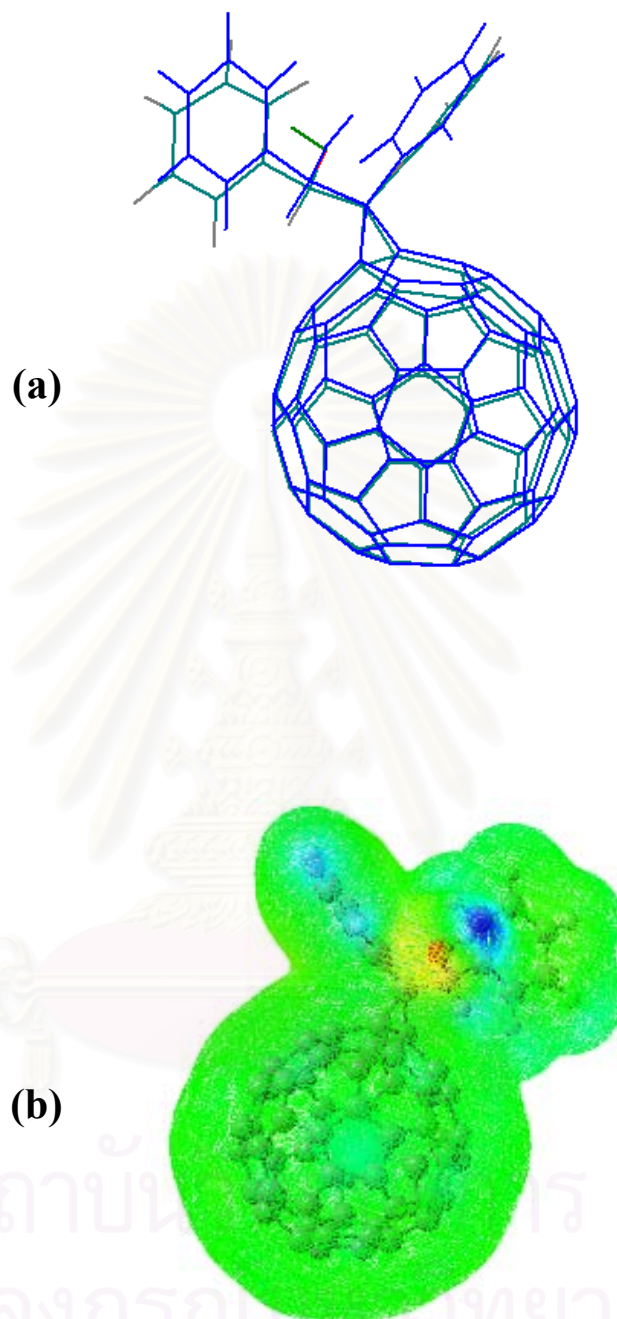


Figure 4.9 (a) Stereoview and (b) electrostatic potential contours plot of the compound **III** comparison between the optional structures obtained from quantum chemical calculation (blue) and molecular dynamics simulations (black).

CHAPTER 5

CONCLUSION

The assessment of structural features and electronic properties of C_{60} derivatives were performed using quantum chemical method. The investigated compounds are classified by the linkage, group 1 and group 2 where their side chains link to the C—C bond of C_{60} surface by the three- and six-membered ring, respectively. The integrated, ONIOM molecular orbital method was applied to optimize the structure of all compounds while the B3LYP/6-31G (d) calculations were performed to examine molecular and electronic properties.

It was found that the energy gaps of C_{60} derivatives depend on the linkage of side chains of compounds. The HOMO-LUMO energy gaps of compounds in group 1 are almost the same as that of C_{60} while those of compounds in group 2 are slightly narrower than that of Buckminsterfullerene (C_{60}). Effect of functional group on the atomic net charges on the C_{60} surface can be observed up to 5 Å far from bridged carbon atoms. The strongest effect takes place on the linked atoms. The effect on atomic net charge of side chain can be classified into 3 levels by the types of side chains.

With the geometry obtained from the ONIOM (B3LYP/6-31G (d): PM3) optimization, changes of the selected bond lengths of all compounds were analyzed. It was found that the bond which links between C_{60} and its side chain for all compounds are longer than those of Buckminsterfullerene (C_{60}). Changes of these bond distances of compounds are clearly due to higher steric effects in the three-membered linkage than that of the six-membered one. Changes of the C—C bonds are observed in the following

orders: $B1 \gg B2 \sim B4 > B3 > B6 > B5$ for compounds in group 1 and $B1 \gg B2 > B4 > B3 \sim B6 > B5$ for compounds in group 2.

In terms of electrostatic potential (ESP), the plots for the selected compounds show two localized ESP regions. The lowest electrostatic potential takes place in the proximity of the lone pair of the hydroxyl oxygen atom, whereas the center for most positive potential lies near the hydroxyl hydrogen atom. The large lateral negative potential in front of the hydroxyl oxygen can be regarded as a nucleophilic region which acts as a magnet toward the electrophilic part of the receptor. This would expect to generate driving force to facilitate the formation of inhibitor-enzyme complex.



สถาบันวิทยบริการ
จุฬาลงกรณ์มหาวิทยาลัย

FURTHER WORKS

All of the results presented here have been gathered with the basic properties of the C₆₀ derivatives as HIV-1 protease inhibitor. Several improvements are possible which have not been done. In continuation from this work, one can study molecular and electronic properties of the series of C₆₀ derivatives. The structure-activity relationship (SAR) can be, then, performed in order to design new and more potent drugs.

As the crystal structure of the complex is not available. Therefore, the study of orientation of C₆₀ derivative in the complex structure using molecular docking method with the force field potential would be also very interesting. Further improvements may be possible by means of molecular dynamics simulations which can show how inhibitor interact with receptor in condensed phase.



สถาบันวิทยบริการ
จุฬาลงกรณ์มหาวิทยาลัย

REFERENCES

1. Pneumocystis pneumonia--Los Angeles. *MMWR Morb. Mortal. Wkly Rep.* **1981**, *30*, 250-252.
2. Kaposi's sarcoma: the role of HHV-8 and HIV-1 in pathogenesis. <http://www-ermm.cbcu.cam.ac.uk/01002733h.htm>.
3. Kaposi's sarcoma and Pneumocystis pneumonia among homosexual men--New York City and California. *MMWR Morb. Mortal. Wkly Rep.* **1981**, *30*, 305-308.
4. Update on acquired immune deficiency syndrome (AIDS)--United States. *MMWR Morb. Mortal. Wkly Rep.* **1982**, *31*, 507-508, 513-514.
5. Barre-Sinoussi, F.; Chermann, J.C.; Rey, M.; Nugeyre, M. T.; Chamaret, S.; Gruest, J.; Dautet, C.; Axler-Blin, C.; Vezinet-Brun, F.; Rouzioux, C.; Rozenbaum, W.; Montagnier, L. Isolation of a T-Lymphotropic Retrovirus from a Patient at Risk for Acquired Immuno Deficiency Syndrome (AIDS). *Science* **1983**, *220*, 868-871.
6. Gallo, R. C.; Salahuddin, S. Z.; Popovic, M.; Shearer, G. M.; Kaplan, M.; Haynes, B. F.; Palker, T. J.; Redfield, R.; Oleske, J.; Safai, B.; White, G.; Foster, P.; Markham, P. D. Frequent Detection and Isolation of Cytopathic Retroviruses (HTLV-III) from Patients With AIDS and at Risk for AIDS. *Science* **1984**, *224*, 500-503.
7. Levy, J. A.; Hoffman, A. D.; Kramer, S. M.; Landis, J. A.; Shimabukuro, J. M.; Oshiro, L. S. Isolation of Lymphocytotropic Retroviruses from San Francisco Patients with AIDS. *Science* **1984**, *225*, 840-842.
8. Brun Vezinet, F.; Rouzioux, C.; Barre Sinoussi, F.; Klatzmann, D.; Saimot, A. G.; Rozenbaum, W.; Christol, D.; Gluckmann, J. C.; Montagnier, L.; Cherman, J. C. Detection of IgG Antibodies to Lymphadenopathy-Associated Virus in Patients with AIDS or Lymphadenopathy Syndrome. *Lancet* **1984**, *1*, 1253-1256.

9. Coffin, J.; Haase, A.; Levy, J. A.; Montagnier, L.; Oroszlan, S.; Teich, N.; Temin, H.; Toyoshima, K.; Varmus, H.; Vogt, P.; Weiss, R. Human immunodeficiency viruses. *Science* **1986**, *232*, 697.
10. UNAIDS. HIV Voluntary Counselling and Testing: A Gateway to Prevention and Care. <http://www.unaids.org/publications/documents/health/counseling/JC729-VCT-Gateway-CS-E.pdf>.
11. UNAIDS. Report on the Global HIV/AIDS Epidemic. Geneva: UNAIDS 2002 <http://www.unaids.org/barcelona/presskit/report.html>.
12. White, D. O.; Fenner, F. J. *Medicinal Virology*. Fourth ed. Academic Press: Sydney, **1994**.
13. Greene, W. C. Aids and the Immune-System. *Scientific American* **1993**, *269*, 98-105.
14. Arthur, L. O.; Bess, J. W.; Jr.; Sowder, R. C. 2nd; Benveniste, R. E.; Mann, D. L.; Chermann, J. C.; Henderson, L. E. Cellular proteins bound to immunodeficiency viruses: implications for pathogenesis and vaccines. *Science* **1992**, *258*, 1935-1938.
15. Turner, B. G.; Summers, M. F. Structural Biology of HIV. *J. Mol. Biol.* **1999**, *285*, 1-32.
16. McDougal, J. S.; Kennedy, M. S.; Sligh, J. M.; Cort, S. P.; Mawle, A.; Nicholson, J. K. Binding of HTLV-III/LAV to T4+ T Cells by a Complex of the 110K Viral Protein and the T4 Molecule. *Science* **1986**, *231*, 382-385.
17. Feng, Y.; Broder, C. C.; Kennedy, P. E.; Berger, E. A. HIV-1 Entry Cofactor: Functional cDNA Cloning of a Seven-Transmembrane, G Protein-Coupled Receptor. *Science* **1996**, *272*, 872-877.
18. Clapham, P. R.; Weiss, R. A. Immunodeficiency Viruses. Spoilt for Choice of Co-Receptors. *Nature* **1997**, *388*, 230-231.
19. Goff, S. P. Retroviral Reverse-Transcriptase – Synthesis, Structure, and Function. *J. Acquir. ImmuneDefic. Syndr. Hum. Retrovirol.* **1990**, *3*, 817-831.

20. Katz, R. A.; Skalka, A. M. The Retroviral Enzymes. *Annu. Rev. Biochem.* **1994**, *63*, 133-173.
21. Whitcomb, J. M.; Hughes, S. H. Retroviral Reverse Transcription and Integration – Progress and Problems. *Ann. Rev. Cell Biol.* **1992**, *8*, 275-306.
22. Ratner, L. HIV Life Cycle and Genetic Approches. *Prospect. Drug. Discovery Des.* **1993**, *1*, 2-22.
23. Reines, D.; Conaway, R. C. The RNA Polymerase II General Elongation Factors. *Trends Biochem. Sci.* **1996**, *21*, 351-355.
24. Herrmann, C. H.; Rice, A. P. Lentivirus Tat Proteins Specifically Associate With a Cellular Protein-Kinase, Tak, That Hyperphosphorylates the Carboxyl-Terminal Domain of the Large Subunit of RNA-Polymerase .2. Candidate For a Tat Cofactor. *J. Virol.* **1995**, *69*, 1612-1620.
25. Wei, P.; Garber, M. E.; Fang, S. M.; Fisher, W. H.; Jones, K. A. A novel CDK9-associated C-type Cyclin Interacts Directly with HIV-1 Tat and Mediates its High-Affinity, Loop-Specific Binding to TAR RNA. *Cell* **1998**, *92*, 451-462.
26. Goldsmith, M. A.; Warmerdam, M. T.; Atchison, R. E.; Miller, M. D.; Greene, W. C. Dissociation of the CD4 Downregulation and Viral Infectivity Enhancement Functions of Human Immunodeficiency Virus Type 1 Nef. *J. Virol.* **1995**, *69*, 4112-4121.
27. <http://www.chem.wisc.edu/~newtrad/CurrRef/AIDStopic/AIDStext/AIDSIntro.-html>.
28. Toh, H.; Ono, M.; Saigo, K.; Miyata, T. Retroviral Protease-Like Sequence in the Yeast Transposon Ty 1. *Nature* **1985**, *315*, 691-692.
29. Pearl, L. H.; Taylor, W. R. A structural model for the retroviral proteases. *Nature* **1987**, *329*, 351-354.
30. Navia, M. A.; Fitzgerald, P. M. D.; McKeever, B. M.; Leu, C. T.; Heimbach, J. C.; Herber, W.K.; Sigal, I. S.; Darke, P. L.; Springer, J. P. Three-Dimensional Structure of Aspartyl Protease from Human Immunodeficiency Virus HIV-1. *Nature* **1989**, *337*, 615-620.

31. Wlodawer, A.; Miller, M.; Jaskolski, M.; Sathyanarayana, B. K.; Baldwin, E.; Weber, I. T.; Selk, L. M.; Clawson, L.; Schneider, J.; Dent, S. B. Conserved folding in retroviral proteases: crystal structure of a synthetic HIV-1 protease. *Science* **1989**, *245*, 616-621.
32. Miller, M.; Schneider, J.; Sathyanarayana, B. K.; Toth, M. V.; Marshall, G. R.; Clawson, L.; Selk, L.; Kent, S. B.; Wlodawer, A. Structure of complex of synthetic HIV-1 protease with a substrate-based inhibitor at 2.3 Å resolution. *Science* **1989**, *246*, 1149-1152.
33. Fitzgerald, P. M.; McKeever, B. M.; Van Middlesworth, J. F.; Springer, J. P.; Heimbach, J. C.; Leu, C. T.; Herber, W. K.; Dixon, R. A.; Darke, P. L. Crystallographic analysis of a complex between human immunodeficiency virus type 1 protease and acetyl-pepstatin at 2.0 Å resolution. *J. Biol. Chem.* **1990**, *265*, 14209-14219.
34. Pettit, S. C.; Michael, S. F.; Swanstrom, R. The Specificity of the HIV-1 Protease. *Prospect. Drug. Discovery Des.* **1993**, *1*, 69-83.
35. Moore, M. L.; Dreyer, G. B. Substrate-Based Inhibitors of HIV-1 Protease. *Prospect. Drug. Discovery Des.* **1993**, *1*, 85-108.
36. Fitzgerald, P. M. D.; Springer, J. P. Structure and Function of Retroviral Proteases. *Annu. Rev. Biophys. Chem.* **1991**, *20*, 299-320.
37. Okimoto, N.; Tsukui, T.; Hata, M.; Hoshino, T.; Tsuda, M. Hydrolysis Mechanism of the Phenylalanine-Proline Peptide Bond Specific to HIV-1 Protease: Investigation by the *Ab Initio* Molecular Orbital Method. *J. Am. Chem. Soc.* **1999**, *121*, 7349-7354.
38. Lee, H.; Darden, T. A.; Pedersen, L. G. An *Ab Initio* Quantum Mechanical Model for the Catalytic Mechanism of HIV-1 Protease. *J. Am. Chem. Soc.* **1996**, *118*, 3946-3950.
39. Rodriguez, E. J.; Angeles, T. S.; Meek, T. D. Use of N-15 Kinetic Isotope Effects to Elucidate Details of the Chemical Mechanism of Human Immunodeficiency Virus-1 Protease. *Biochemistry* **1993**, *32*, 12380-12385.

40. Hyland, L. J.; Tomaszek, T. A.; Roberts, G. D.; Carr, S. A.; Magaard, V. W.; Bryan, H. L.; Fakhoury, S. A.; Moore, M. L.; Minnich, M. D.; Culp, J. S.; Desjarlais, R. L.; Meek, T. D. Human Immunodeficiency Virus-1 Protease .1. Initial Velocity Studies and Kinetic Characterization of Reaction Intermediate by O-18 Isotope Exchange. *Biochemistry* **1991**, *30*, 8441-8453.
41. Hyland, L. J.; Tomaszek, T. A.; Meek, T. D. Human Immunodeficiency Virus-1 Protease .2. Use of Ph Rate Studies and Solvent Kinetic Isotope Effects to Elucidate Details of Chemical Mechanism. *Biochemistry* **1991**, *30*, 8454-8463.
42. Huff, J. R. HIV protease: A novel chemotherapeutic target for AIDS. *J. Med. Chem.* **1991**, *34(8)*, 2305-2314.
43. Tomasselli, A. G.; Howe, W. J.; Sawyer, T. K.; Wlodawer, A.; Heinrikson, R. L. The complexities of AIDS: an assessment of the HIV protease as a therapeutic target. *Chim. Oggi* **1991**, *9*, 6-27.
44. Meek, T. D. Inhibitors of HIV-1 protease, *J. Enzym. Inhib.* **1992**, *6*, 65-98.
45. Abdel-Meguid, S. S. Inhibitors of aspartyl proteinases. *Med. Res. Rev.* **1993**, *13(6)*, 731-778.
46. Appelt, K. Crystal structures of HIV-1 protease-inhibitor complexes. *Perspect. Drug Disc. Design* **1993**, *1*, 23-48.
47. Erickson, J. W. Design and structure of symmetry-based inhibitors of HIV-1 protease. *Perspect. Drug Disc. Design* **1993**, *1*, 109-128.
48. Kramer, R. A.; Schaber, M. D.; Skalka, A. M.; Ganguly, K.; Wong-Staal, F.; Reddy, E. P. HTLV-III gag Protein Is Processed in Yeast Cells by the Virus pol-Protease. *Science* **1986**, *231*, 1580-1585.
49. Kohl, N. E.; Emini, E. A.; Schleif, W. A.; Davis, L. J.; Heimbach, J. C.; Dixon, R. A. F.; Scolnick, E. M.; Sigal, I. S. Active Human Immunodeficiency Virus Protease Is Required For Viral Infectivity. *Proc. Natl. Acad. Sci. USA* **1988**, *85*, 4686-4690.

50. Tomasselli, A. G.; Heinrikson, R. L. Targeting the HIV-protease in AIDS Therapy: A Current Clinical Perspective. *Biochim. Biophys. Acta* **2000**, *1477*, 189-214.
51. De Lucca, G. V.; Erickson-Viitanen, S.; Lam, P. Y. S. Cyclic HIV Protease Inhibitors Capable of Displacing the Active Site Structural Water Molecule. *Drug Discovery Today* **1997**, *2*, 6-18.
52. Kempf, D. J.; Sham, H. L. HIV Protease Inhibitors. *Curr. Pharm. Design* **1996**, *2*, 225-246.
53. Kempf, D. J. Design of Symmetry-Based, Peptidomimetic Inhibitors of Human Immunodeficiency Virus Protease. *Methods Enzymol.* **1994**, *241*, 234-254.
54. Roberts, N. A.; Martin, J. A.; Kinchington, D.; Broadhurst, A. V.; C, C. J.; Duncan, I. B.; Galpin, S. A.; Handa, B. K.; Kay, J.; Kroehn, A.; Lambert, R. W.; Merrett, J. H.; Mills, J. S.; Parkes, K. E. B.; Redshaw, S.; Ritchie, A. J.; Taylor, D. L.; Thomas, G. J.; Machin, P. J. Rational Design of Peptide-Based HIV Proteinase Inhibitors. *Science* **1990**, *248*, 358-364.
55. Jacobsen, H.; Yasargil, K.; Winslow, D. L.; Craig, J. C.; Kroehn, A.; Duncan, I. B.; Mous, J. Characterization of Human Immunodeficiency Virus Type 1 Mutants with Decreased Sensitivity to Proteinase Inhibitor Ro 31-8959. *Virology* **1995**, *206*, 527-534.
56. Markowitz, M.; Mo, H.; Kempf, D. J.; Norbeck, D. W.; Bhat, T. N.; Erickson, J. W.; Ho, D. D. Selection and Analysis of Human Immunodeficiency Virus Type 1 Variants with Increased Resistance to ABT-538, a Novel Protease Inhibitor. *J. Virol.* **1995**, *69*, 701-706.
57. Condra, J. H.; Schleif, W. A.; Blahy, O. M.; Gabryelski, L. J.; Graham, D. J.; Quintero, J. C.; Rhodes, A.; Robbins, H. L.; Roth, E.; Shivapraksh, M.; Titus, D.; Yang, T.; Teppler, H.; Squires, K. E.; Deutsch, P. J.; Emini, E. A. In Vivo Emergence of HIV-1 Variants Resistant to Multiple Protease Inhibitors. *Nature* **1995**, *374*, 569-571.

58. Ridky, T.; Leis, J. Development of Drug Resistance to HIV-1 Protease Inhibitors. *J. Biol. Chem.* **1995**, *270*, 29621-29623.
59. Bursavich, M. G.; Rich, D. H. Designing Non-Peptide Peptidomimetics in the 21st Century: Inhibitors Targeting Conformational Ensembles. *J. Med. Chem.* **2002**, *45*, 541-558.
60. Friedman, S. H.; DeCamp, D. L.; Sijbesma, R. P.; Srdanov, G.; Wudl, F.; Kenyon, G. L. Inhibition of the HIV-1 Protease by Fullerene Derivatives: Model Building Studies and Experimental Verification. *J. Am. Chem. Soc.* **1993**, *115*, 6506-6509.
61. Friedman, S. H.; Ganapathi, P. S.; Rubin, Y.; Kenyon, G. L. Optimizing the Binding of Fullerene Inhibitors of the HIV-1 Protease through Predicted Increases in Hydrophobic Desolvation. *J. Med. Chem.* **1998**, *41*, 2424-2429.
62. Da Ros, T.; Prato, M. Medicinal chemistry with fullerenes and fullerene derivatives. *Chem. Commun.* **1999**, 663-669.
63. Sijbesma, R.; Srdanov, G.; Wudl, F.; Castoro, J. A.; Wikins, C.; Friedman, S. H.; DeCamp, D. L.; Kenyon, G. L. Synthesis of a Fullerene Derivative for the Inhibition of HIV Enzymes. *J. Am. Chem. Soc.* **1993**, *115*, 6510-6512.
64. Schinazi, R. F.; Sijbesma, R. P.; Srdanov, G.; Hill, C. L.; Wudl, F. *Antimicrob. Agents Chemother.* **1993**, *37*, 1707.
65. Schuster, D. I.; Wilson, S. R.; Schinazi, R. F. Anti-Human Immunodeficiency Virus Activity and Cytotoxicity of Derivatized Buckminsterfullerene. *Bioorganic & Medicinal Chemistry Letters* **1996**, *6*, 1253-1256.
66. Frisch, A.; Frisch, M. J. *Gaussian 98 User's Reference*. Pittsburgh, PA: Gaussian Inc., **1998**.
67. Levine, I. N. *Quantum Chemistry*. Boston: Allyn and Bacon, Inc., **1983**.
68. Cook, D. B. *Handbook of Computational Quantum Chemistry*. New York: Oxford University Press, **1998**.
69. HyperChem 5.0 user manuals, Hypercube, Inc., URL – <http://www.hyper.com>.
70. Chem3D 3.5 user manual, CambridgeSoft, MA URL – <http://www.camsoft.com>.

71. Atkins, P.W. *Quanta*. 2nd ed. Oxford University Press, **1991**.
72. Dewar, M. J. S.; Zoebisch, E. G.; Healy, E. F.; Stewart, J. J. P. AM1: A New General Purpose Quantum Mechanical Molecular Model. *J. Amer. Chem. Soc.* **1985**, *107*, 3902.
73. (a) Stewart, J. J. P. Optimisation of Parameters for Semi-empirical Methods I. Method. *Journal of Computational Chemistry* **1989**, *10*, 209-220. (b) Stewart, J. J. P. Optimisation of Parameters for Semi-empirical Methods II. Applications. *Journal of Computational Chemistry* **1989**, *10*, 209-220.
74. Hohenberg, P.; Kohn, W. Inhomogeneous Electron gas. *Phys. Rev.* **1964**, *136*, B864.
75. Vosko, S. J.; Wilk, L. Influence of an improved local-spin-density correlation-energy functional on the cohesive energy of alkali metals. *Phys. Rev. B* **1980**, *22*, 3812.
76. Perdew, J. D.; Wang, Y. Accurate and simple density functional for the electronic exchange energy: Generalized gradient approximation. *Phys. Rev. B* **1986**, *33*, 8800.
77. Lee, C.; Yang, W.; Parr, R. G. Development of the Colle-Savetti Correlation-Energy Formula into a Functional of the Electron Density. *Phys. Rev. B* **1988**, *37*, 785.
78. Svensson, M.; Humbel, S.; Froese, R.; Matsubara, T.; Sieber, S.; Morokuma, K. ONIOM: A multilayered integrated MO+MM method for geometry optimizations and single point energy predictions. A test for Diels-Alder reactions and Pt(P(t - Bu)₃)₂ + H₂ oxidative addition. *Journal of Physical Chemistry* **1996**, *100*, 19357.
79. Maseras, F.; Morokuma, K. IMOMM: A New Integrated Ab Initio + Molecular Mechanics Optimization Scheme of Equilibrium Structure. *Journal of Computational Chemistry* **1995**, *16*, 1170.
80. Humbel, S.; Sieber, S.; Morokuma, K. The IMOMO method: Integration of different levels of molecular orbital approximations for geometry

- optimization of large systems: Test for n-butane conformation and S_N2 reaction: $RCL + Cl^-$. *Journal of Chemical Physics* **1996**, *105*, 1959-1967.
81. Jackson, J. D. *Classical Electromagnetism*. New Delhi: Wiley Eastern, **1978**.
82. Feynman, R. P.; Leighton, R. B.; Sands, M. *Lectures on Physics*. Vol. 2. New York: Addison-Wesley, **1964**.
83. Murray, J. S.; Seminario, J. M.; Concha, M. C.; Politzer, P. Potential Obtained by a Local Density Functional Approach. *Intern. J. Quantum Chem.* **1992**, *44*, 113.
84. Wiener, J. J. M.; Grice, M. E.; Murray, J. S.; Politzer, P. Molecular electrostatic potentials as indicators of covalent radii. *J. Chem. Phys.* **1996**, *104*, 5109.
85. Soliva, R.; Lague, F. J.; Orozco, M. Reliability of MEP and MEP-derived properties computed from DFT methods for molecules containing P, S and Cl. *Theoret. Chem. Accts.* **1997**, *98*, 42.
86. Soliva, R.; Orozco, M.; Lague, F. J. Suitability of density functional methods for calculation of electrostatic properties. *J. Comput. Chem.* **1997**, *18*, 980.
87. Gadre, S. R.; Taspaa, A. Graphics visualization of molecular surfaces. *J. Mol. Graph.* **1994**, *12*, 45.
88. (a) Sorocco, E.; Tomasi, J. *Adv. Quantum Chem. 11*. New York: 116 Ed. P-O Loewdin, Academic, **1978**.
89. Scuseria, G. E. *Ab initio* theoretical predictions of the equilibrium geometries of C_{60} , $C_{60}H_{60}$ and $C_{60}F_{60}$. *Chem. Phys. Lett.* **1991**, *176*, 423.
90. Frisch, M. J.; Trucks, G. W.; Schlegel, H. B.; Scuseria, G. E.; Robb, M. A.; Cheeseman, J. R.; Zakrzewski, V. G.; Montgomery, J. A.; Stratmann, R. E., Jr.; Burant, J. C.; Dapprich, S.; Millam, J. M.; Daniels, A. D.; Kudin, K. N.; Strain, M. C.; Farkas, O.; Tomasi, J.; Barone, V.; Cossi, M.; Cammi, R.; Mennucci, B.; Pomelli, C.; Adamo, C.; Clifford, S.; Ochterski, J.; Peterson, G. A.; Ayala, P. Y.; Cui, Q.; Morokuma, K.; Sal-vador, P.; Dannenberg, J. J.; Malick, D. K.; Rabuck, A. D.; Raghavachari, K.; Foresman, J. B.; Cioslowski, J.; Ortiz, J.V.; Baboul, A. G.; Stefanov, B. B.; Liu, G.;

Liashenko, A.; Piskorz, P.; Komaromi, I.; Gomperts, R.; Martin, R. L.; Fox, D. J.; Keith, T.; Al-Laham, M. A.; Peng, C. Y.; Nanayakkara, A.; Challacombe, M.; Gill, P. M. W.; Johnson, B.; Chen, W.; Wong, M. W.; Andres, J. L.; Gonzalez, C.; Head-Gordon, M.; Replogle, E. S.; Pople, J. A. *Gaussian 98. Revision A.7*. Pittsburgh PA: Gaussian, Inc., **2001**.

91. Aree, T.; Kerdcharoen, T.; Hannongbua, S. Charge transfer, polarizability and stability of Li-C₆₀ complexes. *Chemical Physics Letters* 1998, 285, 221-225.
92. Sanghiran Lee, V.; Promsri, S.; Sompornpisut, P.; Parasuk, V.; Hannongbua, S. Structural Analysis of Lead Fullerene-Based Inhibitor Bound to Human Immunodeficiency Virus Type 1 Protease in Solutions From Molecular Dynamics Simulations. *in preparation*.

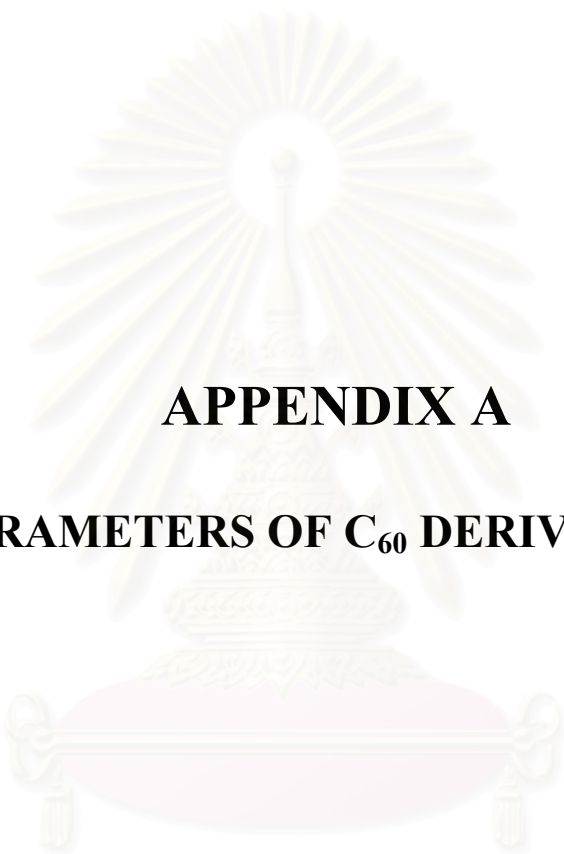


สถาบันวิทยบริการ
จุฬาลงกรณ์มหาวิทยาลัย



APPENDICES

สถาบันวิทยบริการ
จุฬาลงกรณ์มหาวิทยาลัย



APPENDIX A
PARAMETERS OF C₆₀ DERIVATIVES

สถาบันวิทยบริการ
จุฬาลงกรณ์มหาวิทยาลัย

Table A.1 Structural parameters of compound I-VI obtained from ONIOM calculations. Here, R , A, D are distance, bond angle and torsion angle, respectively.

parameters	Compd.I	Compd.II	Compd.III	Compd.IV	Compd.V	Compd.VI
R(1,2)	1.4564	1.4564	1.4564	1.4586	1.4564	1.4564
R(1,6)	1.3845	1.3845	1.3846	1.3843	1.3846	1.3845
R(1,7)	1.4581	1.458	1.458	1.4563	1.458	1.458
R(2,3)	1.3819	1.3818	1.3818	1.3822	1.3818	1.3818
R(2,9)	1.4581	1.4581	1.4581	1.4583	1.4581	1.4581
R(3,4)	1.4564	1.4564	1.4565	1.4577	1.4564	1.4565
R(3,11)	1.4581	1.4581	1.4581	1.4571	1.4581	1.4582
R(4,5)	1.3846	1.3845	1.3845	1.3843	1.3846	1.3846
R(4,12)	1.458	1.458	1.4579	1.4571	1.458	1.458
R(5,6)	1.4579	1.4579	1.4579	1.4573	1.4579	1.4579
R(5,15)	1.4572	1.4573	1.4572	1.4576	1.4572	1.4572
R(6,17)	1.4572	1.4572	1.4572	1.4582	1.4572	1.4572
R(7,8)	1.4586	1.4586	1.4587	1.4569	1.4586	1.4586
R(7,19)	1.3824	1.3825	1.3825	1.3827	1.3825	1.3825
R(8,9)	1.4471	1.4473	1.4471	1.4492	1.4471	1.4471
R(8,20)	1.3859	1.3858	1.3858	1.3807	1.3859	1.3858
R(9,10)	1.3836	1.3835	1.3838	1.3852	1.3837	1.3837
R(10,57)	1.4418	1.4419	1.4415	1.4536	1.4417	1.4417
R(10,59)	1.4558	1.4557	1.4555	1.4555	1.4557	1.4558
R(11,29)	1.4471	1.4472	1.4469	1.4571	1.4471	1.4471
R(11,59)	1.3836	1.3837	1.3839	1.3843	1.3837	1.3839
R(12,13)	1.3825	1.3825	1.3825	1.3843	1.3825	1.3825
R(12,29)	1.4586	1.4585	1.4585	1.4577	1.4586	1.4586
R(13,14)	1.4572	1.4573	1.4572	1.4576	1.4572	1.4572
R(13,39)	1.4578	1.4578	1.4579	1.4573	1.4578	1.4578
R(14,15)	1.3843	1.3843	1.3843	1.3837	1.3843	1.3843
R(14,28)	1.4574	1.4575	1.4575	1.4576	1.4574	1.4575
R(15,16)	1.4577	1.4577	1.4577	1.4577	1.4577	1.4577
R(16,17)	1.4577	1.4577	1.4577	1.4573	1.4577	1.4577
R(16,26)	1.3837	1.3837	1.3837	1.3842	1.3837	1.3837
R(17,18)	1.3843	1.3843	1.3843	1.3844	1.3843	1.3843
R(18,19)	1.4572	1.4572	1.4572	1.4563	1.4572	1.4572
R(18,24)	1.4574	1.4574	1.4575	1.4585	1.4574	1.4574
R(19,22)	1.4578	1.4577	1.4578	1.4572	1.4578	1.4577
R(20,21)	1.4567	1.4568	1.4568	1.4548	1.4568	1.4568
R(20,56)	1.4498	1.4499	1.4497	1.4457	1.4496	1.4497
R(21,22)	1.3834	1.3833	1.3833	1.381	1.3833	1.3833
R(21,54)	1.4568	1.4566	1.4566	1.4468	1.4568	1.4567
R(22,23)	1.4577	1.4578	1.4578	1.4492	1.4578	1.4578
R(23,24)	1.4572	1.4572	1.4572	1.4583	1.4572	1.4572
R(23,52)	1.3824	1.3824	1.3825	1.3851	1.3825	1.3825
R(24,25)	1.3843	1.3843	1.3843	1.3822	1.3843	1.3843
R(25,26)	1.4577	1.4577	1.4577	1.4577	1.4577	1.4576
R(25,50)	1.4572	1.4572	1.4572	1.4571	1.4572	1.4572
R(26,27)	1.4577	1.4577	1.4577	1.4571	1.4577	1.4577

Table A.1 (cont.)

parameters	Compd.I	Compd.II	Compd.III	Compd.IV	Compd.V	Compd.VI
R(27,28)	1.3843	1.3843	1.3843	1.3842	1.3843	1.3843
R(27,49)	1.4572	1.4573	1.4572	1.4577	1.4572	1.4572
R(28,38)	1.4572	1.4573	1.4572	1.4574	1.4572	1.4572
R(29,58)	1.3859	1.3858	1.3857	1.3822	1.3859	1.3858
R(30,31)	1.3859	1.3858	1.3858	1.3827	1.3859	1.3857
R(30,37)	1.4586	1.4586	1.4586	1.4563	1.4586	1.4586
R(30,60)	1.4471	1.4469	1.4472	1.4571	1.4471	1.4469
R(31,32)	1.4497	1.4491	1.4492	1.4569	1.4497	1.4492
R(31,40)	1.4567	1.4567	1.4568	1.4563	1.4568	1.4568
R(32,33)	1.4058	1.4088	1.4059	1.3807	1.4054	1.4072
R(32,41)	1.4924	1.4948	1.4937	1.4491	1.4923	1.4935
R(33,34)	1.4416	1.442	1.4423	1.4548	1.4417	1.4419
R(33,44)	1.4854	1.4869	1.4858	1.4458	1.4863	1.4882
R(34,46)	1.4557	1.4555	1.4558	1.4466	1.4558	1.4554
R(34,60)	1.3836	1.3838	1.3839	1.3809	1.3837	1.3839
R(35,36)	1.4564	1.4565	1.4565	1.4582	1.4564	1.4565
R(35,48)	1.3818	1.3818	1.3818	1.385	1.3818	1.3818
R(35,60)	1.4581	1.4583	1.4584	1.4492	1.4581	1.4582
R(36,37)	1.4581	1.458	1.458	1.4585	1.458	1.458
R(36,49)	1.3845	1.3845	1.3846	1.3823	1.3846	1.3846
R(37,38)	1.3825	1.3824	1.3826	1.3844	1.3825	1.3825
R(38,39)	1.4578	1.4578	1.4577	1.4582	1.4578	1.4578
R(39,40)	1.3834	1.3833	1.3833	1.3843	1.3833	1.3833
R(40,58)	1.4568	1.4564	1.4566	1.4585	1.4568	1.4566
R(41,42)	1.4059	1.4069	1.4065	1.3852	1.4054	1.4064
R(41,58)	1.4498	1.4489	1.4488	1.4583	1.4497	1.449
R(42,43)	1.4858	1.4845	1.4881	1.4538	1.4864	1.4859
R(42,59)	1.4418	1.4417	1.4416	1.4555	1.4416	1.442
R(43,44)	1.8159	1.8259	1.8174	1.4103	1.8104	1.8175
R(43,57)	1.4858	1.4855	1.4873	1.495	1.4863	1.4855
R(43,61)	1.5042	1.5071	1.5027	1.4713	1.506	1.5087
R(44,45)	1.4858	1.4854	1.485	1.4712	1.4863	1.487
R(44,61)	1.5049	1.5052	1.5047	1.9546	1.506	1.5073
R(45,46)	1.4419	1.4414	1.4413	1.4894	1.4417	1.4414
R(45,55)	1.4057	1.4056	1.4052	1.4105	1.4054	1.4057
R(46,47)	1.3836	1.3835	1.3835	1.4534	1.3837	1.3837
R(47,48)	1.4582	1.458	1.4579	1.494	1.4581	1.458
R(47,53)	1.4471	1.4472	1.4473	1.4555	1.4471	1.447
R(48,51)	1.4564	1.4565	1.4565	1.4571	1.4564	1.4565
R(49,50)	1.4579	1.458	1.4579	1.3843	1.4579	1.4579
R(50,51)	1.3845	1.3845	1.3845	1.4555	1.3846	1.3845
R(51,52)	1.4581	1.458	1.4581	1.4532	1.458	1.458
R(52,53)	1.4586	1.4586	1.4585	1.4103	1.4586	1.4586
R(53,54)	1.3859	1.3858	1.3858	1.4708	1.3859	1.3858
R(54,55)	1.4499	1.4497	1.4496	1.4695	1.4496	1.4496
R(55,56)	1.4926	1.4923	1.4924	1.4905	1.4923	1.4924
R(56,57)	1.4056	1.4055	1.406	1.4096	1.4055	1.4054

Table A.1 (cont.)

parameters	Compd.I	Compd.II	Compd.III	Compd.IV	Compd.V	Compd.VI
A(2,1,6)	119.835	119.8354	119.8444	120.0932	119.8385	119.8436
A(2,1,7)	107.8365	107.8366	107.83	107.8441	107.8374	107.8367
A(6,1,7)	120.077	120.0743	120.0744	119.8061	120.076	120.0727
A(1,2,3)	120.1336	120.1262	120.1183	119.9094	120.1271	120.1313
A(1,2,9)	107.8629	107.8731	107.8877	108.0855	107.8685	107.8705
A(3,2,9)	119.7748	119.7771	119.7737	119.8698	119.7779	119.7674
A(2,3,4)	120.1248	120.1302	120.1333	120.0698	120.1294	120.1158
A(2,3,11)	119.7754	119.7565	119.7484	119.7155	119.7751	119.7822
A(4,3,11)	107.8665	107.8692	107.8782	108.1213	107.8668	107.8808
A(3,4,5)	119.8377	119.8383	119.8419	120.0078	119.8377	119.8496
A(3,4,12)	107.8369	107.8472	107.8457	107.9476	107.8373	107.8373
A(5,4,12)	120.0768	120.0636	120.0573	120.0023	120.0762	120.0706
A(4,5,6)	120.0361	120.0313	120.0259	119.9978	120.0335	120.0309
A(4,5,15)	119.9243	119.927	119.9257	119.9937	119.9229	119.9271
A(6,5,15)	107.9977	107.9998	108.0027	107.9987	108.0001	107.9979
A(1,6,5)	120.0327	120.0386	120.0362	119.9178	120.0337	120.0288
A(1,6,17)	119.9227	119.9292	119.9306	120.0497	119.9234	119.9276
A(5,6,17)	108.0012	107.9975	107.9943	107.9988	107.9994	108.0005
A(1,7,8)	108.0109	108.0075	107.9998	107.8257	108.0049	108.0046
A(1,7,19)	119.9274	119.9228	119.9211	120.1535	119.9278	119.9275
A(8,7,19)	119.8968	119.9061	119.9099	119.7094	119.9008	119.9127
A(7,8,9)	107.9666	107.975	107.994	108.4381	107.978	107.9798
A(7,8,20)	120.5596	120.5589	120.5431	120.4374	120.5485	120.5465
A(9,8,20)	119.077	119.0662	119.0552	119.0357	119.0715	119.0711
A(2,9,8)	108.323	108.3076	108.2884	107.804	108.3111	108.3083
A(2,9,10)	120.4468	120.4604	120.4787	120.7253	120.4494	120.442
A(8,9,10)	119.2322	119.2405	119.2526	119.1299	119.2498	119.2564
A(9,10,57)	122.3408	122.3556	122.3641	121.9885	122.3402	122.3254
A(9,10,59)	119.7825	119.772	119.7518	119.0398	119.7698	119.8111
A(57,10,59)	108.4157	108.3505	108.3665	108.9162	108.4065	108.3645
A(3,11,29)	108.3178	108.2957	108.2781	107.8501	108.3145	108.2845
A(3,11,59)	120.449	120.4653	120.4776	120.1246	120.4461	120.4626
A(29,11,59)	119.2433	119.2834	119.2994	120.12	119.2473	119.2824
A(4,12,13)	119.9244	119.9409	119.9515	120.0026	119.9284	119.9309
A(4,12,29)	108.0106	107.9897	107.9744	107.9474	108.0064	107.9937
A(13,12,29)	119.9022	119.8855	119.8789	120.0068	119.8987	119.9092
A(12,13,14)	120.0701	120.0625	120.0582	119.9941	120.0655	120.0671
A(12,13,39)	119.785	119.8088	119.8217	119.9946	119.7925	119.7965
A(14,13,39)	108.0778	108.0719	108.0676	108.0008	108.0763	108.066
A(13,14,15)	120.0066	119.999	119.9976	120.0022	120.0089	120.0038
A(13,14,28)	107.9793	107.9778	107.9754	108.0092	107.9781	107.9834
A(15,14,28)	120.0012	120.0095	120.014	120.0017	120.0036	120.0032
A(5,15,14)	119.996	120.0052	120.008	120.0036	119.9965	119.9989
A(5,15,16)	108.0034	108.0025	108.0021	108.0091	108.0025	108.0046
A(14,15,16)	119.9874	119.9815	119.9792	120.0045	119.9857	119.9823
A(15,16,17)	107.9955	107.9937	107.992	108.0023	107.9948	107.9926
A(15,16,26)	120.0108	120.0092	120.0069	119.9933	120.0103	120.0135

Table A.1 (cont.)

parameters	Compd.I	Compd.II	Compd.III	Compd.IV	Compd.V	Compd.VI
A(17,16,26)	120.0091	120.014	120.015	120.0005	120.0109	120.0141
A(6,17,16)	108.0017	108.006	108.0084	107.9902	108.0028	108.004
A(6,17,18)	119.9966	119.9936	119.9921	120.0598	119.9963	119.9959
A(16,17,18)	119.9849	119.9863	119.9832	119.9201	119.9855	119.9841
A(17,18,19)	120.0084	120.0042	120.003	119.8202	120.0083	120.0063
A(17,18,24)	120.0053	119.9994	120.0012	120.0894	120.0031	120.0011
A(19,18,24)	107.9764	107.9823	107.9835	107.8444	107.9791	107.982
A(7,19,18)	120.0663	120.0741	120.0771	120.1099	120.0666	120.0683
A(7,19,22)	119.7875	119.7832	119.79	119.7476	119.792	119.7842
A(18,19,22)	108.0785	108.0716	108.0679	107.8473	108.0752	108.0712
A(8,20,21)	119.2142	119.2003	119.2159	119.8944	119.2246	119.2114
A(8,20,56)	121.6398	121.6348	121.621	122.5574	121.6127	121.6189
A(21,20,56)	108.7754	108.7877	108.7959	108.1124	108.7703	108.7806
A(20,21,22)	120.4222	120.4437	120.4377	119.7288	120.4186	120.4377
A(20,21,54)	107.8314	107.8236	107.8282	108.1438	107.8313	107.8246
A(22,21,54)	120.4343	120.4012	120.4036	122.6249	120.4174	120.4063
A(19,22,21)	120.1109	120.0987	120.0942	120.482	120.1073	120.099
A(19,22,23)	107.8815	107.8879	107.8909	108.3894	107.8836	107.8889
A(21,22,23)	120.1097	120.1112	120.1072	119.078	120.108	120.1056
A(22,23,24)	108.0776	108.0732	108.072	107.846	108.0752	108.0723
A(22,23,52)	119.7802	119.799	119.7984	119.0981	119.7912	119.7983
A(24,23,52)	120.0679	120.0632	120.0604	120.699	120.0652	120.0646
A(18,24,23)	107.978	107.977	107.9778	108.0706	107.9793	107.9779
A(18,24,25)	120.0013	120.006	120.007	119.9104	120.0024	120.0062
A(23,24,25)	120.008	120.0033	120.002	119.8778	120.0081	120.0047
A(24,25,26)	119.9847	119.985	119.9823	120.0738	119.9855	119.9828
A(24,25,50)	119.9961	120.0004	120.004	119.7227	119.9974	119.999
A(26,25,50)	108.0048	108.0013	108.0007	108.1115	108.0025	108.0033
A(16,26,25)	120.0137	120.0084	120.0102	120.0018	120.0116	120.0107
A(16,26,27)	120.0094	120.0159	120.0201	120.0011	120.012	120.0125
A(25,26,27)	107.9953	107.995	107.9919	107.9516	107.9945	107.9928
A(26,27,28)	119.9864	119.9822	119.9825	120.0053	119.9858	119.981
A(26,27,49)	108.0012	108.0064	108.0091	107.9488	108.0031	108.0059
A(28,27,49)	120.0029	119.9978	119.9928	120.0016	119.9962	119.9989
A(14,28,27)	120.0037	120.0007	119.9964	119.9928	120.0017	120.0064
A(14,28,38)	107.9756	107.9829	107.9908	108.0002	107.9797	107.9806
A(27,28,38)	120.0055	120.0008	120.0037	120.0013	120.0086	120.0018
A(11,29,12)	107.968	107.998	108.0235	108.1209	107.9747	108.0035
A(11,29,58)	119.0797	119.072	119.0578	119.7167	119.0767	119.0547
A(12,29,58)	120.5604	120.5333	120.514	120.0763	120.5492	120.5204
A(31,30,37)	120.5591	120.5556	120.5248	120.1202	120.5493	120.5343
A(31,30,60)	119.0939	119.0385	119.0312	119.731	119.0744	119.0277
A(37,30,60)	107.9641	108.0148	108.0101	107.849	107.9768	108.0156
A(30,31,32)	121.6157	121.6319	121.5688	119.7116	121.6124	121.6075
A(30,31,40)	119.2257	119.2171	119.2182	120.1496	119.2203	119.2443
A(32,31,40)	108.7669	108.8289	108.8037	107.8334	108.7718	108.8033
A(31,32,33)	119.2238	119.3569	119.4549	120.458	119.2647	119.4045

Table A.1 (cont.)

parameters	Compd.I	Compd.II	Compd.III	Compd.IV	Compd.V	Compd.VI
A(31,32,41)	107.3144	107.2081	107.2312	108.4316	107.2993	107.2488
A(33,32,41)	121.7325	121.8926	121.5815	119.0341	121.711	121.8269
A(32,33,34)	118.2239	117.9283	117.9756	119.8627	118.1859	117.941
A(32,33,44)	124.8857	124.8812	124.9163	122.6079	124.8201	125.0074
A(34,33,44)	107.8156	107.8176	107.8243	108.1205	107.8162	107.8757
A(33,34,46)	108.3839	108.3844	108.3826	108.1471	108.4033	108.3856
A(33,34,60)	122.3208	122.4443	122.397	119.7435	122.3322	122.4376
A(46,34,60)	119.8257	119.6726	119.6474	122.6443	119.7727	119.695
A(36,35,48)	120.1362	120.1189	120.0942	120.7036	120.1259	120.1142
A(36,35,60)	107.856	107.8806	107.8916	107.8513	107.8687	107.8847
A(48,35,60)	119.7564	119.7713	119.8094	119.0854	119.778	119.7757
A(35,36,37)	107.8425	107.8392	107.8331	108.0667	107.8367	107.8354
A(35,36,49)	119.8354	119.8371	119.8576	119.8695	119.8406	119.8482
A(37,36,49)	120.0706	120.0719	120.0749	119.9138	120.0762	120.069
A(30,37,36)	108.0086	107.9838	107.9967	107.8449	108.0062	107.9864
A(30,37,38)	119.8909	119.8965	119.9311	119.814	119.9037	119.9025
A(36,37,38)	119.9364	119.9287	119.918	120.0877	119.9275	119.932
A(28,38,37)	120.0617	120.0718	120.0771	119.9198	120.0664	120.0696
A(28,38,39)	108.08	108.0683	108.0617	107.9932	108.0756	108.0683
A(37,38,39)	119.7912	119.7933	119.7825	120.0578	119.7889	119.7972
A(13,39,38)	107.8796	107.8913	107.8969	107.9958	107.8827	107.894
A(13,39,40)	120.1097	120.1005	120.1077	119.9183	120.1096	120.0973
A(38,39,40)	120.1183	120.0994	120.0847	120.0544	120.1074	120.0984
A(31,40,39)	120.4066	120.4289	120.4501	119.8033	120.4221	120.4139
A(31,40,58)	107.8341	107.8479	107.8425	107.8401	107.8309	107.8365
A(39,40,58)	120.4277	120.3994	120.3611	120.0978	120.4151	120.4137
A(32,41,42)	121.7482	121.6529	121.848	119.1134	121.7273	121.6165
A(32,41,58)	107.2829	107.304	107.3366	107.8063	107.3084	107.3171
A(42,41,58)	119.2515	119.3592	119.3981	120.7342	119.2552	119.3915
A(41,42,43)	124.8322	124.9843	124.9734	121.995	124.8125	124.8424
A(41,42,59)	118.1676	118.0737	118.0413	119.0286	118.1951	118.0368
A(43,42,59)	107.7798	107.8423	107.8702	108.9261	107.8162	107.847
A(42,43,44)	112.9227	112.921	112.5934	118.6744	112.9556	113.1923
A(42,43,57)	105.5596	105.4738	105.2719	107.1364	105.4931	105.454
A(42,43,61)	127.1653	127.4409	127.9415	122.8882	127.2026	127.4398
A(44,43,57)	112.8772	112.7976	112.8744	118.1645	112.9571	112.9488
A(57,43,61)	127.1608	126.999	126.7087	107.3437	127.1711	126.968
A(33,44,43)	112.8569	112.6802	113.1046	125.231	112.9658	112.5278
A(33,44,45)	105.5331	105.3878	105.4354	106.3251	105.4974	105.224
A(33,44,61)	127.1992	127.2927	127.8395	111.2844	127.191	127.4251
A(43,44,45)	112.9581	112.7316	112.9422	125.66	112.9699	112.7142
A(45,44,61)	127.1561	127.2494	126.6067	111.0072	127.1764	127.2813
A(44,45,46)	107.7812	107.8921	107.9225	127.8074	107.8137	107.9533
A(44,45,55)	124.7969	124.858	124.8152	107.2793	124.8145	124.8874
A(46,45,55)	118.151	118.2162	118.2853	118.0105	118.1823	118.1609
A(34,46,45)	108.4045	108.354	108.3226	125.6622	108.4065	108.3489
A(34,46,47)	119.7261	119.8467	119.8991	118.8466	119.7781	119.8336

Table A.1 (cont.)

parameters	Compd.I	Compd.II	Compd.III	Compd.IV	Compd.V	Compd.VI
A(45,46,47)	122.3788	122.3185	122.2725	122.7358	122.3303	122.3495
A(46,47,48)	120.466	120.4573	120.4195	107.1614	120.4473	120.4532
A(46,47,53)	119.2262	119.2494	119.2557	121.9558	119.2496	119.2513
A(48,47,53)	108.3141	108.311	108.316	119.0798	108.3115	108.3032
A(35,48,47)	119.7896	119.7415	119.7394	108.9026	119.7755	119.7477
A(35,48,51)	120.1203	120.1452	120.1497	120.0719	120.1282	120.1372
A(47,48,51)	107.8691	107.8709	107.8623	108.1138	107.8678	107.8747
A(27,49,36)	119.9212	119.9272	119.9319	119.7265	119.9234	119.9272
A(27,49,50)	108.0023	107.9922	107.9914	107.8622	107.9993	107.9958
A(36,49,50)	120.0323	120.0369	120.0366	120.1126	120.0331	120.0317
A(25,50,49)	107.996	108.0046	108.0065	120.1155	108.0001	108.0017
A(25,50,51)	119.9226	119.9251	119.927	120.4875	119.9231	119.926
A(49,50,51)	120.0353	120.0364	120.0218	107.8271	120.0322	120.0294
A(48,51,50)	119.8406	119.8255	119.8401	120.4982	119.84	119.8392
A(48,51,52)	107.8331	107.8374	107.8455	119.0726	107.838	107.8355
A(50,51,52)	120.0775	120.0683	120.0627	121.9481	120.075	120.069
A(23,52,51)	119.9262	119.9378	119.942	108.8856	119.9295	119.935
A(23,52,53)	119.9042	119.885	119.8946	107.1958	119.9015	119.8946
A(51,52,53)	108.011	108.001	107.998	122.6575	108.0046	107.9971
A(47,53,52)	107.9727	107.9795	107.978	118.8442	107.9779	107.9894
A(47,53,54)	119.066	119.073	119.0978	118.029	119.0749	119.0607
A(52,53,54)	120.5644	120.5502	120.5364	107.2407	120.547	120.5405
A(21,54,53)	119.1987	119.244	119.2511	125.514	119.2267	119.2457
A(21,54,55)	108.7882	108.7763	108.759	111.3626	108.7673	108.78
A(53,54,55)	121.6465	121.6276	121.6013	111.3906	121.6103	121.6199
A(45,55,54)	119.2391	119.221	119.2153	106.427	119.2685	119.2647
A(45,55,56)	121.7488	121.8731	121.7581	127.7967	121.719	121.7985
A(54,55,56)	107.2749	107.3179	107.3382	125.6137	107.308	107.3015
A(20,56,55)	107.3069	107.2718	107.2563	107.3475	107.3006	107.2902
A(20,56,57)	119.2152	119.2413	119.2767	118.2551	119.2734	119.2535
A(55,56,57)	121.8042	121.8179	121.8686	125.2911	121.7201	121.667
A(10,57,43)	107.7723	107.8149	107.9259	107.1704	107.8152	107.8673
A(10,57,56)	118.2036	118.1725	118.1234	118.6527	118.1672	118.2037
A(43,57,56)	124.8207	124.8687	124.6951	122.8113	124.8185	124.9031
A(29,58,40)	119.2067	119.2639	119.3072	119.9021	119.2267	119.2542
A(29,58,41)	121.6193	121.5766	121.5647	119.866	121.614	121.5774
A(40,58,41)	108.779	108.7872	108.7637	108.0859	108.767	108.7716
A(10,59,11)	119.7713	119.7687	119.7697	120.5077	119.7815	119.7345
A(10,59,42)	108.3999	108.358	108.4029	107.8227	108.405	108.3739
A(11,59,42)	122.3488	122.3534	122.3453	120.5169	122.3277	122.3678
A(30,60,34)	119.2435	119.2888	119.2898	120.4927	119.248	119.2821
A(30,60,35)	108.3287	108.2814	108.2684	108.3859	108.3115	108.2777
A(34,60,35)	120.436	120.5106	120.4851	119.0831	120.4483	120.4947
D(6,1,2,3)	-0.0063	-0.0061	-0.0106	0.5138	0.0011	-0.0088
D(6,1,2,9)	-142.224	-142.232	142.2403	-141.884	-142.221	-142.221
D(7,1,2,3)	142.3146	142.3107	142.3088	142.708	142.3259	142.3159
D(2,1,6,5)	0.0098	0.0067	-0.0014	-0.6277	0.0004	0.0061

Table A.1 (cont.)

parameters	Compd.I	Compd.II	Compd.III	Compd.IV	Compd.V	Compd.VI
D(2,1,6,17)	138.1344	138.1431	138.1274	137.5107	138.1243	138.1308
D(7,1,6,5)	-137.738	-137.738	137.7469	-138.371	-137.753	-137.748
D(2,1,7,8)	-0.1178	-0.1216	-0.1125	0.0073	-0.1088	-0.1101
D(2,1,7,19)	-142.484	-142.493	142.4779	-142.072	-142.474	-142.495
D(6,1,7,8)	142.0951	142.0886	142.1042	142.3295	142.1101	142.1124
D(1,2,3,4)	-0.0047	-0.0023	0.0199	0.0562	-0.0027	0.0069
D(1,2,3,11)	-137.792	-137.774	137.7611	-138.04	-137.797	-137.803
D(9,2,3,4)	137.7872	137.8014	137.8342	138.0757	137.7948	137.799
D(1,2,9,8)	-0.0398	-0.0157	-0.0153	-0.5093	-0.0595	-0.0579
D(1,2,9,10)	142.2745	142.3095	142.3281	141.2705	142.2722	142.2718
D(3,2,9,8)	-142.417	-142.397	142.3985	-142.925	-142.437	-142.432
D(2,3,4,5)	0.0122	0.0101	-0.0176	-0.5085	0.0029	-0.0027
D(2,3,4,12)	-142.312	-142.307	142.3258	-143.073	-142.321	-142.332
D(11,3,4,5)	142.2245	142.2003	142.1749	141.8784	142.2209	142.2291
D(2,3,11,29)	142.4171	142.4163	142.439	143.6522	142.433	142.442
D(2,3,11,59)	0.0876	0.0265	0.0296	0.867	0.1049	0.073
D(4,3,11,29)	0.0491	0.0596	0.075	1.1088	0.0571	0.0617
D(3,4,5,6)	-0.0087	-0.0095	0.0056	0.3942	-0.0013	0
D(3,4,5,15)	-138.134	-138.136	138.1163	-137.78	-138.125	-138.122
D(12,4,5,6)	137.7435	137.7436	137.7515	138.4994	137.7509	137.7616
D(3,4,12,13)	142.484	142.4639	142.4574	142.5652	142.4747	142.4696
D(3,4,12,29)	0.1129	0.1291	0.1411	-0.0002	0.1101	0.1011
D(5,4,12,13)	0.2662	0.2477	0.2452	-0.0017	0.2569	0.2386
D(4,5,6,1)	-0.0023	0.0011	0.0037	0.1748	-0.0003	-0.0019
D(4,5,6,17)	-142.535	-142.545	142.5377	-142.426	-142.533	-142.537
D(15,5,6,1)	142.5329	142.5374	142.5349	142.782	142.5322	142.5316
D(4,5,15,14)	0.1159	0.1225	0.113	-0.3249	0.1151	0.1134
D(4,5,15,16)	142.7162	142.7233	142.7126	142.3226	142.7119	142.7103
D(6,5,15,14)	-142.469	-142.46	142.4625	-142.934	-142.466	-142.466
D(1,6,17,16)	-142.713	-142.721	142.7147	-142.549	-142.711	-142.705
D(1,6,17,18)	-0.1189	-0.1222	-0.1198	-0.0013	-0.1144	-0.1098
D(5,6,17,16)	-0.132	-0.1262	-0.1266	-0.0064	-0.1295	-0.1253
D(1,7,8,9)	0.0934	0.1121	0.1032	-0.3242	0.0722	0.0745
D(1,7,8,20)	-141.607	-141.58	141.5756	-142.444	-141.62	-141.617
D(19,7,8,9)	142.473	142.4911	142.4736	141.954	142.4494	142.466
D(1,7,19,18)	-0.113	-0.1098	-0.1219	-0.0323	-0.1179	-0.0983
D(1,7,19,22)	138.0052	138.0005	137.9962	137.6544	138.001	138.0039
D(8,7,19,18)	-138.059	-138.056	138.057	-137.686	-138.059	-138.056
D(7,8,9,2)	-0.0332	-0.0596	-0.0543	0.5151	-0.0079	-0.0102
D(7,8,9,10)	-142.881	-142.92	142.9358	-141.979	-142.866	-142.86
D(20,8,9,2)	142.33	142.2998	142.29	143.2505	142.3447	142.3408
D(7,8,20,21)	-0.9872	-1.0195	-1.0226	0.1453	-0.9692	-0.9734
D(7,8,20,56)	140.0642	140.0254	140.042	142.5662	140.0445	140.0493
D(9,8,20,21)	-138.566	-138.597	138.5962	-138.078	-138.545	-138.549
D(2,9,10,57)	-142.367	-142.296	142.39	-140.198	-142.336	-142.246
D(2,9,10,59)	0.116	0.0563	-0.0248	1.4274	0.1036	0.1524
D(8,9,10,57)	-4.0517	-3.9765	-4.0612	-2.6014	-4.0128	-3.9291

Table A.1 (cont.)

parameters	Compd.I	Compd.II	Compd.III	Compd.IV	Compd.V	Compd.VI
D(9,10,57,43)	155.0185	155.1003	155.0761	143.9851	154.9543	155.0735
D(9,10,57,56)	6.5556	6.5279	6.7297	-0.6151	6.4832	6.3079
D(59,10,57,43)	8.8729	9.0586	9.0344	-1.0033	8.8494	8.9795
D(9,10,59,11)	-0.0278	0.0003	0.1072	-0.5719	0.0024	-0.09
D(9,10,59,42)	-147.161	-147.072	147.0218	-144.525	-147.114	-147.163
D(57,10,59,11)	147.132	147.0701	147.1879	145.6074	147.1274	147.0032
D(3,11,29,12)	0.0208	0.0204	0.0124	-1.109	0.0111	0.0009
D(3,11,29,58)	-142.349	-142.334	142.3251	-143.665	-142.345	-142.317
D(59,11,29,12)	142.8794	142.9283	142.9382	141.6782	142.8652	142.8876
D(3,11,59,10)	-0.0742	-0.0421	-0.1095	-0.577	-0.1067	-0.0232
D(3,11,59,42)	142.3696	142.3165	142.3317	138.86	142.3289	142.3333
D(29,11,59,10)	-138.4	-138.411	138.4879	-138.852	-138.428	-138.366
D(4,12,13,14)	0.1163	0.1473	0.137	-0.3215	0.1174	0.1307
D(4,12,13,39)	-138.002	-137.985	137.9998	-138.496	-138.003	-137.979
D(29,12,13,14)	138.0653	138.0563	138.0232	137.7824	138.0593	138.0681
D(4,12,29,11)	-0.0828	-0.0925	-0.095	0.6865	-0.075	-0.0631
D(4,12,29,58)	141.6247	141.6082	141.5915	143.0833	141.6221	141.599
D(13,12,29,11)	-142.464	-142.452	142.4435	-141.877	-142.453	-142.441
D(12,13,14,15)	-0.3824	-0.4074	-0.3942	0.3215	-0.3752	-0.3779
D(12,13,14,28)	-142.987	-143.015	143.0041	-142.32	-142.985	-142.988
D(39,13,14,15)	142.0653	142.0637	142.0878	142.9282	142.0774	142.0697
D(12,13,39,38)	143.4433	143.4599	143.4428	142.4236	143.4346	143.4338
D(12,13,39,40)	0.6396	0.6848	0.6763	-0.1819	0.6457	0.6607
D(14,13,39,38)	0.8696	0.8768	0.8565	-0.1829	0.8614	0.8666
D(13,14,15,5)	0.266	0.2718	0.2686	0.0017	0.2586	0.2554
D(13,14,15,16)	-137.905	-137.903	137.9055	-138.218	-137.909	-137.915
D(28,14,15,5)	138.4281	138.4322	138.429	138.2147	138.4255	138.424
D(13,14,28,27)	142.6053	142.6032	142.5992	142.3341	142.6113	142.6141
D(13,14,28,38)	0.0019	0.0018	-0.0125	-0.2818	-0.0005	0.0068
D(15,14,28,27)	-0.0018	0.0005	-0.0035	-0.3071	-0.0013	0.0036
D(5,15,16,17)	-0.2133	-0.2189	-0.2154	0.2824	-0.2106	-0.2084
D(5,15,16,26)	-142.86	-142.869	142.8619	-142.336	-142.858	-142.863
D(14,15,16,17)	142.3908	142.3923	142.397	142.9296	142.3909	142.3959
D(15,16,17,6)	0.2134	0.2133	0.2114	-0.1705	0.2102	0.2062
D(15,16,17,18)	-142.386	-142.389	142.3874	-142.78	-142.391	-142.394
D(26,16,17,6)	142.8604	142.8611	142.8543	142.4443	142.8575	142.8604
D(15,16,26,25)	138.2141	138.216	138.213	137.7951	138.2134	138.2168
D(15,16,26,27)	-0.0016	-0.001	-0.0071	-0.3069	-0.0015	0.0056
D(17,16,26,25)	0.0029	0.0033	0.0055	-0.3896	0.0017	-0.0007
D(6,17,18,19)	-0.2643	-0.27	-0.2625	0.2187	-0.2579	-0.2605
D(6,17,18,24)	-138.43	-138.431	138.4273	-137.54	-138.425	-138.427
D(16,17,18,19)	137.9005	137.9007	137.9058	138.3594	137.9096	137.9066
D(17,18,19,7)	0.3805	0.3861	0.3838	-0.2017	0.3744	0.3647
D(17,18,19,22)	-142.068	-142.055	142.0681	-142.321	-142.077	-142.07
D(24,18,19,7)	142.9908	142.9886	142.9898	142.1323	142.9843	142.9726
D(17,18,24,23)	142.6135	142.6042	142.6062	141.911	142.6125	142.6097
D(17,18,24,25)	0.0057	-0.0003	0.0015	-0.4821	0.0011	0.0013

Table A.1 (cont.)

parameters	Compd.I	Compd.II	Compd.III	Compd.IV	Compd.V	Compd.VI
D(19,18,24,23)	0.0019	-0.0005	-0.0006	-0.3029	0.0003	-0.0005
D(7,19,22,21)	-0.657	-0.6653	-0.6674	0.1864	-0.6458	-0.6481
D(7,19,22,23)	-143.45	-143.454	143.4474	-141.997	-143.434	-143.429
D(18,19,22,21)	141.9143	141.9045	141.9112	142.4674	141.9271	141.9124
D(8,20,21,22)	0.385	0.4035	0.4118	0.0413	0.3791	0.3669
D(8,20,21,54)	144.0883	144.0657	144.0769	147.2311	144.0472	144.0316
D(56,20,21,22)	-145.194	-145.165	145.1659	-147.22	-145.158	-145.178
D(8,20,56,55)	-143.7	-143.622	143.6319	-156.274	-143.635	-143.604
D(8,20,56,57)	0.0769	0.1635	0.2659	-7.5123	0.0627	-0.0378
D(21,20,56,55)	0.8851	0.9482	0.9602	-10.0725	0.9217	0.9526
D(20,21,22,19)	0.4384	0.4404	0.4348	-0.2068	0.4298	0.4453
D(20,21,22,23)	138.7368	138.7347	138.722	138.0544	138.7241	138.7335
D(54,21,22,19)	-138.749	-138.713	138.7223	-142.517	-138.725	-138.709
D(20,21,54,53)	-144.061	-144.12	144.0726	-138.573	-144.044	-144.101
D(20,21,54,55)	1.5272	1.4809	1.4644	10.1051	1.487	1.4933
D(22,21,54,53)	-0.3632	-0.4391	-0.3928	7.4622	-0.3754	-0.423
D(19,22,23,24)	0.8798	0.8838	0.8685	-0.4708	0.8613	0.868
D(19,22,23,52)	143.4432	143.4572	143.4347	141.9946	143.4309	143.4416
D(21,22,23,24)	-141.914	-141.899	141.9058	-143.271	-141.9265	-141.91
D(22,23,24,18)	-0.5456	-0.5466	-0.537	0.4779	-0.5332	-0.5367
D(22,23,24,25)	142.0592	142.0591	142.0699	142.8855	142.0756	142.0723
D(52,23,24,18)	-142.982	-143.003	142.9875	-141.271	-142.9817	-142.993
D(22,23,52,51)	-137.998	-138.004	138.0051	-138.999	-138.0007	-137.998
D(22,23,52,53)	-0.0425	-0.0784	-0.0649	2.5519	-0.0566	-0.0703
D(24,23,52,51)	0.1099	0.1172	0.1083	-1.4093	0.115	0.1218
D(18,24,25,26)	0.258	0.2627	0.2594	-0.0739	0.2566	0.2579
D(18,24,25,50)	138.4277	138.4328	138.4298	138.0206	138.4253	138.4264
D(23,24,25,26)	-137.904	-137.897	137.9018	-138.079	-137.9097	-137.906
D(24,25,26,16)	-0.2623	-0.2642	-0.263	0.5084	-0.2581	-0.2582
D(24,25,26,27)	142.3879	142.3899	142.3965	143.0687	142.3927	142.3901
D(50,25,26,16)	-142.865	-142.87	142.8707	-141.883	-142.861	-142.861
D(24,25,50,49)	-142.467	-142.463	142.4599	-143.637	-142.4672	-142.46
D(24,25,50,51)	0.1119	0.1325	0.1153	-0.8589	0.1121	0.1205
D(26,25,50,49)	0.1311	0.1361	0.1383	-1.0912	0.1304	0.1361
D(16,26,27,28)	0.2568	0.2593	0.2585	-0.0047	0.2583	0.2519
D(16,26,27,49)	142.8685	142.864	142.8586	142.557	142.8603	142.8562
D(25,26,27,28)	-142.395	-142.392	142.3966	-142.565	-142.3924	-142.396
D(26,27,28,14)	-0.2551	-0.259	-0.2531	0.3118	-0.2569	-0.2565
D(26,27,28,38)	137.9021	137.9004	137.9192	138.493	137.9097	137.9086
D(49,27,28,14)	-138.431	-138.431	138.4228	-137.791	-138.4253	-138.427
D(26,27,49,36)	-142.715	-142.711	142.7044	-143.07	-142.7094	-142.703
D(26,27,49,50)	-0.1354	-0.129	-0.118	-0.6717	-0.1291	-0.1247
D(28,27,49,36)	-0.1109	-0.1133	-0.1089	-0.5066	-0.1119	-0.1061
D(14,28,38,37)	142.9869	142.992	142.9729	142.7787	142.9803	142.9846
D(14,28,38,39)	0.5363	0.5407	0.5425	0.1687	0.5336	0.5294
D(27,28,38,37)	0.3843	0.3907	0.3644	0.1665	0.3716	0.3753
D(11,29,58,40)	138.5464	138.543	138.6347	138.0309	138.5456	138.5184

Table A.1 (cont.)

parameters	Compd.I	Compd.II	Compd.III	Compd.IV	Compd.V	Compd.VI
D(11,29,58,41)	-2.4659	-2.5109	-2.4242	0.0271	-2.4668	-2.489
D(12,29,58,40)	0.9599	0.9514	1.0449	-0.076	0.9675	0.961
D(37,30,31,32)	140.0538	140.1248	140.0208	137.7088	140.0453	140.0486
D(37,30,31,40)	-0.9597	-1.0269	-0.9774	0.0428	-0.9638	-1.0561
D(60,30,31,32)	2.4555	2.5186	2.4796	0.0282	2.4665	2.4884
D(31,30,37,36)	-141.639	-141.578	141.5854	-142.137	-141.624	-141.573
D(31,30,37,38)	0.7454	0.7663	0.8024	0.1866	0.7581	0.7881
D(60,30,37,36)	0.0859	0.1162	0.0507	-0.031	0.0722	0.0763
D(31,30,60,34)	-0.485	-0.645	-0.5976	-0.1875	-0.5071	-0.6076
D(31,30,60,35)	142.366	142.3286	142.3154	142.014	142.3475	142.325
D(37,30,60,34)	-142.865	-143.017	142.9022	-142.468	-142.863	-142.931
D(30,31,32,33)	0.0147	0.2632	0.1121	0.1845	0.0425	0.2079
D(30,31,32,41)	-143.66	-143.714	143.4854	-141.95	-143.6267	-143.773
D(40,31,32,33)	144.5727	144.9244	144.6447	142.4692	144.5932	144.8447
D(30,31,40,39)	0.3804	0.4431	0.3456	-0.2486	0.3727	0.4702
D(30,31,40,58)	144.055	144.1172	143.9723	142.0724	144.041	144.1332
D(32,31,40,39)	-145.159	-145.206	145.1519	-142.338	-145.16	-145.134
D(31,32,33,34)	-4.2914	-4.7263	-4.4076	-0.2372	-4.3434	-4.5978
D(31,32,33,44)	-147.187	-147.072	146.9176	-142.708	-147.0515	-147.318
D(41,32,33,34)	134.0316	133.8464	133.8824	138.0018	133.9811	134.0271
D(31,32,41,42)	142.6189	142.6805	142.8886	141.9683	142.6003	142.7847
D(31,32,41,58)	0.0276	-0.0054	-0.1736	-0.5231	-0.0063	0.0712
D(33,32,41,42)	0.0525	-0.1824	0.2315	-0.7915	0.0115	-0.1338
D(32,33,34,46)	-139.739	-139.282	139.4822	-147.176	-139.6433	-139.443
D(32,33,34,60)	6.4082	6.7588	6.4339	0.0776	6.4497	6.6327
D(44,33,34,46)	8.9437	8.9569	8.9015	0.1455	8.8601	9.1387
D(32,33,44,43)	8.1951	7.8893	7.6444	7.8019	8.0427	8.2637
D(32,33,44,45)	132.0095	131.2141	131.524	156.3114	131.9143	131.3647
D(34,33,44,43)	-137.866	-137.574	137.9808	-138.429	-137.8371	-137.525
D(33,34,46,45)	-0.0616	0.1368	0.0707	-10.3119	-0.0059	0.0485
D(33,34,46,47)	147.0679	147.2538	147.1299	138.6742	147.1129	147.1966
D(60,34,46,45)	-147.198	-147.005	146.9416	-156.411	-147.1152	-147.116
D(33,34,60,30)	-3.9947	-4.0589	-3.9178	0.1352	-4.0002	-4.0158
D(33,34,60,35)	-142.322	-142.477	142.2744	-138.143	-142.3201	-142.393
D(46,34,60,30)	138.4628	138.3442	138.3539	142.5135	138.424	138.418
D(48,35,36,37)	142.2956	142.3338	142.3649	141.262	142.3239	142.3492
D(48,35,36,49)	-0.0229	0.0154	0.0235	-1.1353	-0.0028	0.0269
D(60,35,36,37)	0.1159	0.117	0.0991	-0.478	0.1029	0.1253
D(36,35,48,47)	-137.789	-137.802	137.8056	-140.153	-137.7945	-137.814
D(36,35,48,51)	0.0166	-0.0276	-0.0435	1.4578	-0.0001	-0.0345
D(60,35,48,47)	-0.0339	-0.004	0.0335	-2.566	0.0019	-0.0081
D(36,35,60,30)	-0.0632	-0.0455	-0.0682	0.4598	-0.0586	-0.0786
D(36,35,60,34)	142.2646	142.3931	142.3205	143.2802	142.2692	142.3224
D(48,35,60,30)	-142.412	-142.417	142.4607	-142.004	-142.4347	-142.453
D(35,36,37,30)	-0.1247	-0.144	-0.0927	0.3141	-0.1082	-0.1246
D(35,36,37,38)	-142.489	-142.474	142.4863	-141.888	-142.4797	-142.473
D(49,36,37,30)	142.0889	142.0697	142.1519	142.6918	142.1135	142.0992

Table A.1 (cont.)

parameters	Compd.I	Compd.II	Compd.III	Compd.IV	Compd.V	Compd.VI
D(35,36,49,27)	138.1356	138.1279	138.1274	138.058	138.1257	138.1154
D(35,36,49,50)	0.0119	0.0071	0.0015	-0.0436	0.003	-0.0043
D(37,36,49,27)	0.3856	0.3795	0.3553	0.0679	0.3705	0.362
D(30,37,38,28)	-138.056	-138.021	138.0744	-138.354	-138.0607	-138.035
D(30,37,38,39)	0.0635	0.0949	0.0206	-0.2109	0.0543	0.0837
D(36,37,38,28)	-0.1098	-0.1247	-0.1181	-0.6058	-0.1132	-0.1196
D(28,38,39,13)	-0.8685	-0.8756	-0.8642	0.0088	-0.8617	-0.8624
D(28,38,39,40)	141.9315	141.9	141.9125	142.5542	141.9282	141.9101
D(37,38,39,13)	-143.439	-143.45	143.4248	-142.54	-143.4311	-143.438
D(13,39,40,31)	138.726	138.6943	138.7538	138.3642	138.7264	138.6767
D(13,39,40,58)	-0.4316	-0.4809	-0.3838	0.6262	-0.4294	-0.4751
D(38,39,40,31)	0.4199	0.4087	0.469	0.224	0.4312	0.3922
D(31,40,58,29)	-144.035	-144.025	144.1433	-142.688	-144.0498	-144
D(31,40,58,41)	1.5018	1.5272	1.4135	-0.3053	1.4876	1.5162
D(39,40,58,29)	-0.3694	-0.3381	-0.4782	-0.4987	-0.3784	-0.3372
D(32,41,42,43)	8.719	8.8024	8.6114	2.6194	8.7235	8.5806
D(32,41,42,59)	-133.898	-134.05	134.2218	-139.018	-133.9882	-133.959
D(58,41,42,43)	147.0485	147.1941	147.4309	140.2087	147.0759	146.9919
D(32,41,58,29)	143.6032	143.6653	143.8662	142.9105	143.6437	143.5837
D(32,41,58,40)	-0.9433	-0.9385	-0.765	0.5115	-0.9137	-0.9791
D(42,41,58,29)	-0.0907	-0.0321	-0.2655	1.1447	-0.0539	-0.1105
D(41,42,43,44)	-8.0271	-8.0581	-8.2588	0.7685	-8.0694	-7.6712
D(41,42,43,57)	-131.8	-131.671	131.6296	-143.946	-131.9158	-131.627
D(59,42,43,44)	137.773	137.9041	137.6684	145.7613	137.8168	137.9978
D(41,42,59,10)	139.5715	139.6226	139.5374	144.5189	139.6367	139.5075
D(41,42,59,11)	-6.5389	-6.4216	-6.5694	0.5697	-6.4692	-6.5183
D(43,42,59,10)	-8.871	-9.0617	-9.1212	-1.6714	-8.8663	-8.864
D(42,43,44,33)	-0.0823	0.0292	0.4543	-5.7455	0.021	-0.4022
D(42,43,44,45)	-119.698	-119.107	119.2024	-148.126	-119.6359	-119.206
D(57,43,44,33)	119.5572	119.4977	119.4802	133.1558	119.6555	119.3479
D(42,43,57,10)	-13.9999	-14.2907	-14.2684	-0.0265	-13.9634	-14.0886
D(42,43,57,56)	131.8412	131.6377	131.4741	142.7564	131.8747	132.0486
D(44,43,57,10)	-137.801	-137.981	137.4598	-142.903	-137.8088	-138.198

สถาบันวิทยบริการ
จุฬาลงกรณ์มหาวิทยาลัย

Table A.2 Structural parameters of compound **VII-X** obtained from ONIOM calculations. Here, R , A, D are distance, bond angle and torsion angle, respectively.

parameters	Compd. VII	Compd. VIII	Compd. IX	Compd. X
R(1,2)	1.4577	1.4571	1.4572	1.4576
R(1,6)	1.3826	1.3829	1.3828	1.3825
R(1,7)	1.457	1.4569	1.4571	1.4574
R(2,3)	1.3866	1.3865	1.3866	1.3867
R(2,9)	1.4449	1.4458	1.4457	1.4447
R(3,4)	1.4585	1.4585	1.4584	1.4584
R(3,11)	1.4448	1.4447	1.4445	1.4452
R(4,5)	1.3831	1.383	1.383	1.3831
R(4,12)	1.4573	1.4575	1.4575	1.4573
R(5,6)	1.4583	1.4583	1.4583	1.4584
R(5,15)	1.4565	1.4566	1.4565	1.4565
R(6,17)	1.4585	1.4584	1.4583	1.4585
R(7,8)	1.4446	1.4457	1.4458	1.4446
R(7,19)	1.3868	1.3864	1.3866	1.3867
R(8,9)	1.5051	1.5035	1.5028	1.5049
R(8,20)	1.3865	1.3881	1.3893	1.3874
R(9,10)	1.389	1.3883	1.3899	1.388
R(10,57)	1.5488	1.5487	1.5466	1.5455
R(10,59)	1.4342	1.4353	1.4345	1.4346
R(10,77)	2.7722	1.4592	1.4589	1.4593
R(11,29)	1.4594	1.3875	1.3873	1.388
R(11,59)	1.3882	1.3849	1.3848	1.3848
R(12,13)	1.3849	1.4567	1.4567	1.4569
R(12,29)	1.4569	1.4571	1.4571	1.4571
R(13,14)	1.4571	1.4576	1.4575	1.4574
R(13,39)	1.4574	1.3844	1.3844	1.3844
R(14,15)	1.3844	1.4577	1.4576	1.4577
R(14,28)	1.4577	1.4578	1.4578	1.4579
R(15,16)	1.4579	1.4566	1.4566	1.4565
R(16,17)	1.4565	1.3845	1.3844	1.3844
R(16,26)	1.3844	1.3829	1.383	1.3831
R(17,18)	1.3831	1.4583	1.4584	1.4584
R(18,19)	1.4583	1.4577	1.4575	1.4573
R(18,24)	1.4574	1.4445	1.4447	1.4453
R(19,22)	1.4454	1.4346	1.4348	1.434
R(20,21)	1.4331	1.5503	1.5449	1.5459
R(20,56)	1.5448	1.3869	1.3873	1.3879
R(21,22)	1.3876	1.4548	1.4549	1.4555
R(21,54)	1.4554	2.3943	1.4591	1.4591
R(22,23)	1.4589	1.4586	1.4567	1.4569
R(23,24)	1.4569	1.4568	1.3811	1.381
R(23,52)	1.3811	1.3809	1.3848	1.3848
R(24,25)	1.3847	1.3847	1.4571	1.4571
R(25,26)	1.4571	1.4571	1.4575	1.4574

Table A.2 (cont.)

parameters	Compd. VII	Compd. VIII	Compd. IX	Compd. X
R(25,50)	1.4575	1.4576	1.4576	1.4576
R(26,27)	1.4576	1.4576	1.3838	1.3838
R(27,28)	1.3838	1.3838	1.4576	1.4577
R(27,49)	1.4576	1.4577	1.4577	1.4576
R(28,38)	1.4576	1.4576	1.381	1.3811
R(29,58)	1.3811	1.3811	1.383	1.3831
R(30,31)	1.3831	1.383	1.4565	1.4565
R(30,37)	1.4565	1.4566	1.4583	1.4584
R(30,60)	1.4585	1.4584	1.4584	1.4583
R(32,41)	1.4449	1.4446	1.4572	1.4574
R(33,34)	1.4572	1.4566	1.4458	1.4444
R(33,44)	1.4444	1.4452	1.457	1.4575
R(34,46)	1.4575	1.4571	1.3828	1.3825
R(34,60)	1.3825	1.3828	1.4566	1.4565
R(35,36)	1.4566	1.4566	1.383	1.3831
R(35,48)	1.3831	1.3829	1.4583	1.4584
R(35,60)	1.4583	1.4582	1.4578	1.4579
R(36,37)	1.4579	1.4578	1.3844	1.3844
R(36,49)	1.3843	1.3844	1.3844	1.3844
R(37,38)	1.3844	1.3845	1.4571	1.4571
R(38,39)	1.4571	1.4571	1.3849	1.3848
R(39,40)	1.3848	1.3847	1.4567	1.457
R(40,58)	1.457	1.4568	1.3875	1.388
R(41,42)	1.3879	1.3871	1.4591	1.4593
R(41,58)	1.4591	1.4588	1.4352	1.4347
R(42,43)	1.4335	1.435	1.4546	1.4555
R(42,59)	1.4554	1.4545	1.389	1.3877
R(43,44)	1.3881	1.3897	1.5487	1.5473
R(43,57)	1.5499	1.5467	1.5041	1.5053
R(44,45)	1.5047	1.5038	1.4456	1.4446
R(45,46)	1.4452	1.4456	1.3882	1.388
R(45,55)	1.3868	1.3909	1.3866	1.3865
R(46,47)	1.3865	1.3864	1.4583	1.4584
R(47,48)	1.4585	1.4585	1.4449	1.4452
R(47,53)	1.4452	1.4443	1.4576	1.4572
R(48,51)	1.4573	1.4574	1.4571	1.4571
R(52,53)	1.4597	1.4594	1.3872	1.3882
R(53,54)	1.388	1.3875	1.4351	1.435
R(54,55)	1.4357	1.4359	1.5459	1.5502
R(55,56)	1.5497	1.5515	1.6931	1.6749
R(56,57)	1.68	1.7139	1.5953	1.5594
R(56,61)	1.567	1.5876	1.5954	1.5621
R(57,64)	1.5643	1.5801	1.5261	1.5255
A(2,1,6)	120.3319	120.3578	120.3524	120.2899
A(2,1,7)	108.0031	107.9227	107.9294	108.0083
A(6,1,7)	120.2266	120.2944	120.3164	120.2455

Table A.2 (cont.)

parameters	Compd. VII	Compd. VIII	Compd. IX	Compd. X
A(1,2,3)	119.4727	119.4011	119.3977	119.5271
A(1,2,9)	108.9099	108.8745	108.8886	108.8249
A(3,2,9)	120.9986	121.1519	121.1731	120.954
A(2,3,4)	120.3013	120.392	120.3891	120.2765
A(2,3,11)	118.8847	118.7952	118.8335	118.9416
A(4,3,11)	108.281	108.2159	108.2039	108.2585
A(3,4,5)	119.954	119.9157	119.9186	119.9427
A(3,4,12)	107.8547	107.891	107.8913	107.8652
A(5,4,12)	119.9743	119.953	119.9677	119.9814
A(4,5,6)	119.8939	119.872	119.8723	119.9112
A(4,5,15)	120.0849	120.0763	120.0621	120.074
A(6,5,15)	107.9888	108.0093	108.0166	107.9843
A(1,6,5)	120.0404	120.0552	120.064	120.0479
A(1,6,17)	120.0714	120.0908	120.0718	120.0602
A(5,6,17)	107.9643	107.9362	107.9376	107.9704
A(1,7,8)	108.737	108.8782	108.8107	108.7915
A(1,7,19)	119.5871	119.4316	119.4417	119.5739
A(9,8,20)	120.351	120.4003	120.5298	120.4481
A(2,9,8)	107.0074	107.1485	107.1151	107.1468
A(2,9,10)	120.2975	120.2586	120.1284	120.2394
A(8,9,10)	120.6598	120.2381	120.3382	120.322
A(9,10,57)	124.5606	125.5159	125.1607	124.9207
A(9,10,59)	118.1922	118.0322	118.1296	118.4119
A(57,10,59)	110.198	110.1079	110.1315	110.1268
A(3,11,29)	108.0724	108.1428	108.1637	108.091
A(3,11,59)	119.4055	119.3162	119.3046	119.4433
A(29,11,59)	120.5089	120.5267	120.458	120.4798
A(4,12,13)	119.9952	120.0281	120.026	119.9927
A(4,12,29)	107.8351	107.8241	107.825	107.8454
A(13,12,29)	119.9452	119.8951	119.8912	119.9337
A(12,13,14)	119.9697	119.9523	119.9444	119.9709
A(12,13,39)	119.9914	120.0207	119.9964	119.9883
A(14,13,39)	107.9882	107.9859	108.0063	107.9942
A(13,14,15)	120.0074	119.9981	120.0043	120.007
A(13,14,28)	108.0296	108.0238	108.0133	108.0265
A(15,14,28)	119.9468	119.9595	119.9575	119.9466
A(5,15,14)	119.9678	119.9913	119.9948	119.9734
A(5,15,16)	108.0322	108.0235	108.0129	108.0303
A(14,15,16)	120.0105	120.0034	120.0123	120.0142
A(15,16,17)	108.0177	108.0029	108.0132	108.0229
A(15,16,26)	120.0259	120.021	120.0129	120.0223
A(17,16,26)	119.9672	119.9917	119.9922	119.972
A(6,17,16)	107.9921	108.022	108.0141	107.9876
A(6,17,18)	119.9382	119.8869	119.8872	119.9286
A(19,18,24)	107.8636	107.8791	107.8916	107.8598
A(7,19,18)	120.2807	120.4253	120.3738	120.2684

Table A.2 (cont.)

parameters	Compd. VII	Compd. VIII	Compd. IX	Compd. X
A(7,19,22)	119.0237	118.8049	118.8724	118.9728
A(18,19,22)	108.2204	108.19	108.2002	108.2553
A(8,20,21)	118.8199	118.1558	118.2388	118.5772
A(8,20,56)	124.9812	125.8434	125.1061	124.8457
A(21,20,56)	110.1557	110.1788	110.1491	110.1895
A(20,21,22)	121.6834	122.2453	122.1727	121.7815
A(20,21,54)	108.3601	108.3171	108.3477	108.4136
A(22,21,54)	119.982	119.9318	119.7111	119.818
A(19,22,21)	119.4141	119.3125	119.3128	119.4464
A(19,22,23)	108.1499	108.2068	108.169	108.1014
A(22,23,24)	107.8945	107.8781	107.8998	107.9294
A(22,23,52)	119.713	119.6959	119.81	119.7623
A(24,23,52)	120.136	120.1676	120.0974	120.1047
A(18,24,23)	107.87	107.8434	107.8378	107.8525
A(18,24,25)	119.9739	120.0114	120.0202	119.9827
A(23,24,25)	119.9129	119.8625	119.8943	119.9264
A(24,25,26)	119.9653	119.9387	119.9464	119.969
A(24,25,50)	119.9735	119.9909	120.0047	119.9791
A(26,25,50)	108.0088	108.0134	107.9985	108.0021
A(16,26,25)	120.0263	120.0199	120.0071	120.0144
A(16,26,27)	119.9468	119.9567	119.9567	119.9455
A(25,26,27)	108.0174	108.006	108.0171	108.0221
A(26,27,28)	120.0273	120.0229	120.03	120.0326
A(26,27,49)	107.9562	107.9706	107.9682	107.9551
A(27,28,38)	120.0321	120.0232	120.0299	120.0359
A(11,29,12)	107.9555	107.9242	107.9142	107.9383
A(11,29,58)	119.823	119.8136	119.7909	119.809
A(12,29,58)	120.0542	120.0674	120.1211	120.0759
A(31,30,37)	120.0517	120.0444	120.069	120.0612
A(31,30,60)	119.9254	119.892	119.8835	119.9213
A(37,30,60)	107.9921	108.0145	108.012	107.9842
A(30,31,32)	119.9194	119.8729	119.9067	119.932
A(30,31,40)	120.004	119.9963	119.9716	119.994
A(32,31,40)	107.8488	107.8762	107.8792	107.8616
A(31,32,33)	120.267	120.3871	120.3791	120.2618
A(31,32,41)	108.2743	108.2056	108.2253	108.2622
A(33,32,41)	118.9208	118.8218	118.8227	118.9492
A(32,33,34)	119.5756	119.4755	119.436	119.567
A(32,33,44)	121.0075	121.1726	121.1298	120.9455
A(34,33,44)	108.82	108.8409	108.8811	108.8015
A(33,34,46)	107.9907	107.9058	107.9519	108.0076
A(33,34,60)	120.2473	120.28	120.321	120.2587
A(46,34,60)	120.3409	120.3957	120.3102	120.2772
A(36,35,48)	120.0849	120.0855	120.058	120.0737
A(36,35,60)	107.9812	108.0052	108.0118	107.9817
A(48,35,60)	119.8997	119.8552	119.8819	119.921

Table A.2 (cont.)

parameters	Compd. VII	Compd. VIII	Compd. IX	Compd. X
A(35,36,37)	108.0336	108.0235	108.0147	108.0292
A(35,36,49)	119.98	119.9894	119.9918	119.9726
A(37,36,49)	120.0122	120.0025	120.013	120.0183
A(30,37,36)	108.016	108.0059	108.0146	108.0254
A(30,37,38)	119.9787	119.9886	119.9853	119.9766
A(37,38,39)	120.0176	120.0209	120.0086	120.0119
A(13,39,38)	108.0081	108.0131	107.9943	108.0009
A(13,39,40)	119.973	119.9908	120.0003	119.9821
A(38,39,40)	119.9589	119.9431	119.95	119.9671
A(31,40,39)	119.9884	120.0058	120.0147	119.9886
A(31,40,58)	107.8445	107.8475	107.8333	107.8499
A(39,40,58)	119.9292	119.8737	119.905	119.9308
A(32,41,42)	119.4034	119.3374	119.3429	119.4565
A(32,41,58)	108.0973	108.1864	108.1415	108.0923
A(42,41,58)	120.4515	120.4785	120.508	120.4699
A(41,42,43)	121.9224	122.228	122.2288	121.8343
A(41,42,59)	119.81	119.8304	119.6748	119.7356
A(43,42,59)	108.4622	108.3591	108.3513	108.4117
A(42,43,44)	118.4288	118.1188	118.078	118.4619
A(42,43,57)	110.1849	110.1452	110.0948	110.0437
A(44,43,57)	124.7629	125.7038	125.2551	125.1454
A(33,44,43)	120.1663	120.1674	120.2313	120.2338
A(33,44,45)	107.2133	107.2591	107.1135	107.2052
A(43,44,45)	120.5784	120.3189	120.5051	120.2485
A(44,45,46)	107.1317	107.0254	107.1956	107.1416
A(44,45,55)	120.4493	120.4704	120.1541	120.4438
A(46,45,55)	120.281	120.3534	120.1468	120.3121
A(34,46,45)	108.8304	108.9499	108.8415	108.8305
A(34,46,47)	119.4926	119.3606	119.4442	119.5565
A(45,46,47)	121.0139	121.2139	121.1226	120.9488
A(46,47,48)	120.2789	120.4032	120.3764	120.2591
A(46,47,53)	118.8876	118.7212	118.8602	118.9203
A(47,48,51)	107.8714	107.884	107.8946	107.8547
A(27,49,36)	119.9447	119.9585	119.9558	119.9438
A(27,49,50)	108.0324	108.0239	108.0146	108.0281
A(36,49,50)	119.995	119.9973	120.01	120.0062
A(25,50,49)	107.9849	107.9858	108.0013	107.9924
A(25,50,51)	120.0032	120.0211	119.9999	119.9898
A(49,50,51)	119.97	119.9481	119.9482	119.9711
A(48,51,50)	120.0109	120.0362	120.0145	119.9919
A(48,51,52)	107.8348	107.8133	107.8427	107.8423
A(50,51,52)	119.9411	119.8952	119.8923	119.9396
A(23,52,51)	120.0328	120.0618	120.1108	120.0598
A(23,52,53)	119.8927	119.8341	119.7819	119.8296
A(51,52,53)	107.9562	107.9396	107.8909	107.956
A(47,53,52)	108.0628	108.1216	108.177	108.057

Table A.2 (cont.)

parameters	Compd. VII	Compd. VIII	Compd. IX	Compd. X
A(47,53,54)	119.4019	119.3201	119.3348	119.4548
A(52,53,54)	120.5375	120.5897	120.455	120.5241
A(21,54,53)	119.4691	119.4747	119.7706	119.5982
A(21,54,55)	108.5198	108.4349	108.3436	108.472
A(53,54,55)	121.9795	122.4692	122.1409	121.905
A(45,55,54)	118.2876	117.7092	118.2522	118.3197
A(45,55,56)	125.0458	125.4696	125.3979	124.9376
A(54,55,56)	109.8295	110.0588	110.1	109.9938
A(20,56,55)	99.5617	99.0646	110.7096	99.5066
A(20,56,57)	113.3555	112.1038	110.6175	113.5148
A(20,56,61)	107.7237	109.4343	109.3283	109.3549
A(55,56,57)	113.3559	112.7198	99.4495	113.4993
A(55,56,61)	110.7293	112.9254	113.2569	111.2144
A(10,57,64)	111.3876	111.313	108.3915	110.6762
A(43,57,56)	113.5518	112.7244	99.4355	113.4012
A(43,57,64)	110.2343	111.9767	113.1242	110.5439
A(56,57,64)	108.3963	108.4096	112.9801	108.9109
A(29,58,40)	120.1065	120.1516	120.0854	120.0884
A(29,58,41)	119.7799	119.7346	119.7804	119.799
A(40,58,41)	107.9337	107.8818	107.9188	107.9321
A(10,59,11)	122.0485	122.2833	122.2488	121.8798
A(10,59,42)	108.4759	108.2916	108.4849	108.3901
A(11,59,42)	119.6234	119.6116	119.7829	119.7041
A(30,60,34)	120.0592	120.086	120.0674	120.0543
A(30,60,35)	107.9722	107.9448	107.9412	107.9749
A(34,60,35)	120.0208	120.0467	120.0771	120.0402
D(6,1,2,3)	0.3394	0.2593	0.2758	0.2283
D(6,1,2,9)	144.6377	144.8431	144.8811	144.6191
D(7,1,2,3)	143.7987	143.7587	143.8163	143.6722
D(2,1,6,5)	0.3431	0.4429	0.4087	0.3824
D(2,1,6,17)	138.6341	138.7321	138.6854	138.6795
D(7,1,6,5)	138.7112	138.6015	138.6747	138.6459
D(2,1,7,8)	1.1095	1.2436	1.2059	1.111
D(2,1,7,19)	143.688	143.9553	143.8655	143.7371
D(6,1,7,8)	144.6143	144.7704	144.762	144.5742
D(1,2,3,4)	-0.8075	-0.7947	-0.7815	-0.6864
D(1,2,3,11)	138.3116	138.1783	138.1946	138.1959
D(9,2,3,4)	139.8918	139.9657	140.0362	139.8594
D(1,2,9,8)	0.7876	0.9225	0.9523	0.7832
D(1,2,9,10)	143.5692	143.1234	143.1159	143.1011
D(11,3,4,5)	142.0684	141.9738	141.9946	142.0421
D(2,3,11,29)	142.4701	142.5093	142.5435	142.5165
D(2,3,11,59)	-0.3653	-0.338	-0.1993	-0.3428
D(4,3,11,29)	0.3676	0.4509	0.4582	0.4148
D(3,4,5,6)	0.0877	0.0755	0.0827	0.0765
D(3,4,5,15)	138.0487	138.0538	138.0393	138.0609

Table A.2 (cont.)

parameters	Compd. VII	Compd. VIII	Compd. IX	Compd. X
D(12,4,5,6)	137.8942	137.8616	137.8956	137.8966
D(3,4,12,13)	142.3351	142.2877	142.286	142.3413
D(3,4,12,29)	0.0389	0.0505	0.0571	0.0538
D(5,4,12,13)	0.0237	0.0197	-0.0061	0.0259
D(4,5,6,1)	-0.5542	-0.6083	-0.586	-0.5332
D(4,5,6,17)	143.3036	143.3717	143.3299	143.2814
D(15,5,6,1)	142.0633	141.9942	142.0022	142.0814
D(4,5,15,14)	0.3156	0.343	0.3103	0.3041
D(4,5,15,16)	142.9592	142.9926	142.9654	142.9587
D(6,5,15,14)	142.2175	142.1693	142.1941	142.2386
D(1,6,17,16)	142.0514	141.983	142.001	142.0796
D(1,6,17,18)	0.5726	0.6018	0.6027	0.5418
D(5,6,17,16)	0.6844	0.7647	0.7395	0.6632
D(1,7,8,9)	-0.6196	-0.6705	-0.6154	-0.623
D(1,7,8,20)	142.9232	143.0226	143.2263	143.1386
D(19,7,8,9)	143.6102	143.8093	143.7474	143.6557
D(1,7,19,18)	0.6349	0.878	0.8106	0.7022
D(1,7,19,22)	138.2004	138.276	138.2516	138.2398
D(8,7,19,18)	139.8293	139.9834	139.894	139.8394
D(7,8,9,2)	-0.1034	-0.1553	-0.2074	-0.0988
D(7,8,9,10)	142.7225	142.3654	142.2758	142.3794
D(9,8,20,21)	135.7662	135.4345	135.3758	135.6352
D(2,9,10,57)	150.4452	151.4084	151.0148	150.7495
D(2,9,10,59)	-2.7823	-2.2589	-2.3701	-2.0114
D(8,9,10,57)	-12.6976	-14.0866	-13.801	-13.3342
D(9,10,57,43)	132.8266	132.4428	109.5645	133.2343
D(9,10,57,56)	11.8281	12.8158	133.0722	12.4085
D(59,10,57,43)	-17.0188	-18.7397	99.6935	-17.6792
D(9,10,59,11)	4.8876	4.5889	4.888	4.0808
D(9,10,59,42)	140.6042	140.9393	141.2296	141.1774
D(57,10,59,11)	156.8942	158.1983	157.9464	157.1325
D(3,11,29,12)	-0.343	-0.4191	-0.4224	-0.3808
D(3,11,29,58)	142.7709	142.8154	142.8682	142.8049
D(59,11,29,12)	142.0061	141.8951	141.8116	142.0222
D(3,11,59,10)	-3.3182	-3.298	-3.6088	-2.9068
D(3,11,59,42)	138.5031	138.5221	138.86	138.5879
D(29,11,59,10)	141.5136	141.5185	141.7485	141.151
D(4,12,13,14)	0.1261	0.1575	0.1583	0.1299
D(4,12,13,39)	137.9823	137.9647	137.9539	137.9872
D(29,12,13,14)	137.9136	137.8987	137.8922	137.9161
D(4,12,29,11)	0.1864	0.2257	0.2236	0.2003
D(4,12,29,58)	142.5117	142.5092	142.5227	142.5058
D(13,12,29,11)	142.1321	142.0708	142.0655	142.1134
D(12,13,14,15)	-0.0527	-0.0822	-0.0745	-0.0666
D(12,13,14,28)	142.6336	142.665	142.6475	142.6423
D(39,13,14,15)	142.4996	142.4953	142.4788	142.4903

Table A.2 (cont.)

parameters	Compd. VII	Compd. VIII	Compd. IX	Compd. X
D(12,13,39,38)	142.5307	142.5364	142.5297	142.5484
D(12,13,39,40)	0.0028	0.0062	0.001	0.0044
D(28,14,15,5)	138.0114	138.0055	137.9997	138.022
D(13,14,28,27)	142.8149	142.8208	142.8198	142.8124
D(13,14,28,38)	0.1435	0.1523	0.1529	0.1389
D(15,14,28,27)	0.2073	0.221	0.2262	0.2101
D(5,15,16,17)	-0.0029	-0.0074	-0.0036	-0.0059
D(5,15,16,26)	142.6266	142.6468	142.6475	142.6402
D(14,15,16,17)	142.6219	142.637	142.6438	142.6307
D(15,16,17,6)	-0.4214	-0.4684	-0.4552	-0.4064
D(15,16,17,18)	142.9947	142.9834	142.9817	142.9688
D(26,16,17,6)	142.2283	142.1839	142.1978	142.2501
D(15,16,26,25)	138.392	138.3913	138.3923	138.3813
D(15,16,26,27)	0.21	0.2255	0.2247	0.2103
D(17,16,26,25)	0.1789	0.1769	0.1698	0.1568
D(6,17,18,19)	-0.1222	-0.1547	-0.1037	-0.1147
D(6,17,18,24)	137.9106	137.9007	137.8995	137.915
D(16,17,18,19)	138.0393	137.9738	138.0358	138.0376
D(17,18,19,7)	-0.4837	-0.5918	-0.6086	-0.511
D(17,18,19,22)	142.0831	141.9576	142.0387	142.0547
D(24,18,19,7)	141.8366	141.6791	141.6923	141.8139
D(17,18,24,23)	142.266	142.2118	142.2475	142.2606
D(17,18,24,25)	0.0049	0.0257	0.0031	-0.0111
D(19,18,24,23)	0	-0.0019	-0.0229	-0.0286
D(7,19,22,21)	0.2249	0.233	0.2732	0.3227
D(18,19,22,21)	142.3858	142.3256	142.376	142.4454
D(8,20,21,22)	-3.7614	-4.4182	-4.5663	-4.0048
D(8,20,21,54)	141.6842	141.7098	141.0753	141.3599
D(21,20,56,55)	18.0306	18.912	-98.4046	17.5889
D(20,21,22,19)	2.8096	3.316	3.2795	2.8592
D(20,21,22,23)	141.005	141.5651	141.4555	141.1061
D(54,21,22,19)	138.766	139.0559	138.6406	138.7124
D(20,21,54,53)	145.9067	146.6252	146.7285	146.0463
D(20,21,54,55)	0.277	0.3474	-0.0747	0.114
D(22,21,54,53)	0.2293	0.4231	-0.0964	0.1151
D(19,22,23,24)	0.3824	0.5022	0.3856	0.3889
D(19,22,23,52)	142.7281	142.8583	142.7955	142.7908
D(21,22,23,24)	141.9509	141.8189	141.8819	142.0151
D(22,23,24,18)	-0.2346	-0.3066	-0.2222	-0.221
D(22,23,24,25)	142.0537	141.946	142.0783	142.0759
D(52,23,24,18)	142.3919	142.4524	142.5043	142.4705
D(22,23,52,51)	137.8731	137.8002	137.8519	137.8967
D(22,23,52,53)	0.1212	0.1183	-0.0304	0.0431
D(24,23,52,51)	-0.1101	-0.0466	0.0085	-0.0411
D(18,24,25,26)	-0.1707	-0.1796	-0.1616	-0.144
D(18,24,25,50)	137.9434	137.9294	137.9514	137.9713

Table A.2 (cont.)

parameters	Compd. VII	Compd. VIII	Compd. IX	Compd. X
D(23,24,25,26)	137.9441	137.8837	137.9157	137.9177
D(24,25,26,16)	0.0766	0.0764	0.073	0.069
D(24,25,26,27)	142.6649	142.6581	142.6533	142.6462
D(50,25,26,16)	142.4676	142.4701	142.4866	142.4803
D(24,25,50,49)	142.5748	142.5448	142.5305	142.5553
D(24,25,50,51)	-0.0208	-0.0043	0.0041	-0.0063
D(26,25,50,49)	-0.0342	-0.0214	0.0033	-0.0104
D(16,26,27,28)	-0.2094	-0.2254	-0.2239	-0.2067
D(16,26,27,49)	142.4624	142.4504	142.4477	142.4614
D(49,27,28,14)	138.2117	138.2223	138.2233	138.2139
D(26,27,49,36)	142.4472	142.4514	142.446	142.4597
D(26,27,49,50)	0.1399	0.1459	0.157	0.1398
D(28,27,49,36)	0.2178	0.2183	0.2251	0.2062
D(14,28,38,37)	142.4504	142.4517	142.4526	142.4619
D(14,28,38,39)	-0.1509	-0.1591	-0.1534	-0.1395
D(27,28,38,37)	-0.2254	-0.2224	-0.2142	-0.2126
D(11,29,58,40)	137.9212	137.8826	137.8674	137.9128
D(11,29,58,41)	0.0283	0.0884	0.0336	0.0213
D(12,29,58,40)	0.0008	0.0155	-0.0269	0.0134
D(37,30,31,32)	138.023	137.9902	138.0284	138.0462
D(37,30,31,40)	0.2349	0.2313	0.2503	0.2299
D(60,30,31,32)	-0.1169	-0.131	-0.1123	-0.0871
D(31,30,37,36)	142.9711	142.9843	142.9801	142.9553
D(31,30,37,38)	-0.3073	-0.3299	-0.3315	-0.2936
D(60,30,37,36)	-0.4219	-0.4714	-0.4536	-0.4116
D(31,30,60,34)	0.5961	0.6104	0.5882	0.5401
D(31,30,60,35)	143.293	143.3492	143.3507	143.2682
D(37,30,60,34)	142.0089	141.9699	142.0201	142.0654
D(30,31,32,33)	-0.5984	-0.6024	-0.6104	-0.5321
D(30,31,32,41)	142.0769	141.9701	141.9961	142.0364
D(40,31,32,33)	141.7211	141.682	141.6786	141.8038
D(30,31,40,39)	-0.0133	0.0183	-0.0143	-0.0202
D(30,31,40,58)	142.2597	142.2221	142.2352	142.2632
D(32,31,40,39)	142.2951	142.2112	142.2744	142.3285
D(31,32,33,34)	0.8245	0.8452	0.8444	0.691
D(31,32,33,44)	139.8778	140.0042	139.9506	139.8595
D(33,32,41,42)	0.3178	0.2812	0.3168	0.3316
D(32,33,34,46)	143.8746	143.9141	143.886	143.6941
D(32,33,34,60)	-0.3439	-0.3635	-0.3663	-0.2368
D(44,33,34,46)	1.1304	1.281	1.2352	1.1593
D(32,33,44,43)	1.0274	1.4608	1.1423	1.3023
D(32,33,44,45)	143.783	143.8346	143.7187	143.5663
D(34,33,44,43)	143.3856	143.0352	143.2803	142.9789
D(33,34,46,45)	-1.1996	-1.417	-1.2936	-1.158
D(33,34,46,47)	143.716	143.8526	143.7676	143.7296
D(60,34,46,45)	144.6899	144.9175	144.818	144.6072

Table A.2 (cont.)

parameters	Compd. VII	Compd. VIII	Compd. IX	Compd. X
D(33,34,60,30)	-0.3677	-0.365	-0.3512	-0.3796
D(33,34,60,35)	138.6256	138.6507	138.6478	138.6647
D(46,34,60,30)	138.7089	138.6832	138.7172	138.6481
D(48,35,36,37)	142.9636	142.9718	142.9772	142.9626
D(48,35,36,49)	0.2993	0.3261	0.3224	0.3034
D(60,35,36,37)	0.431	0.4823	0.468	0.4068
D(36,35,48,47)	138.0704	138.0352	138.049	138.0499
D(36,35,48,51)	-0.245	-0.2541	-0.2372	-0.2486
D(60,35,48,47)	0.0602	0.0749	0.0724	0.097
D(36,35,60,30)	-0.6914	-0.773	-0.7477	-0.6609
D(36,35,60,34)	142.0224	141.9831	142.0104	142.0734
D(48,35,60,30)	143.3058	143.3642	143.3347	143.2841
D(35,36,37,30)	-0.0056	-0.0068	-0.0089	0.003
D(35,36,37,38)	142.6482	142.6464	142.6447	142.6397
D(49,36,37,30)	142.6445	142.6332	142.6366	142.642
D(35,36,49,27)	138.0203	138.0069	138.003	138.0236
D(35,36,49,50)	-0.1398	-0.1615	-0.1628	-0.1439
D(36,37,38,28)	0.2215	0.2252	0.2173	0.2109
D(28,38,39,13)	0.1008	0.1051	0.0953	0.0868
D(28,38,39,40)	142.6349	142.6564	142.6462	142.6373
D(37,38,39,13)	142.4665	142.4769	142.4871	142.4846
D(13,39,40,31)	137.9624	137.9417	137.9589	137.985
D(13,39,40,58)	0.191	0.2216	0.2057	0.2009
D(38,39,40,31)	-0.14	-0.173	-0.145	-0.1297
D(31,40,58,29)	142.4924	142.4956	142.491	142.5191
D(31,40,58,41)	-0.2041	-0.2989	-0.2493	-0.2232
D(39,40,58,29)	-0.193	-0.2329	-0.1926	-0.2101
D(32,41,42,43)	3.1505	3.2593	3.3427	2.7877
D(32,41,42,59)	138.7498	138.991	138.6184	138.7282
D(58,41,42,43)	141.3036	141.5224	141.5732	141.0394
D(32,41,58,29)	142.7883	142.8774	142.8091	142.8338
D(32,41,58,40)	0.355	0.495	0.4317	0.4093
D(42,41,58,29)	0.483	0.5283	0.4744	0.419
D(41,42,43,44)	-4.4817	-4.378	-4.6915	-3.8219
D(41,42,43,57)	157.331	158.6469	157.7898	157.3032
D(59,42,43,44)	141.1552	141.5954	140.971	141.4622
D(41,42,59,10)	146.6714	146.9198	146.884	146.2384
D(41,42,59,11)	0.2023	0.3136	-0.2111	0.0957
D(43,42,59,10)	0.1848	-0.0102	0.1951	0.1015
D(42,43,44,33)	2.3444	1.9719	2.3937	1.7441
D(42,43,44,45)	135.4736	135.5435	135.2217	135.6632
D(57,43,44,33)	150.9209	151.8442	151.0375	150.8827
D(42,43,57,10)	17.1366	18.7351	-99.8882	17.7311
D(42,43,57,56)	138.2163	138.6405	17.7924	138.6497
D(43,44,45,46)	142.4643	142.0975	142.3617	142.2601
D(44,45,46,34)	0.8036	0.9996	0.8525	0.7105

Table A.2 (cont.)

parameters	Compd. VII	Compd. VIII	Compd. IX	Compd. X
D(44,45,46,47)	143.4815	143.5088	143.515	143.5999
D(55,45,46,34)	143.3718	143.5511	142.8339	143.3224
D(44,45,55,54)	135.2007	134.5804	135.3481	135.4248
D(44,45,55,56)	-12.7949	-13.6209	-14.0208	-12.8146
D(46,45,55,54)	-2.4402	-2.9993	-1.7715	-2.2737
D(34,46,47,48)	-0.7594	-0.8881	-0.7497	-0.7344
D(34,46,47,53)	138.221	138.223	138.1628	138.243
D(45,46,47,48)	139.8382	140.0585	139.9677	139.8625
D(46,47,48,35)	0.6203	0.6809	0.5957	0.5494
D(46,47,48,51)	141.7051	141.5966	141.7204	141.7709
D(53,47,48,35)	142.0558	141.942	141.9982	142.0362
D(46,47,53,52)	142.4394	142.4951	142.5552	142.4954
D(46,47,53,54)	-0.4275	-0.4369	-0.2393	-0.4085
D(48,47,53,52)	0.3812	0.4788	0.4729	0.4101
D(35,48,51,50)	0.0357	0.0226	-0.0033	0.0391
D(35,48,51,52)	142.2731	142.2103	142.2438	142.2532
D(47,48,51,50)	142.3624	142.2951	142.2807	142.3402
D(27,49,50,25)	-0.0653	-0.077	-0.0991	-0.08
D(27,49,50,51)	142.634	142.6497	142.6565	142.6372
D(36,49,50,25)	142.4996	142.5032	142.48	142.4919
D(25,50,51,48)	137.997	137.9747	137.9512	137.9961
D(25,50,51,52)	-0.1927	-0.2417	-0.1992	-0.2083
D(49,50,51,48)	0.1234	0.1415	0.1625	0.1201
D(48,51,52,23)	142.5992	142.5637	142.4881	142.5481
D(48,51,52,53)	0.18	0.2311	0.2494	0.2034
D(51,52,53,47)	-0.3475	-0.4398	-0.4474	-0.3797
D(47,53,54,21)	138.5014	138.5123	138.8002	138.5779
D(47,53,54,55)	-3.027	-3.6901	-3.1605	-2.9469
D(52,53,54,21)	0.2868	0.2311	0.5942	0.3142
D(21,54,55,45)	140.7053	140.3836	141.5406	140.9398
D(21,54,55,56)	11.8272	12.4315	12.2112	11.7259
D(53,54,55,45)	4.4595	5.3935	4.1605	4.2839
D(45,55,56,20)	132.4606	131.5573	132.9361	132.9695
D(45,55,56,57)	11.7539	12.8783	12.2112	12.043
D(54,55,56,20)	-17.7964	-18.6653	-18.4348	-17.4866
D(20,56,57,10)	0.6577	0.7958	0.7433	0.234
D(20,56,57,43)	112.0575	110.7148	112.1744	112.434
D(55,56,57,10)	113.2117	111.5528	111.1053	112.9148

Table A.3 The net charges (in a.u.) of atoms of C₆₀ derivatives in group-1 obtained using B3LYP/6-31G (d).

Carbon atom	Compd. I	Compd. II	Compd. III	Compd. IV	Compd. V	Compd. VI
1	-0.00185	-0.00034	-0.00129	-0.00117	-0.00156	-0.00167
2	-0.00004	0.000796	0.000632	-0.00059	-0.00053	-0.00016
3	0.000486	0.000112	-0.00023	-0.00276	-0.00044	-0.00026
4	-0.0016	-0.00037	-0.00137	-0.00054	-0.0014	-0.00133
5	-0.00057	0.000247	-0.00063	-0.00082	-0.00065	-0.00062
6	0.000453	0.00041	-0.00067	-0.00029	-0.00087	-0.00121
7	-0.00212	-0.0013	-0.0008	0.000062	-0.0014	-0.00136
8	-0.0038	-0.00535	-0.00508	-0.01399	-0.00543	-0.00559
9	-0.00987	-0.0126	-0.01312	-0.00478	-0.0153	-0.01248
10	-0.00047	0.004031	0.005214	0.00428	0.002942	0.00224
11	-0.0109	-0.01283	-0.01377	-0.00058	-0.01531	-0.01309
12	-0.00178	-0.00073	-0.00063	-0.00036	-0.00178	-0.00123
13	-0.00203	-0.00115	-0.00259	-0.00065	-0.00246	-0.00272
14	-0.00083	0.000314	-0.00048	-0.00057	-0.00088	-0.00127
15	-0.00063	0.00005	-0.00014	-0.00106	-0.00081	-0.00077
16	-0.0007	-0.00013	-0.00092	-0.00049	-0.00146	-0.00081
17	-0.00094	-0.00021	-0.00079	-0.00067	-0.00096	-0.00038
18	-0.00029	-0.00075	-0.00021	-0.0016	-0.00094	-0.00147
19	-0.00122	-0.00256	-0.00298	0.001972	-0.00231	-0.00263
20	-0.00053	0.0034	0.001421	0.00898	0.001733	0.002055
21	0.001274	0.001791	0.000667	0.004467	0.000338	0.000941
22	-0.0016	-0.00174	-0.0015	-0.01386	-0.00184	-0.00204
23	-0.00085	-0.00265	-0.00229	-0.00638	-0.00257	-0.00285
24	-0.00142	-0.00078	-0.00038	-0.00036	-0.00101	-0.00119
25	-0.00071	-0.00037	-0.00044	-0.00321	-0.00104	-0.00046

Table A.3 (cont.)

Carbon atom	Compd. I	Compd. II	Compd. III	Compd. IV	Compd. V	Compd. VI
26	-0.00121	-0.00023	-0.00103	-0.00035	-0.00149	-0.00179
27	-0.00078	-0.0006	-0.00028	-0.00046	-0.00078	-0.00074
28	-0.00048	-0.00024	0.000192	-0.00046	-0.00099	-0.00082
29	-0.00028	-0.00602	-0.00615	-0.00292	-0.00505	-0.00562
30	-0.00478	-0.00248	-0.00436	-0.00011	-0.00478	-0.00544
31	-0.0002	0.009092	-0.00045	0.001212	0.002147	0.0006
32	0.004223	-0.02125	-0.01466	-0.01772	-0.00253	-0.01622
33	0.029582	0.029429	0.071131	0.006206	0.045119	0.050136
34	0.002409	0.000693	-0.00078	0.002797	0.003658	0.000846
35	-0.00128	0.001267	0.00075	-0.00642	-0.00033	-0.00018
36	-0.00184	0.000225	-0.00036	-0.00088	-0.00118	-0.00104
37	-0.00249	0.002147	-0.00083	-0.00183	-0.00169	-0.00166
38	-0.0007	0.001252	-0.00292	0.000276	-0.00221	-0.00211
39	-0.00179	0.001479	-0.00054	-0.00119	-0.00227	-0.00058
40	0.002487	0.005503	0.000311	-0.00133	0.000739	0.000312
41	-0.00625	-0.01787	-0.01418	-0.00531	-0.0027	-0.01465
42	0.049842	0.046489	0.037981	0.003226	0.044121	0.051654
43	-0.09483	-0.10557	-0.08954	-0.00417	-0.10648	-0.10412
44	-0.08441	-0.09079	-0.08564	0.029899	-0.10565	-0.09215
45	0.03771	0.035073	0.037184	-0.03042	0.044095	0.032953
46	0.002055	0.004262	0.004137	0.040022	0.003865	0.004231
47	-0.00959	-0.0134	-0.01309	-0.01461	-0.01491	-0.01447
48	-7.5E-05	0.000569	0.000225	0.002824	-0.00026	-0.00052
49	-0.00056	0.000939	-0.00141	-0.00245	-0.00077	-0.00132
50	0.000284	0.000426	-0.00043	-0.00098	-0.0006	-0.00092
51	-0.00183	-0.00044	-0.00069	-0.0006	-0.00128	-0.00191

Table A.3 (cont.)

Carbon atom	Compd. I	Compd. II	Compd. III	Compd. IV	Compd. V	Compd. VI
52	-0.0022	-0.00073	-0.00164	0.003472	-0.00122	-0.00177
53	-0.00391	-0.00537	-0.00429	-0.01246	-0.00525	-0.00612
54	-0.00138	0.003583	0.001057	0.038844	0.002113	0.00168
55	-0.00559	-0.00073	-0.00224	-0.06745	-0.00237	-0.00128
56	-0.00077	-0.0033	-0.00176	0.044386	-0.00279	-0.00481
57	0.016427	0.048306	0.039572	-0.00516	0.044598	0.049712
58	-0.00412	-0.00533	0.000816	-0.00122	0.001567	-5.8E-05
59	0.004156	0.004728	0.001091	-0.00019	0.003134	0.00265
60	-0.01073	-0.01268	-0.01192	-0.01527	-0.01491	-0.01359
61	-0.07204	0.023269	0.009455	-0.17518	-0.06862	0.023891



สถาบันวิทยบริการ
จุฬาลงกรณ์มหาวิทยาลัย

Table A.4 The net charges (in a.u.) of atoms of C₆₀ derivatives in group 2 obtained using B3LYP/6-31G (d).

Carbon atom	Compd. VII	Compd. VIII	Compd. IX	Compd. X
1	0.00298	0.003306	0.002224	0.003672
2	0.003798	0.004051	-0.00025	0.002852
3	-0.00671	-0.00604	-0.00967	-0.00598
4	-0.00258	-0.00299	-0.00331	-0.00243
5	-0.00057	-0.00114	-0.00214	-0.00104
6	-0.00359	-0.00344	-0.00331	-0.00248
7	0.002244	0.004015	0.002072	0.002849
8	-0.03108	-0.03195	-0.02613	-0.02759
9	-0.02658	-0.032	-0.01103	-0.02726
10	0.041327	0.037519	0.056216	0.043193
11	-0.0145	-0.0227	-0.02447	-0.01169
12	-0.00165	-0.00088	-0.00182	-0.00128
13	-0.00028	-0.00032	-0.00085	0.000135
14	-0.00128	-0.00081	-0.00137	-0.00107
15	-0.00182	-0.00072	-0.00152	-0.00148
16	-0.00103	-0.00112	-0.00099	-0.00046
17	-0.00082	-0.00116	-0.00186	-0.00119
18	-0.00303	-0.00276	-0.00379	-0.00286
19	-0.00535	-0.00553	-0.00656	-0.00511
20	0.043089	0.051959	0.038517	0.044703
21	0.020623	0.015913	0.02304	0.017852
22	-0.01324	-0.0287	-0.01978	-0.01318
23	-0.00159	-0.00044	-0.00081	-0.00014
24	-0.00149	-0.00088	-0.00114	-0.00085
25	-0.00017	-0.0002	-0.00031	-0.00083

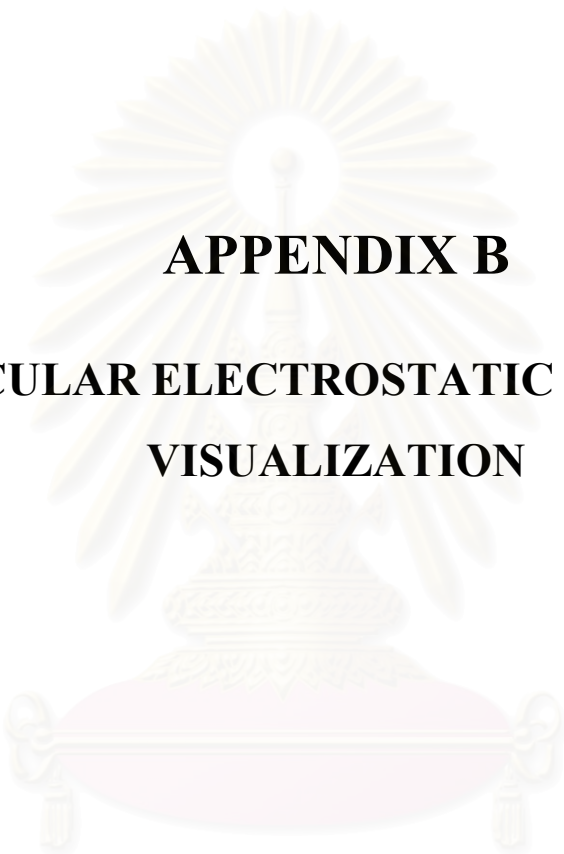
Table A.4 (cont.)

Carbon atom	Compd. VII	Compd. VIII	Compd. IX	Compd. X
26	-0.00113	-0.00072	-0.00102	-0.0011
27	-0.00117	-0.0014	-0.00231	-0.00071
28	-0.00049	-0.00112	-0.00126	-0.00108
29	-0.00027	-0.00016	-0.00034	-0.00028
30	-0.0012	-0.00151	-0.00129	-0.00135
31	-0.00301	-0.00243	-0.00309	-0.00206
32	-0.0062	-0.00788	-0.00785	-0.00596
33	0.003374	0.002537	0.002779	0.003719
34	0.00261	0.002634	0.003246	0.004184
35	-0.00088	-0.0012	-0.00243	-0.00125
36	-0.00071	-0.00107	-0.00078	-0.00085
37	-0.00118	-0.00081	-0.00139	-0.00073
38	-0.00102	-0.00103	-0.00133	-0.00018
39	-0.00083	-0.00033	-0.00018	-0.00025
40	-0.00095	-0.00134	-0.00161	-0.00121
41	-0.01473	-0.01607	-0.02014	-0.01171
42	0.043549	0.031527	0.012302	0.016234
43	0.049706	0.040082	0.030449	0.041902
44	-0.02765	-0.02895	-0.02356	-0.0237
45	-0.01584	-0.03015	-0.0273	-0.02285
46	0.006142	0.004728	0.002787	0.004938
47	-0.00498	-0.00868	-0.00704	-0.00609
48	-0.00293	-0.00208	-0.00298	-0.00253
49	-0.0014	-0.0008	-0.0008	-0.00086
50	-0.00031	-0.00039	-0.00099	0.000232
51	-0.00156	-0.00089	-0.00175	-0.00048

Table A.4 (cont.)

Carbon atom	Compd. VII	Compd. VIII	Compd. IX	Compd. X
52	0.000184	-0.00037	-0.00003	-0.00047
53	-0.0106	-0.01569	-0.01792	-0.01181
54	0.025098	0.036635	0.027763	0.015959
55	0.05444	0.046419	0.043923	0.036362
58	-0.00124	-0.00053	-0.00144	0.000049
59	0.032836	0.017651	0.051454	0.016772
60	-0.00276	-0.00292	-0.00311	-0.0024
61	-0.35046	-0.10852	-0.12232	-0.29698
64	0.15449	-0.08466	-0.15236	-0.2811

สถาบันวิทยบริการ
จุฬาลงกรณ์มหาวิทยาลัย



APPENDIX B
MOLECULAR ELECTROSTATIC POTENTIAL
VISUALIZATION

สถาบันวิทยบริการ
จุฬาลงกรณ์มหาวิทยาลัย

APPENDIX B

Molecular Electrostatic Potential Visualization

In order to get the three-dimensional plots showing molecular electrostatic potential (MESP) isosurfaces for all compounds in this study, the schematic representative methodology details and calculations are demonstrated in Figure A.1.

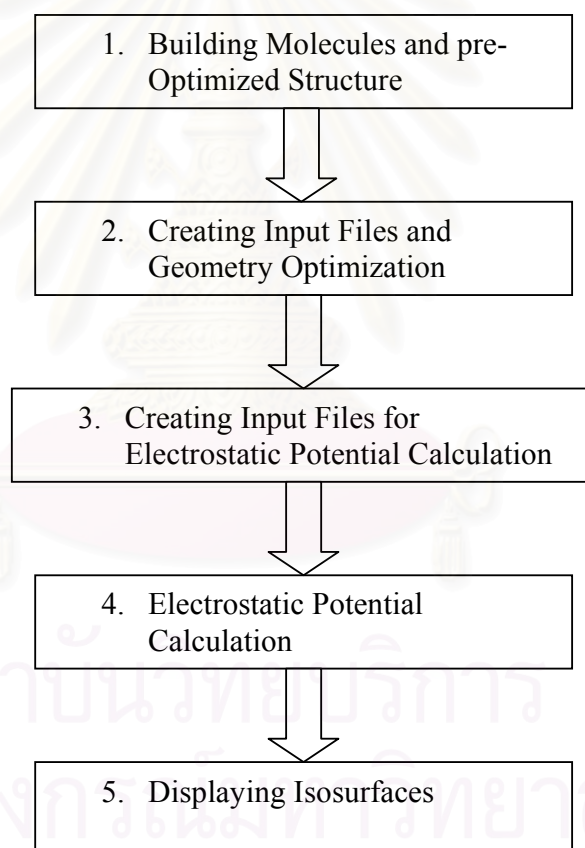


Figure B.1 Schematic representation of methodology details and calculations of molecular electrostatic maps.

1. Building Molecules and pre-Optimized Structure

The facility in HyperChem that constructs 3D models of chemical structures from 2D drawings. HyperChem uses built-in rules to assign standard bond lengths, bond angles, torsion angles, and stereochemistry. The Model Builder also assigns atom types for the currently active force field, and can automatically add hydrogens to complete valence requirements. These are approximate structures and might require refinement by geometry optimization.

Creates a 3D molecular model from selected atoms you created with the Drawing tool or if nothing is selected, from all the atoms and bonds. After building molecule is finished, every structures studied was pre-optimized at the MM+ using conformational search in HyperChem package.

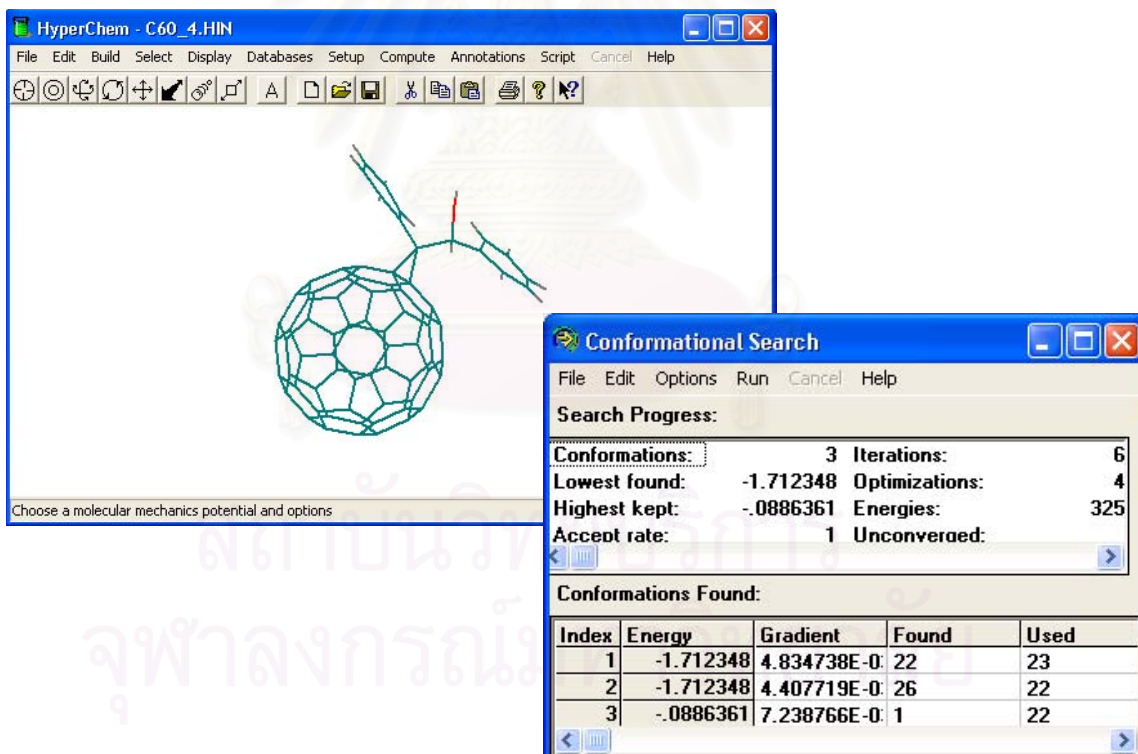


Figure B.2 Dialog boxes of drawing tools and conformational search in HyperChem package.

2. Creating Input Files and Geometry Optimization

After molecule building from HyperChem package, .hin file was created. Easier way to create input file for ONIOM optimization is created by *Gaussview* program. One has to convert .hin file to .ent file and then open with *Gaussview* program. In this program, option in edit menu allows to assign atoms to ONIOM layers.

Select Layer: Assigning Atoms to ONIOM Layers

Assigns atoms to layers graphically. This option is used for ONIOM calculations.

The following figure illustrates ONIOM layer assignment.

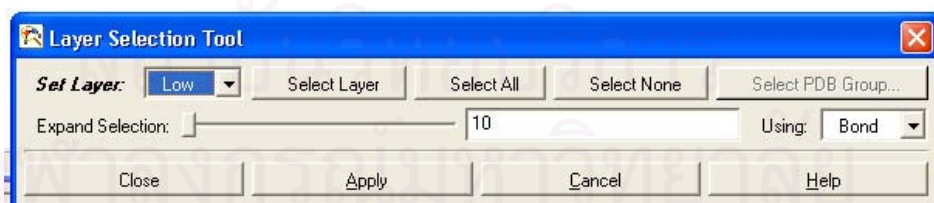


Figure B.3 ONIOM layer assignment illustration in *Gaussview* program.

To create an input file, **Save** option under the **File** menu was selected. The molecular structure and the options selected (or their defaults) in this dialog box make up the *Gaussian* input file.

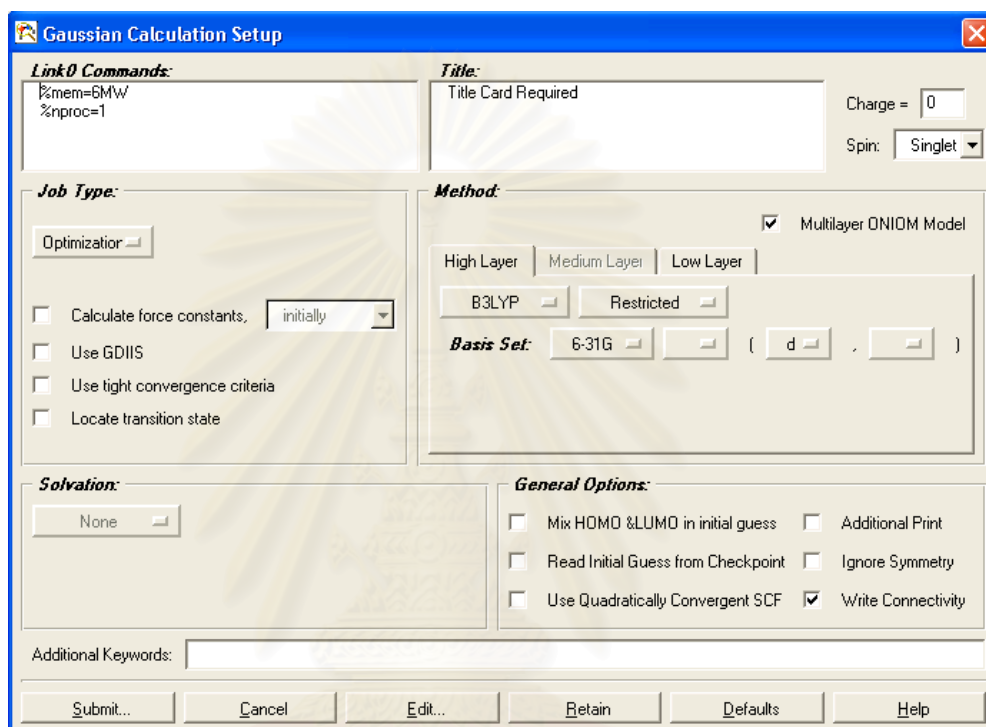


Figure B.4 Dialog Box of *Gaussian* Calculation Setup in *Gaussview* program.

สถาบันวิทยบริการ
จุฬาลงกรณ์มหาวิทยาลัย

Example Input File for Multilayer ONIOM Calculation

```

%mem=6MW
%nproc=1
%chk=opt4c2.chk
# opt oniom=(b3lyp/6-31g*:pm3) geom=connectivity

```

Title Card Required

```

0 1
C      0  2.378227 -0.434033  3.432911 L
C      0  1.162204 -1.218056  3.315130 L
C      0  2.010022  0.970092  3.365072 L
C      0  0.566486  1.049463  3.208823 L
C      0  0.047961 -0.294412  3.176419 L
C      0 -0.993672 -0.600496  2.341880 L H   57
C      0  0.061230 -2.713038  1.730134 L
C      0  2.034152 -3.464575  0.715883 L
C      0  4.389498  0.073193  2.143654 L
C      0  4.043777  1.395132  2.082612 L
C      0  2.818777  1.855816  2.710661 L
C      0  0.015736  2.007436  2.398175 L H   56
C      0  4.742715 -0.508031 -1.465830 L
C      0  4.241669 -1.780283 -1.495703 L
C      0  0.590912 -3.374796  0.564666 L
C      0  1.144950 -1.049296 -3.328184 L
C      0  0.328541 -1.926992 -2.664760 L H   32
C      0 -0.921991 -1.479090 -2.065432 H
C      0 -1.281012 -0.141488 -2.152508 H

```

C	0	-0.362459	0.782431	-2.790118	L H	33
C	0	2.587649	-1.138795	-3.173475	L	
C	0	3.132559	-2.104338	-2.374573	L	
C	0	0.909183	-2.949212	-1.816755	L	
C	0	-1.098958	-2.229102	-0.807420	H	
C	0	-1.629284	-1.616732	0.319956	H	
C	0	-2.199972	-0.233104	0.310874	H	
C	0	-2.000290	0.582166	-1.060419	H	
C	0	-1.286983	1.888943	-0.934865	H	
C	0	-0.367616	2.021544	-2.046699	L H	45
C	0	0.776843	2.765824	-1.942166	L	
C	0	2.000884	2.305379	-2.576753	L	
C	0	1.120482	3.376643	-0.683199	L	
C	0	0.300004	3.201425	0.400391	L H	55
C	0	-0.944688	2.452966	0.286245	H	
C	0	-1.123742	1.702410	1.543055	H	
C	0	-1.642467	0.414978	1.537466	H	
C	0	0.044855	-3.120352	-0.665909	L H	41
C	0	-0.986685	-1.841358	1.600377	L H	42
C	0	0.789422	0.346563	-3.387613	L	
C	0	-5.595738	2.436770	1.719378	H	
O	0	-4.679711	-0.118797	-2.506523	H	
H	0	-4.594159	0.547023	1.943450	H	
H	0	-6.038287	2.397478	2.710834	H	
H	0	-6.485911	4.337206	1.220317	H	
H	0	-8.246224	-3.099637	1.478958	H	
H	0	-5.905925	-3.207689	2.322948	H	
H	0	-4.081706	-2.148418	1.063045	H	
H	0	-5.258520	0.616686	-2.240498	H	

3. Creating Input Files for Electrostatic Potential Calculation

After geometry optimization is finished, then, a most stable conformation of the structure was obtained. Create input file again with coordinates of the most stable structure for electrostatic potential calculation. Add the *'%chk=jobname.chk'* line and *cube* keyword to your *gaussian* input file.

Example Input File for Electrostatic Potential Calculation

```
$RunGauss
%chk=elec4
#p b3lyp/6-31g* gfinput iop(6/7=3) cube=potential,prop
```

optimized structure of opt4

```
0 1
C      2.344669 -0.589011  3.449133
C      1.127451 -1.371679  3.284659
C      1.141483 -2.523307  2.521233
C      2.373509 -2.959403  1.878325
C      3.531760 -2.216876  2.033422
C      3.516921 -1.001637  2.838702
C      1.973449  0.820872  3.440423
C      0.527472  0.905207  3.267791
C      0.009216 -0.442562  3.173071
C     -1.037784 -0.705142  2.307197
C      0.038253 -2.800021  1.608879
C      2.026453 -3.506877  0.572407
C      2.857509 -3.288425 -0.510625
```


C	-1.022252	-1.917328	1.501711
C	0.828971	0.523432	-3.394888
C	-3.358886	0.300745	-0.537497
C	-4.203910	1.417815	0.043348
C	-4.820261	1.275229	1.293509
C	-5.676659	2.262574	1.779372
C	-5.938455	3.404437	1.019112
C	-5.336540	3.553596	-0.230629
C	-4.472973	2.567925	-0.713998
C	-4.222671	-0.679148	-1.408828
C	-5.315302	-1.393386	-0.618131
C	-6.641779	-0.946346	-0.638816
C	-7.632936	-1.608353	0.086622
C	-7.314837	-2.735985	0.844330
C	-5.998973	-3.201327	0.860453
C	-5.010796	-2.539071	0.131164
O	-4.715851	0.022176	-2.537693
H	-4.630894	0.385950	1.886080
H	-6.143084	2.136684	2.753100
H	-6.605246	4.173820	1.400116
H	-5.528990	4.440508	-0.829060
H	-3.984157	2.703955	-1.674550
H	-3.554628	-1.435279	-1.823022
H	-6.917510	-0.085872	-1.240325
H	-8.656637	-1.244062	0.052833
H	-8.087271	-3.254514	1.406615
H	-5.740583	-4.089890	1.431388
H	-3.995560	-2.923204	0.133914
H	-5.232611	0.775520	-2.217005

4. Electrostatic Potential Calculation

One way to get the electrostatic potential is convert the binary checkpoint file to a formatted one with the **formchk** utility:

```
formchk jobname.chk jobname.fchk
```

From a formatted checkpoint file, create one cube file containing density and one containing the electrostatic potential, calculate with the *gaussians* **cubegen** utility:

```
cubegen 0 density jobname.fchk jobname_dens.cube
```

```
cubegen 0 potential jobname.fchk jobname_esp.cube
```

then, these command provide the files that contain density and electrostatic potential to create an isodensity surface colorcoded with the electrostatic potential.

5. Displaying Isosurfaces

The *Gaussview* surfaces facility allows to display various chemical data in three dimensions. The surface data may be generated from a *Gaussian* checkpoint file or be read-in from a cube file (.CUB). In this study, *cube* files which contain density and electrostatic potential were used.

Start *Gaussview*, open the filename of the density cube and select 'Surfaces' in **Results** menu:

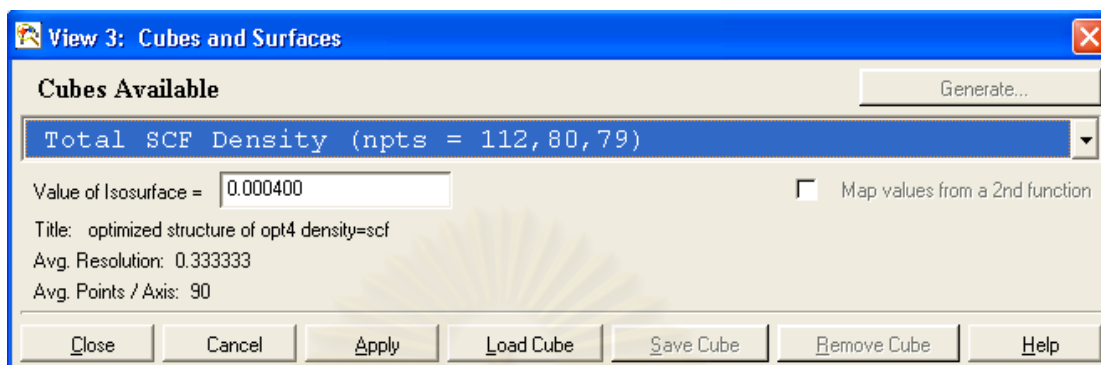


Figure B.5 Show the section in the Cubes and Surfaces dialog box.

Gaussview also allows to map the values of one property on an isosurface of a different property. Now click 'Load Cube' in dialog box to open another cube file that contain electrostatic potential. This is accomplished by checking the **Map values from a 2nd function** checkbox on **Cubes and Surfaces** dialog. Then select 2nd function, which is electrostatic potential cube file. This will bring up the following Figure.

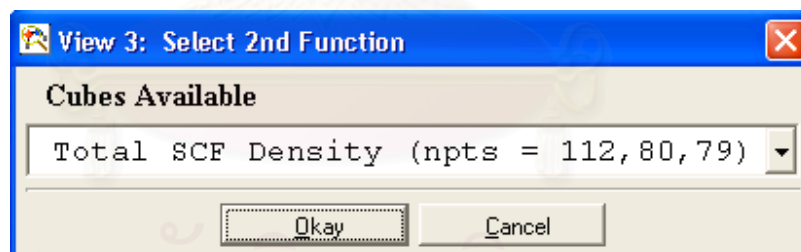


Figure B.6 Show the section of map values from a 2nd function in the Cubes and Surfaces dialog box.

Click on 'Apply' in checkbox on **Cubes and Surfaces** dialog. *Gaussview* will report the maximum and minimum value of the electrostatic potential it encounters on the isodensity surface.

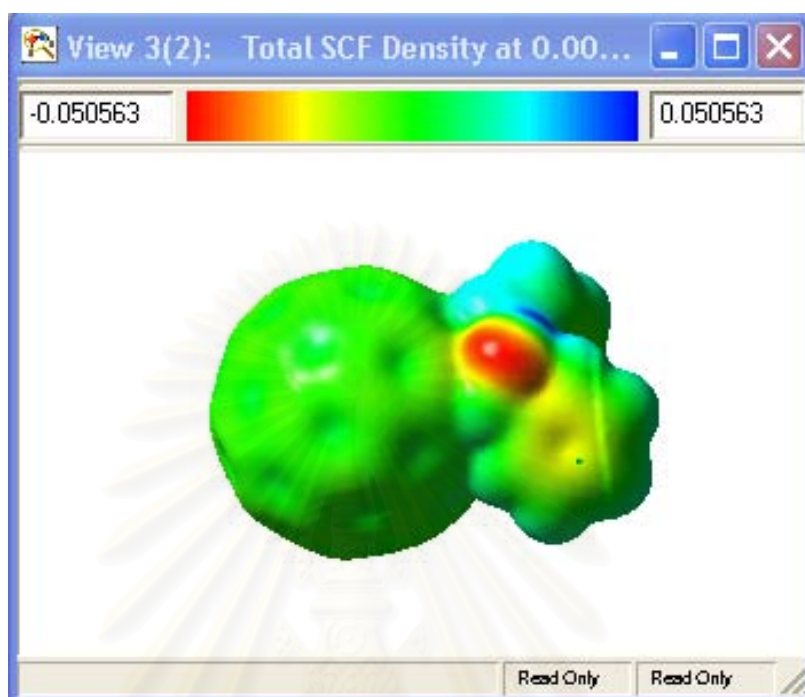


Figure B.7 Three-dimensional plot showing MESP isosurface (displayed in solid mode).

Figure A.6 is an example of a mapped surface, which display in solid mode. The surface display may be modified using the **Change View Format** dialog's **Surface** tab.

สถาบันวิทยบริการ
จุฬาลงกรณ์มหาวิทยาลัย

APPENDIX C

Manuscript

Molecular and Electronic Properties of HIV-1 Protease
Inhibitor C₆₀-derivatives as Study by ONIOM Method

Siriporn Promsri, Parawan Chuichay,
Vannajan Sanghiran Lee, Vudhichai Parasuk,
Supot Hannongbua

In preparation.

สถาบันวิจัยบริการ
จุฬาลงกรณ์มหาวิทยาลัย

Molecular and Electronic Properties of HIV-1 Protease Inhibitor C₆₀- derivatives as Study by ONIOM Method

Siriporn Promsri¹, Parawan Chuichay¹, Vannajan Sanghiran², Vudhichai Parasuk¹, Supot Hannongbua¹

¹ Department of Chemistry, Faculty of Science, Chulalongkorn University, Bangkok, 10330 Thailand.

² Department of Chemistry, Faculty of Science, Chiangmai University, Chiangmai, Thailand.

Abstract

Quantum chemical methods were performed to study structure and electronic properties of a series of C₆₀ derivatives. The integrated, ONIOM molecular orbital method was applied to optimize the structure of all compounds while the DFT/B3LYP (6-31G (d)) calculations were performed to examine molecular and electronic properties. It was found that strongest effect of functional group on the net charges takes place on the linked atoms between C₆₀ and its side chain. The functional group leads to the changes of atomic net charges on the C₆₀ surface up to 5 Å far from C—C bond where the functional group binds to the surface. Two localized electrostatic potential regions are observed, for the selected compounds, near the hydroxyl oxygen and the hydroxyl hydrogen. The hydroxyl hydrogen atom is the center for most positive potential. These electrostatic features are likely to be the modulator of hydrophobicity or lipophilicity of the compounds and, hence, indicate how they interact with the receptor.

Introduction

HIV protease (HIV PR) is one of the most intensely studied aspartic peptidase, needed for viral replication implicated in AIDS, during the last 20 years [1]. It was found that water-soluble methanofullerene derivative was a competitive inhibitor for this purpose [2, 3]. Therefore, various sizes of fullerene derivatives have been synthesized and their

biological activities have been widely measured and reported. On the basis of molecular modeling, Friedman et. al. [2] anticipated that a C_{60} molecule fits nicely into the hydrophobic cavity of the protease specific for HIV-1 because of steric bulk of C_{60} and its complementarity to the active site surface of HIV-PR. The core fullerene moiety was observed to bind snugly into the active site. This was confirmed experimentally that the binding affinity of C_{60} derivatives is in the low-micromolar to nanomolar range [4]. In addition, the main mechanism of action of these derivatives is hydrophobic interaction.

It is known that binding of drug to HIV-1 protease alters their physicochemical properties and the potency of binding correlates with the hydrophobicity of the drug. Therefore, understanding of their structural and the electrostatic features of these compounds would lead directly to an understanding of the mechanism of their action [5]. As receptor recognized stereo-electronic effects, studies of molecular and electronic properties by means of quantum chemical calculations could also provide essential information in the field of the structure based drug design.

The present study is an assessment of structural features and electronic properties toward an improved understanding of structure-activity relationship of C_{60} derivatives to enable a prediction of potent antiviral activity. The study encompassed 10 compounds as shown in Figure 1. We have made detailed molecular modeling studies on C_{60} derivatives using Own N-layered Integrated molecular Orbital and molecular Mechanics or ONIOM algorithm [6]. The ONIOM scheme allows treating a selected area of a large system at a high level, whereas the rest of the system is treated using a computationally more feasible level of theory. Conformational analysis, a detailed analysis of electrostatic potential (ESP), and molecular properties study have been correlated with antiviral activity.

1. Computational details:

1.1. Optimized Geometry of the C₆₀ Derivatives

Fullerene (C₆₀) derivatives were selected as targets for this study. Starting parameters for C₆₀ have been taken from literature. They were then entirely optimized, using ONIOM algorithm at the ONIOM2 level. All computational calculations were carried out using the Gaussian 98 program for 10 C₆₀-derivatives. Schematic representations of these compounds, **I-X**, are shown in Figure 1. Their antiviral activities as measured by *K_i* and *EC₅₀* values are also given. These compounds are classified into two groups by the membered ring bridge between C₆₀ and side chain of each derivatives, 3-membered and 6-membered rings for compounds **I-VI** and **VII-X**, respectively. This method was applied with semiempirical; PM3 and density functional theory (DFT); B3LYP/6-31G*, at low and high level, respectively. The regions for each level were assigned as shown in Figure 2.

1.2. Electronic Properties of the C₆₀ Derivatives

The optimal geometry obtained from the density functional theory (DFT) with B3LYP functionals has been applied to evaluate electronic properties of the compounds. The standard 6-31G (d) basis set was used to determine stabilization energy, HOMO-LUMO energies and electronic properties such as charge distribution on the solubilizing group and electrostatic potential of C₆₀ derivatives. Electrostatic potentials were calculated using CUBEGEN routine which is a utility in Gaussian 98 program.

Molecular electrostatic potential maps for compounds **III**, **VIII**, **IX** and **X** were visualized using the Gaussview program. The electrostatic potentials were sampled over the entire accessible surface of a molecule. Three-dimensional isosurfaces of the molecular electrostatic potentials represent electrostatic potentials superimposed onto a surface of electron density. The most negative electrostatic potential indicated by red, whereas the most positive electrostatic potential is blue.

2. Results and discussion:

2.1. Effect of functional groups on the molecular orbital properties

The HOMO-LUMO energy gaps of all compounds were shown in Table 1. The results show that the energy gaps of C₆₀ derivatives in group 1 (compounds **I-VI**) are almost the same as that of C₆₀ which those of compounds in group 2 (compounds **VII-X**) are slightly narrower than that of C₆₀. However, no significant difference in the HOMO-LUMO energy gap is found among the derivatives in the same group.

2.2. Effect of functional groups on the atomic net charge

To visualize effect of functional groups on the atomic net charges of the C₆₀ derivatives, their structures were fully optimized based on ONIOM (B3LYP/6-31G (d): PM3) calculations. Atomic net charges on carbon atoms around C—C bond which links between C₆₀ and its side chain have been analyzed and plotted separately for the two groups of compounds, compounds **I-VI** (group 1) and **VII-X** (group 2), in Figures 3a and 3b. The selected atoms were labeled and given as an insert of Figure 3, in which atom numbers C₁-C₁₄ and C₁₅-C₁₆ are those of C₆₀ surface and its side chain, respectively. It is interesting to note here, therefore, that effect of functional group on the atomic net charges on the C₆₀ surface can be observed up to 5 Å far from bridged carbon atoms (C₁-C₂).

Atomic net charge on the C₆₀ surface

As expected, strongest effect of functional group on the net charges takes place on the linked atoms, C₁ and C₂. The calculated values are between -0.10 and -0.09 for both groups of derivatives in which the side chains are linked to the C₆₀ surface by the three- and six-membered rings, respectively. Second set of atoms where the net charge of 0.02 – 0.05 is independent of linking type, are C₃-C₆. Effect of linkage has been significantly observed for C₁₁-C₁₄ where the six-membered linkage leads to less negative atomic charges than those of the three-membered ring.

Atomic net charge on the side chain

Effect of side chains and of linkage types is displayed also in Figure 4 in terms of atomic net charges of C_{15} and $C_{15}-C_{16}$ for compounds group 1 and group 2, respectively.

Interesting is centered on C_{15} of the three-membered ring linkage, compound **I-VI**, in which its net charge can be classified into 3 levels. The compounds that their side chains consist of two symmetric benzene rings, compounds **I** and **V**, lead the electron density about -0.07. This value is significantly lower than that between 0.01 and 0.02 obtained from the compounds that their side chains consist of the single benzene ring, compounds **II**, **III** and **VI**. In addition to the above 2 sets of compounds, the lowest negative charge takes place when the benzene rings are replaced by the open chain, compound **IV**. The calculated value of -0.18 is much lower than those of the other compounds in group 1.

For the second group of compounds, **VII-X**, carbon atoms of the linked six-membered ring, C_1 and C_2 , are almost less negative than those of the three-membered rings, compound **I-VI**. The =NO and -OMe functional groups on the six-membered ring of compound **VII** and the -O group of compound **X** donate more electrons into the rings, in comparison to those of compounds **VIII** and **IX**. An unsymmetric distribution taken place for compound **VII**, charge of C_{15} of about 0.5 atomic unit is much lower than that of C_{16} , is clearly due to the presence of the electron donor -OMe group on C_{15} (see Figure 1).

2.3. Effect of functional groups on the molecular geometry

With the geometry obtained from the ONIOM (B3LYP/6-31G (d): PM3) optimization, changes of the selected bond lengths of all compounds relative to those of Buckminsterfullerene (C_{60}) were plotted in Figures 4a and 4b. Six types of C—C bonds on the C_{60} surface which are in the region 5 Å from the bridged atoms were labeled by B1-B6 in an insert of Figure 4. B3 is only double bond of all investigated ones. B5 and B6 obtained from PM3 only. The average C-C bond lengths of the Buckminsterfullerene

which share by the 2 six-membered rings of 1.44 Å and by five- and six-membered ring of 1.37 Å yielded from our previous work [7] have been used for comparison.

It was found in Figure 4 that B1 for all compounds which links between C₆₀ and its side chain are more than 0.37 Å for compounds **I-VI** (Figure 4A) and 0.22 Å for compound **VII-X** (Figure 4B) longer than those of Buckminsterfullerene. The corresponding C—C distances of the two groups of derivatives, which longer than 1.81 Å and 1.67 Å for compounds in group 1 and group 2, respectively, indicate that B1 bond for all compounds are totally broken. It is found that the three-membered linkage effect B1 distance more than the six-membered one. For compound **IV**, dramatic increase of B1 by 0.5 Å relates directly to an increase of electron density on C₁₁, and hence of the three-membered ring connected to C₆₀ surface.

Exclude compound **IV**, interest is centered on B2. Increases of this C—C bond of group 2 compounds (0.11 Å) are significantly longer than those of group 1 (0.03 Å – 0.05 Å). This fact can be described by a constrain due to an increase of B1, i.e., B2 of compounds in group 1 is higher constrained due to a much higher increase of B2 bond of this group of compounds than that of group 2. Therefore, the trends in increasing B1 and B2 are opposite; the longer B1 bonds with the shorter B2 bonds. As a consequence of increasing B1, B4 bonds for group 1 compounds are slightly longer than those of group 2. In addition, increases of B3 and B5 bonds for compounds in group 1 are superior, in comparison to those of group 2.

Another clear conclusion which can be made from Figure 4 is that side chain effects play stronger role on the bond lengths of the six- than those of the five-membered ring of the C₆₀ surface. Changes of the C—C bonds are observed in the following orders: B1 >> B2 ~ B4 > B3 > B6 > B5 for compounds **I-VI** (excluded compound **IV**) and B1 >> B2 > B4 > B3 ~ B6 > B5 for compounds **VII-X**.

2.4. Electrostatic Potential (ESP)

Three-dimensional isosurfaces of ESP superimposed onto total electron density and electrostatic potential map of compounds **III**, **VIII**, **IX** and **X** are presented in Figure 5. The plots for all compounds show two localized ESP regions. The lowest electrostatic potential (red region) is in the proximity of the lone pair of the hydroxyl oxygen atom, whereas the center for most positive potential (most blue region) lies near the hydroxyl hydrogen atom. These long-range electrostatic features indicate the potential for the inhibitor to participate in intermolecular formation of hydrogen bond with the receptor. The large lateral negative potential in front of the hydroxyl oxygen can be regarded as a nucleophilic region which acts as a magnet toward the electrophilic part of the receptor. This would generate driving force to facilitate the formation of inhibitor-enzyme complex. This fact is known to relate directly to their antiviral activity.

To visualize reliability of the gas phase properties yielded from quantum chemical calculations as described before, the results were compared to those obtained from molecular dynamics (MD) simulations [8]. Compound **III**, which is the most active compound ($K_i = 150$ nM) among the investigated compounds, was selected. Their structures obtained from the DFT calculations and from MD simulation were compared in Figure 6a. The ESP potential for the MD structure was shown in Figure 6b.

The plot shows that the two structures are almost identical with the root mean square displacement (RMSD) of 1.02 Å. As a consequence, no difference was found in terms of positive and negative regions of the electrostatic potential obtained from the quantum calculations (compound **III** in Figure 5) and MD (Figure 6b) geometries. However, it was found that the lowest negative ESP from the quantum calculations structure is slightly higher than that of the MD one will the trend is opposite for lowest positive interaction.

Acknowledgement

The authors are grateful to Prof. Keiji Morokuma for suggestions and discussions in using the ONIOM method. Special thanks to Asst. Prof. Dr. Surapong Pinitglang for all the help and good advise. Acknowledgement is made to Computational Chemistry Unit Cell (CCUC), Department of Chemistry, Faculty of Science, Chulalongkorn University, Bangkok, Thailand for the use of its resources.



สถาบันวิทยบริการ
จุฬาลงกรณ์มหาวิทยาลัย

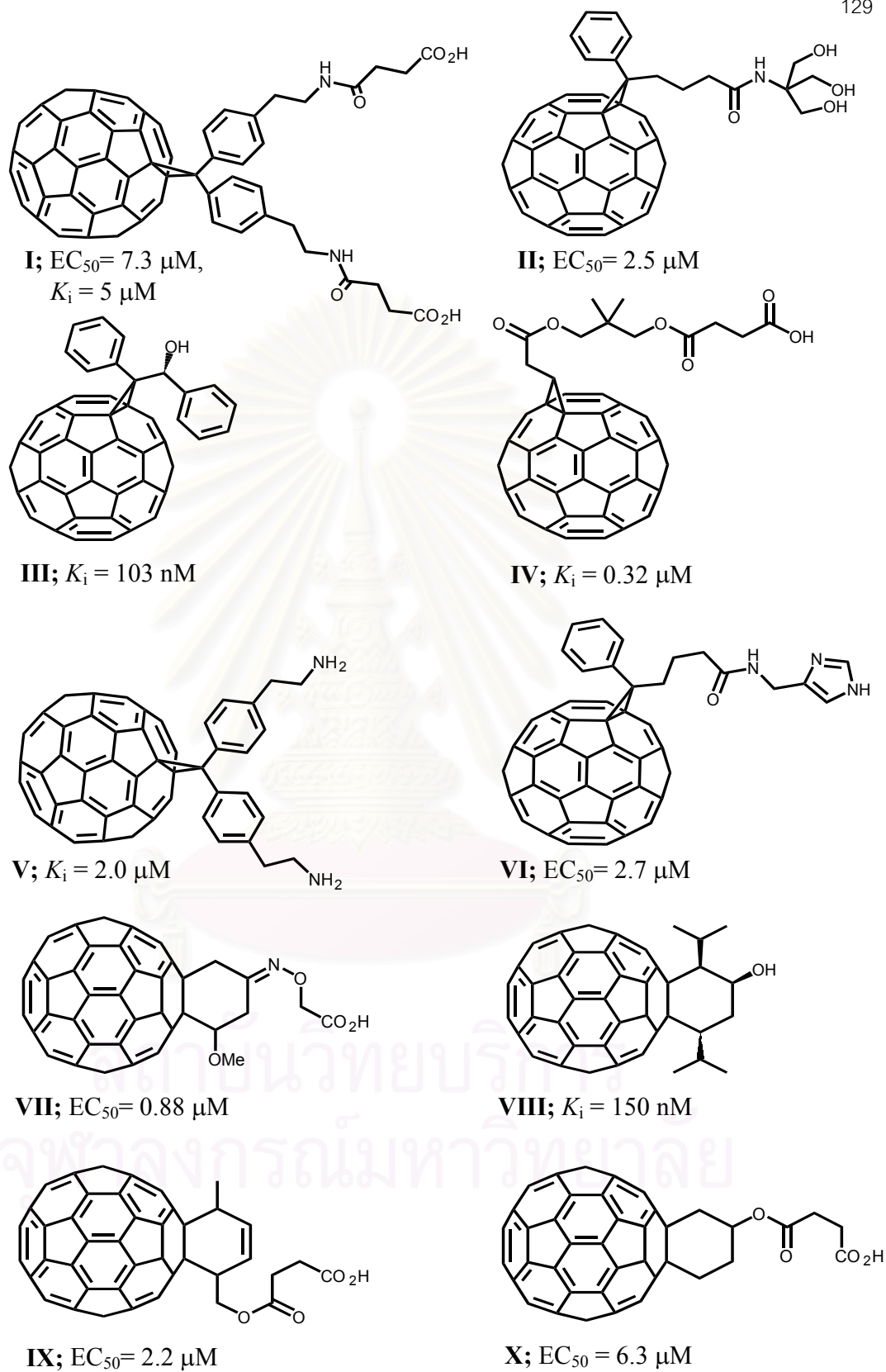


Figure 1 Fullerene (C_{60}) derivatives used in this study.

Table 1 The HOMO-LUMO energy gaps of all 10 C₆₀ derivatives and of C₆₀.

Compound.	HOMO-LUMO energy gap(ev)
I	2.73
II	2.74
III	2.74
IV	2.79
V	2.73
VI	2.73
VII	2.65
VIII	2.63
IX	2.63
X	2.64
C ₆₀	2.73

สถาบันวิทยบริการ
จุฬาลงกรณ์มหาวิทยาลัย

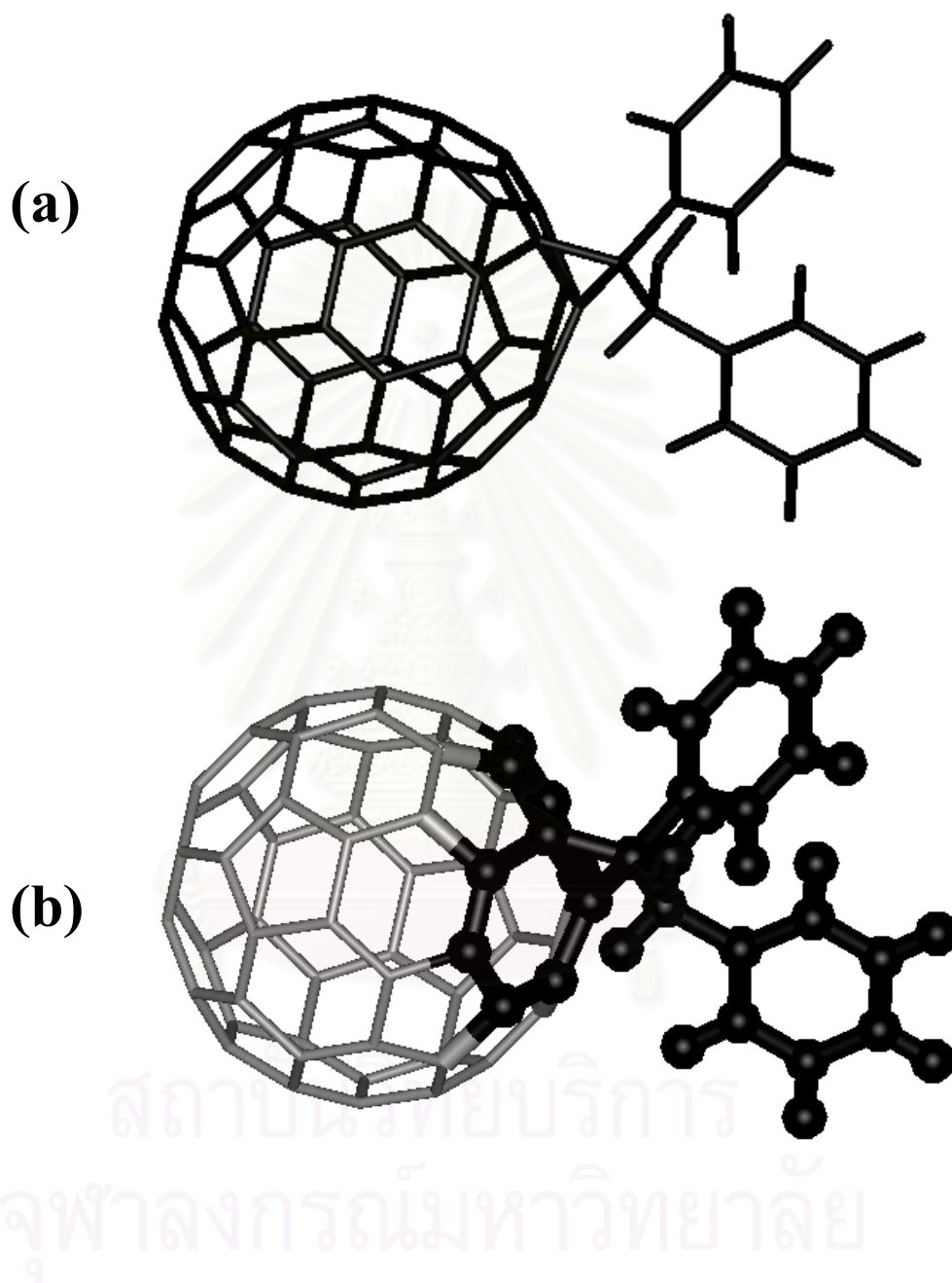


Figure 2 Optimized structure of C_{60} derivatives using ONIOM method; (a) low level region and (b) high level region (ball and stick).

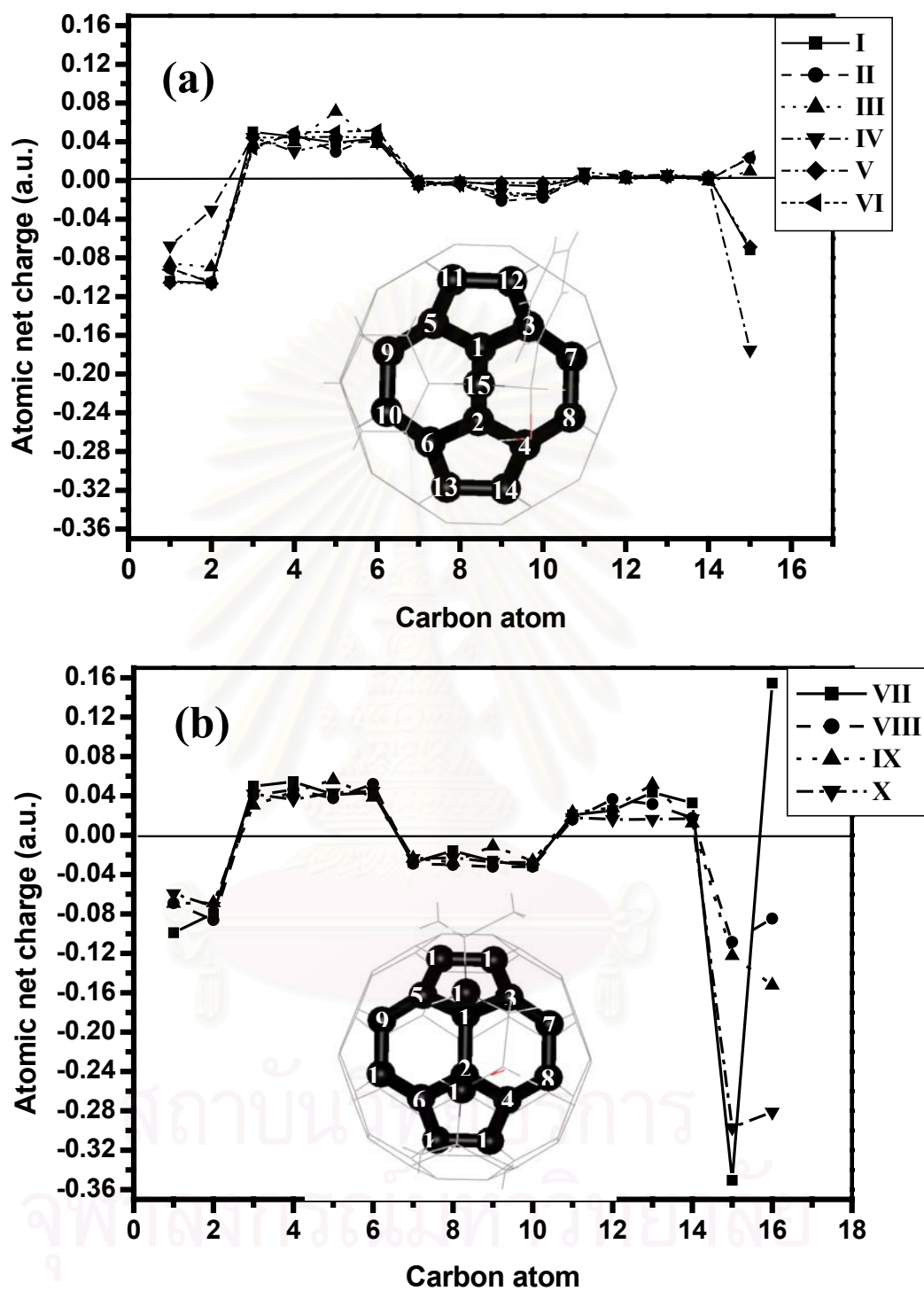


Figure 3 The plots of atomic net charges of all 10 C₆₀ derivatives; (a) compounds I-VI and (b) compounds VII-X.

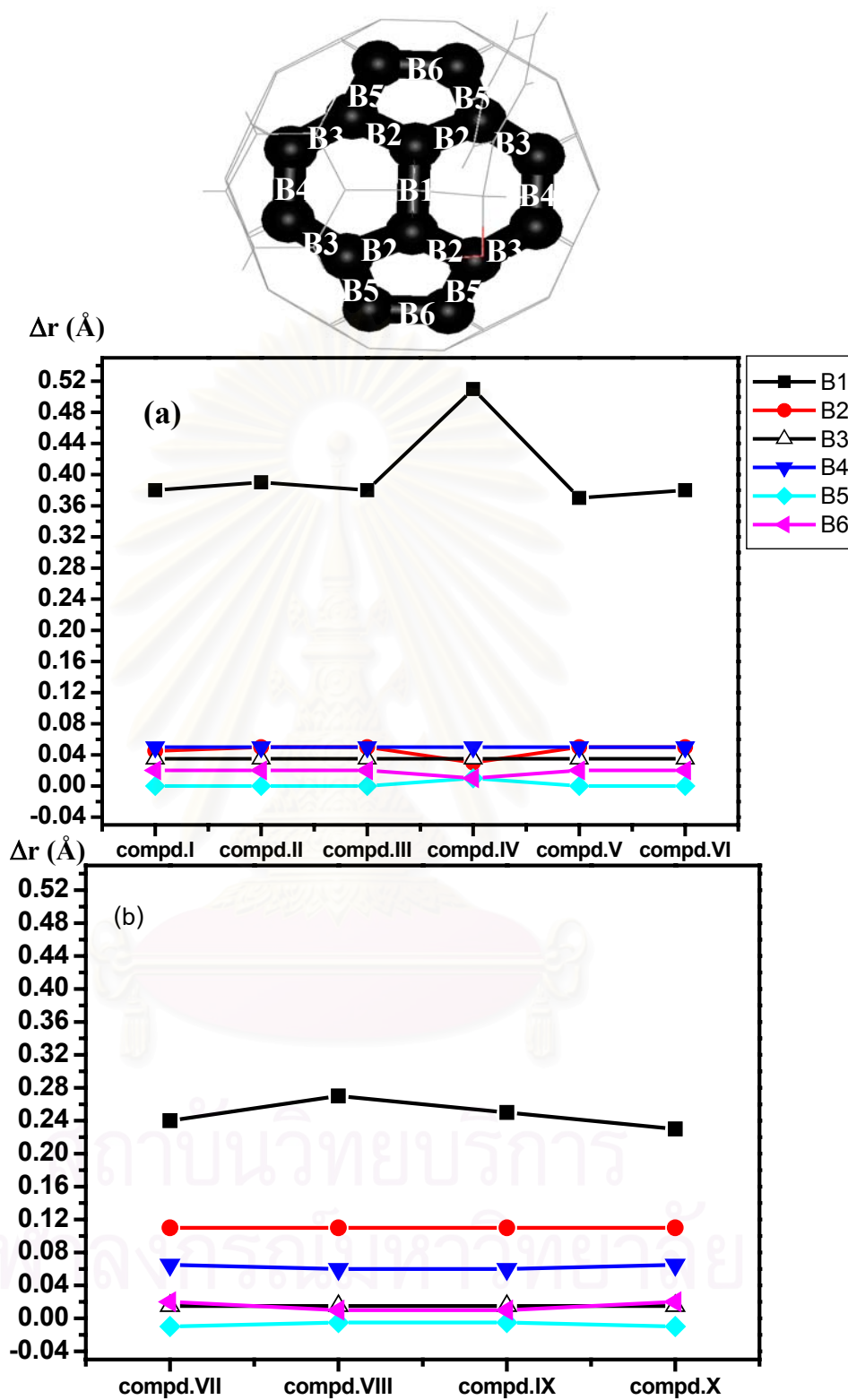


Figure 4.6 The plots of selected bond-length of all compounds; (a) compounds I-VI and (b) compounds VII-X.

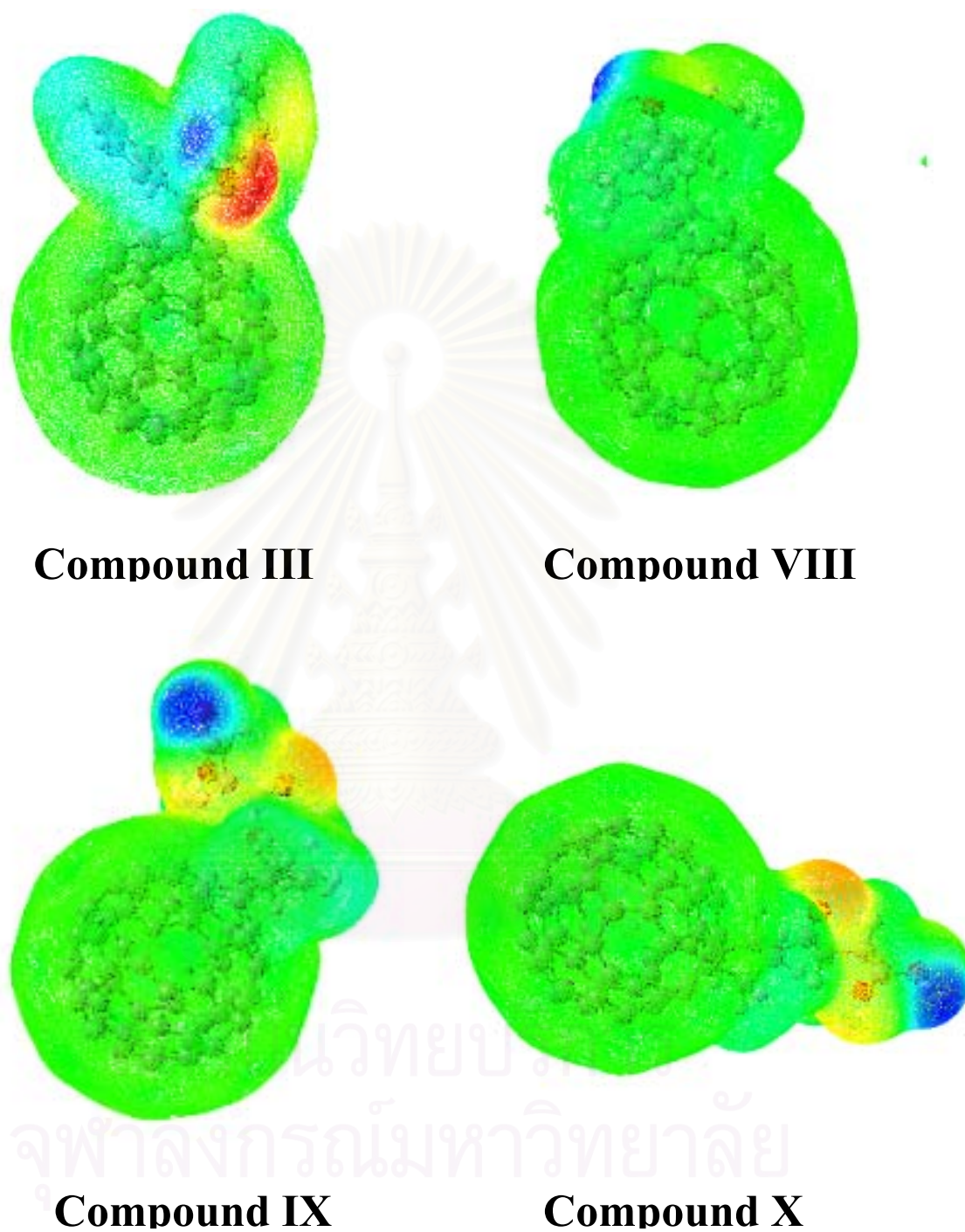


Figure 5 Molecular electrostatic potential energy isosurfaces of the selected compounds superimposed onto their total electron density (0.004 e/au^3).

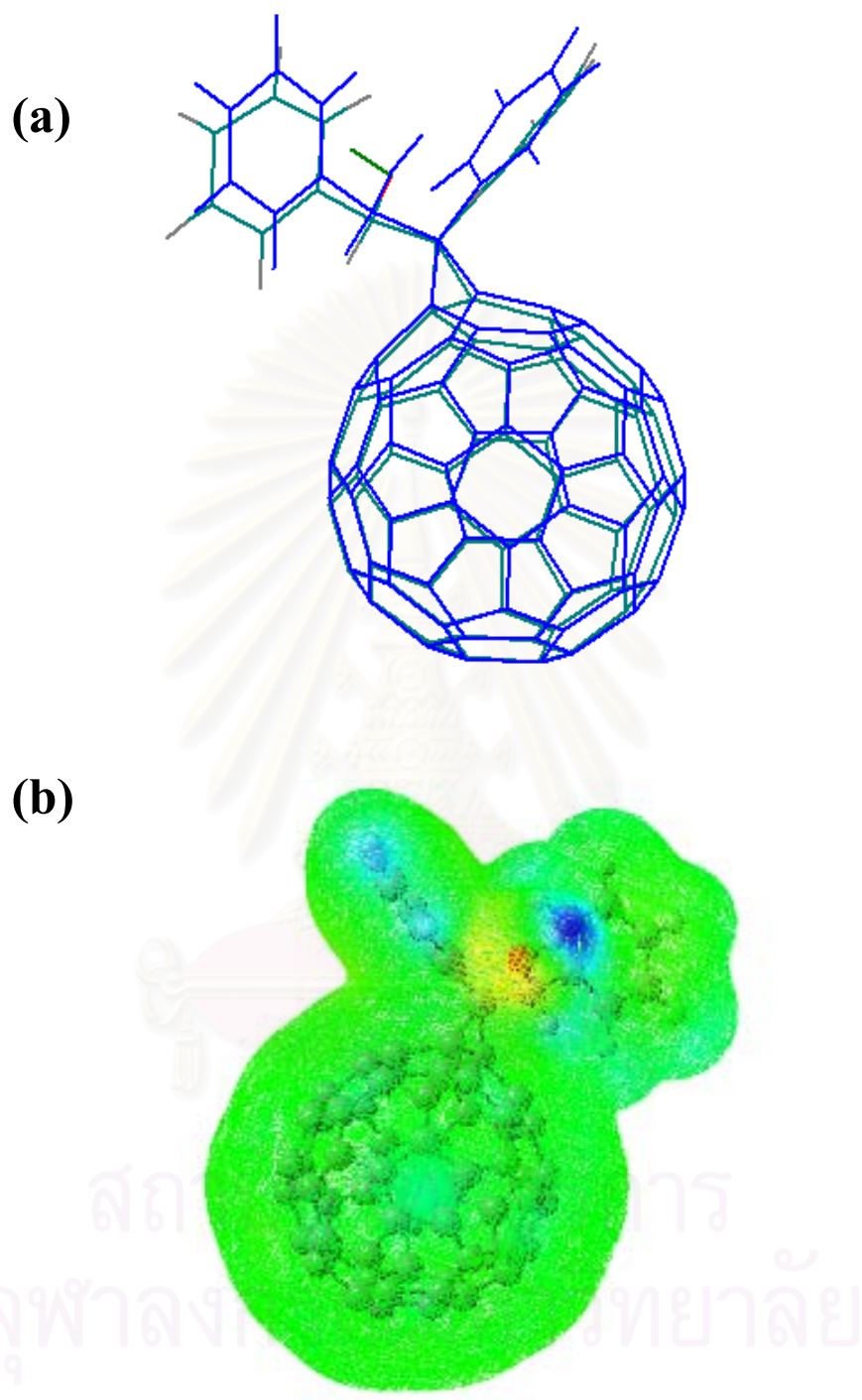


Figure 6 (a) Stereoview and (b) electrostatic potential contours plot of the compound **III**; comparison between the optional structure obtained from quantum chemical calculation (blue) and molecular dynamics simulations (black).

VITAE

NAME: Siriporn Promsri

DATE AND PLACE OF BIRTH: 20 March 1979 in Nakorn Ratchasima, Thailand

ELEMENTARY SCHOOL:

1984-1990 Ratgaroon Withaya School, Nakorn Ratchasima

SECONDARY SCHOOL:

1990-1996 Suranaree Withaya School, Nakorn Ratchasima

UNIVERSITY EDUCATION:

1996-2000 B. Sc. in Chemistry, Department of Chemistry, Faculty of Science, Khon Kaen University, Khon Kaen

2000-2002 M. Sc. in Physical Chemistry, Department of Chemistry, Faculty of Science, Chulalongkorn University, Bangkok

สถาบันวิทยบริการ
จุฬาลงกรณ์มหาวิทยาลัย